Volume 1 | Issue 2 | 2019

Technical Journal

Engineering excellence around the globe

SNC LAVALIN

Foreword

Chris Hendy

Editor-in-Chief SNC-Lavalin Technical Journal

Professional Head of Bridge Engineering and Transportation Technical Director, EDPM

Welcome to the second edition of our SNC-Lavalin Technical Journal, established to showcase the fantastic depth and breadth of our engineering expertise across a wide range of disciplines and domains and to demonstrate that technical excellence is at the heart of everything we do. This second edition again highlights our impressive asset management and design credentials across all of our Sectors.

In the field of asset management, we have pioneered long-term camera-based monitoring of the expansion joints and cables of the world's third longest span suspension bridge, the Great Belt Bridge in Denmark. We have supported Oil and Gas operators to continue producing economically from their fields without production outages through our Design and Operability Review Process, which identifies causes and contributory factors and allows early intervention. And we have developed a next-generation portable system to test for early warning of degradation of the jacket and insulation of electrical cables used extensively in Nuclear Power Plants, particularly in the control and safety systems, again to facilitate early intervention.

In design, we are leading the way in establishing best practice in detailing continuous welded rail for railways, eliminating expensive and maintenance-intensive track joints, and proposing new rules for adoption in global railway track standards. To address the complex retrieval of hardpan nuclear waste, we have designed a Mechanical Waste Gathering System which breaks up the waste and moves it to the surface without the introduction of liquid to the tank bottom, which is not desirable in compromised leaking tanks due to the risk of environmental release. And the design of a new 135 MW hydroelectric generating station in Canada showcases our approach to safety by design whereby the initial concept for the intake, considering deep water penetration of an existing dam, was modified to use safer and more economical shallow water construction.

The above examples provide only a small insight into the wealth of innovative papers presented in this journal and the far wider contribution that SNC Lavalin makes day to day.

I hope you enjoy the selection of technical papers included in this edition as much as we have enjoyed compiling them.

Editor-in-Chief

Chris Hendy
Editor-in-Chief

FREng, MA (Cantab) CEng FICE Eur Ing
Technical Director, Atkins Fellow,
Professional Head of Bridge
Engineering
Engineering, Design and Project
Management
Epsom, UK

2019 Editorial Board Members

Ramy Azar
Ph.D, Ing.

Vice-President, Engineering & Chief
Technology Officer
Clean Power
Montreal, Canada

Vinod Batta
Ph.D., P.Eng.

Vice-President, Engineering & Chief
Technology Officer, Hydro
Clean Power
Vancouver, Canada

Eric Chui Hon Man
BEng CEng ACGI MHKIE MIMM MICE
MIStructE RPE(GEL, CVL, STL)

Divisional Director
Tunnel and Ground Engineering, EDPM
Hong Kong, China

Chad Gvozdenovic
P. Eng.

Vice President, Global Technical Lead
Oil & Gas
Calgary, Canada

Donna Huey
GISP

Atkins Fellow and Sr. Vice President,
Client Technology Director
Engineering, Design and Project
Management
Orlando, FL, USA

Matt Keys
PhD BEng CEng

Fellow, Technical Director, Global
Technical Authority – Offshore
Structures
Oil & Gas
Perth, Australia

Adrian Lindon
BA(Hons) Dip. Arch, ARB, RIBA

Managing Director, Design and
Engineering (Middle East)
Engineering, Design and Project
Management
Dubai, UAE

Navil Shetty
PhD, DIC, FIAM

Atkins Fellow and Technical Chair for
Asset Management
Centre of Excellence for Digital Asset
Management & Operations
Bangalore, India

Patrick Sikka
P. Eng

Vice-President
Mining & Metallurgy – North America
Toronto, Canada

Richard Moura
P.Eng.

Director, Business Development Rail
& Transit
Global Business Development,
Transportation-Major Projects
Infrastructure
Toronto, Canada

Tim Milner
CSci CChem MRSC

Atkins Fellow and Chief Technology
Officer
Nuclear
Columbia, SC, USA

Samuel Fradd

Technology Manager
Engineering, Design and Project
Management
Epsom, UK

Akshaye Sikand
MS, P.Eng.

Manager, Knowledge Management
Global Projects Support
Toronto, Canada

Production Team

Dorothy Gartner
MLIS

Librarian
Global Projects Support
Montreal, Canada

Samantha Morley
CAPM

Operations Coordinator
Technical Professional Organization,
Atkins North America
Denver, CO, USA

Cheryl Law
MEng CEng MICE

Associate Engineer, Infrastructure
Engineering, Design and Project
Management
Epsom, UK

Graphic Design Team

Montreal, Canada

Volume 1 | Issue 2 | 2019

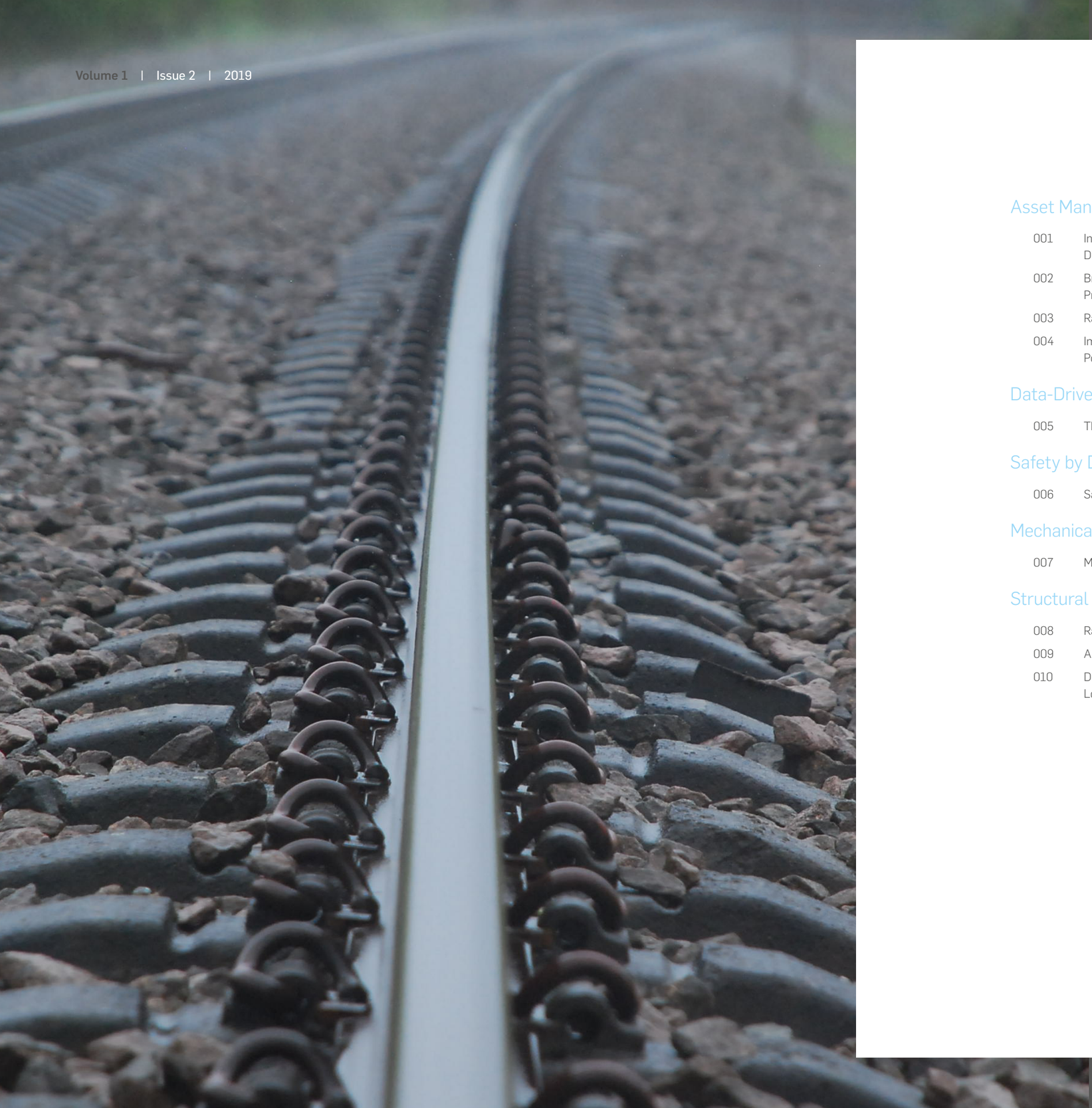

Innovative Long-Term Monitoring of the Great Belt Bridge Expansion Joint Using Digital Image Correlation

Jan Winkler

PhD
Professional Head of Geomatics, DIC Team Lead, Engineering, Design and Project Management
Copenhagen, Denmark

Martin Duus Havelykke

Maintenance Manager, Sund & Bælt Holding A/S—Structures and Landworks
Copenhagen, Denmark

Abstract

Informed decisions on timely intervention for effective bridge maintenance activities rely on good quality, accurate and reliable asset condition data. Although proper functioning of the expansion joint is critical for bridge performance, its long-term condition monitoring has been considered challenging due to costs associated with installation of different sensors and data processing. Digital image correlation (DIC) is a non-contact photogrammetry technique that can be used for monitoring by imaging a bridge component periodically and computing strain and deformation from images recorded at different times or operating conditions. This paper describes the outcome of 1-month long monitoring campaign where the DIC system was used as a cost effective data gathering tool providing real-time information on movement and rotation of the Great Belt Bridge expansion joint. Outcome of the monitoring provided previously unavailable data, helped to better understand the behaviour of the expansion joint and informed next steps with respect to the maintenance strategy. The results of the monitoring showed good agreement between the data collected using DIC and the temperature data received from the Danish Meteorological Institute (DMI). From the collected data a mathemathical model was established, which relates the air temperature to deformations in the joint. Such a model allows for real-time evaluation of monitoring data and for cost-efficient identification of problems in the functioning of the joint. To the authors knowledge this is one of the first applications of the DIC technique for long-term monitoring of a suspension bridge.

Keywords

Suspension bridge; Expansion joint; Monitoring; Digital image correlation

This paper received the International Association for Bridge and Structural Engineering (IABSE) Award 2019 (Category: Outstanding Paper)

1. Introduction

1.1. Bridge Monitoring – Challenges

The principal difficulty with adding lots of monitoring systems to bridges is that they produce vast quantities of data. Bridge operators typically do not know what to do with this data unless there are very clear trigger levels defined associated with this data and clear interventions defined if they are exceeded. This means that the structural engineer needs to identify what the most likely deterioration mechanisms are for the particular bridge and design bespoke monitoring that can be used to specifically measure performance in such a way that an acceptable level can be set and checked.

Instruments such as strain gauges, accelerometers, fiber optic sensors and displacement transducers are becoming increasingly common in structural health monitoring. These types of sensors can however possess drawbacks such as the need for external power and cabling/antenna for data transmission, high data acquisition channel counts and the limitation of only measuring at discrete points or along a line, so it is necessary to have an idea of where to expect damage when placing the instrumentation. These sensors can be used effectively to continuously monitor for abnormalities that indicate damage, but the type and severity of the damage can still be difficult to identify from discrete point measurements. Furthermore, asset managers are continously searching for new technologies that will allow them gathering information about their structures without traffic disruption.

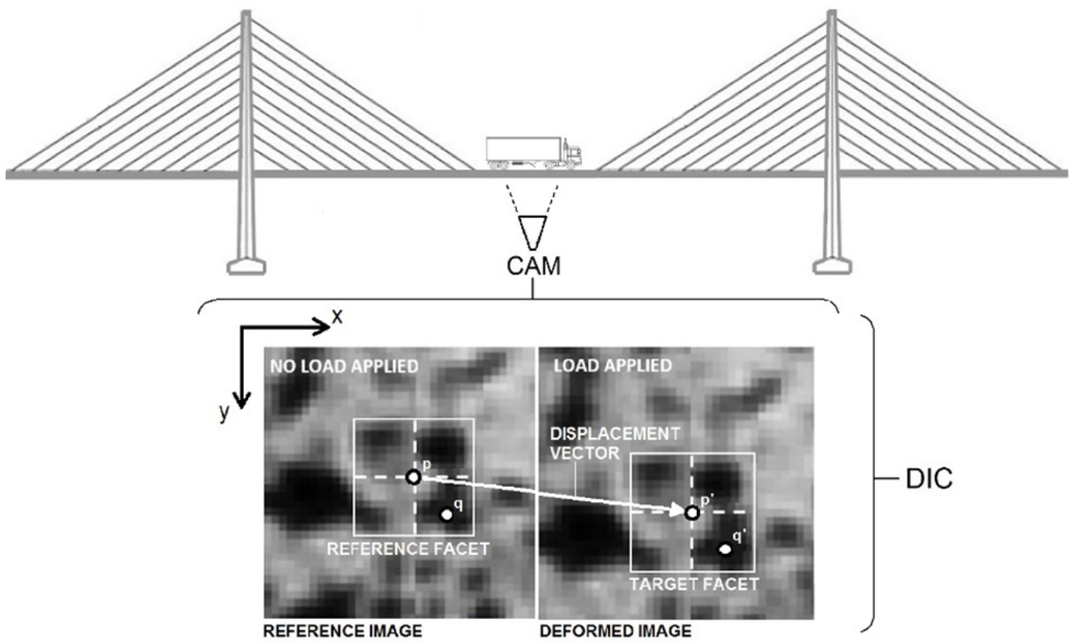

Figure 1: Digital image correlation method

1.2. Digital Image Correlation (DIC)

DIC represents a photogrammetry technique used for accurate measurements of surface deformation. The digitized images (e.g of a bridge deck) are compared to match facets from one image to another by using an image correlation algorithm (Figure 1). Image analysis involves capturing a reference image of a bridge component surface in its undeformed state. As the load is applied (e.g truck load), additional images are collected. The algorithm, involves a stage-wise analysis, in which each stage consists of one image resulting in a description of displacements occurring on the surface of the bridge component. The evaluation of a correlation measurement results in coordinates, deformations and strains of the surface.

Assuming a locally homogeneous deformation over a small facet of the specimen, the deformed coordinates (x'_q, y'_q) of a material point q in the neighborhood of a point p, at undeformed location (x_p, y_p), are given by equations (1.a),(1.b) [1]:

$$x'_q = x_q + u_p + \frac{\partial u_p}{\partial x}\Delta x_q + \frac{\partial u_p}{\partial y}\Delta y_q \qquad (1.a)$$

$$y'_q = y_q + v_p + \frac{\partial v_p}{\partial y}\Delta y_q + \frac{\partial v_p}{\partial x}\Delta x_q \qquad (1.b)$$

where u_p and v_p are the x and y components of the displacement vector of point p, respectively, xq and yq ,are the undeformed coordinates of point q,
$\Delta x_q = x_q - x_p$ and $\Delta y_q = y_q - y_p$.

DIC method allows high precision surface deformation measurement that can reach the accuracy of a few micrometers. DIC measurement can provide information about strain, vertical and horizontal displacement, crack size, rotation and acceleration. DIC is independent of scale and material.

1.3. Image Analysis in Bridge Engineering

Research activity on the application of photogrammetry in bridge-related projects has been minimal and widely dispersed within the last 25 years [2]. Early applications of this technique include measurement of the deflection of a continuous three span steel bridge under dead load [3] and identification of the bridge deformation [4]. DIC was also employed to measure the geometry of a suspension bridge [5] and deformation of steel connection of a pedestrian bridge [6]. It was shown that DIC is a complementary tool of the conventional measuring systems such as LVDTs and strain gages. The last few years have seen an increased application of the DIC in the measurement of the vertical deflections of steel and concrete bridges due to traffic [7-13] and train transit [14]. In general, it was concluded that DIC system accuracy is comparable to existing displacement measurement techniques and DIC is an easier way to measure displacement of multiple points at once. DIC was also proposed as a method to asses dynamic characteristics of suspension bridge hanger cables [15]. In this study, a non-contact sensing method to estimate the tension of hanger cables by using digital image processing based on a portable digital camcorder was proposed. Moreover, DIC technique has been used to record the strain on a concrete girder during a full scale bridge failure test [16] and for the measurement of the displacement field on a cracked concrete girder during a bridge loading test [17]. In both cases the photogrammetry method was able to detect a change in loading condition and locate cracks. Recent applications of DIC include fatigue testing of monostrands for bridge stay cables. Here, the vision-based system allowed for the measurement of the interwire movement (fretting fatigue) being the governing mechanism responsible for the fatigue life reduction in modern stay cable assemblies [18,19]. DIC was also employed in structural monitoring to measure strain at fatigue-sensitive bridge detail with a view to avoiding the need for strengthening [20].

This paper describes the outcome of 1-month long monitoring campaign where the DIC system was used as a cost effective data gathering tool providing information on movement and rotation of the Great Belt Bridge expansion joint. Outcome of the monitoring provided previously unavailable data, helped to better understand the behaviour of the expansion joint and informed next steps with respect to the maintenance strategy.

2. Great Belt Bridge

The Great Belt East Bridge has a central span of 1624 m with 535 m side spans, carrying a four lane motorway plus emergency lanes and pylons reaching up to 254 meters. The 31 m wide welded steel box girder is continuous between the anchor blocks over the whole suspension bridge length. Hence there are expansion joints located at the anchor blocks (Figure 2) but there are no expansion joints at the towers. Expansion joints are a critical components of any large structure, their correct functioning are of fundamental importance for structural integrity, thus inspection and maintenance need to assure their flawless functioning at any time.

In October 2016, Atkins was appointed by Sund & Bælt to provide a long-term monitoring system in order to analyse the rotation and movement (expansion & contraction) of the Great Belt East Bridge expansion joint due to temperature change. Monitoring was undertaken during the course of 1-month (November – December 2016). The long-term DIC monitoring system was designed and set up within 2.5 weeks. The system was remotely controlled via LAN connection from the Atkins office. The scope of work comprised of synchronized monitoring of the movement and rotation of the edge beam.

The expansion joint is an assembly comprised of centre beams and edge beams that run parallel to the structural edges (Figure 3a). In order to avoid material fatigue, the traffic loads are transmitted to the adjoining reinforced concrete structure via anchor plates which are rigidly connected to the edge beams. Dependent on the size of movement numerous centre beams are arranged between the edge beams. The beams slide on obliquely arranged swivelling support bars, resting on elastic sliding bearings (Figure 3b). The monitoring data are describing the movement and rotation of the edge beam.

Figure 2: Great Belt East Bridge expansion joint

2.1. Measurement Methodology

A synchronized camera system with a selection of lenses was designed to provide sufficient resolution to make the measurements. The system was set up to capture the expansion joint movement and rotation periodically (every 30 min). The camera location was varying depending upon the measurement requirements. The normalized greyscale correlation tracking algorithms were used for the image analysis. The camera was mounted on a steel plate designed to provide a required field of view. Calibration was achieved by measuring a distance within the image. These measurements allowed the bridge components (expansion joint) to be defined in real units for measurement purposes. No editing of the raw data has been undertaken.

2.2. Validation and Calibration of DIC System

Image processing and analysis of the expansion beam movement was carried out using programming language. A general validation (cross check) of the image-based sensors was conducted by the author previously [18]. Calibration is a measuring process during which the image pixels coordinate frame is adjusted such that the dimensional consistency is ensured. The field of view (the area of the structure captured on the camera's image) was treated as a grid of discrete elements and the calibration was done by specifying real world distances between points in an image. The relevant distances were taken from the drawings. Locations of interest in a field of view were described as a system of continuously varying coordinates.

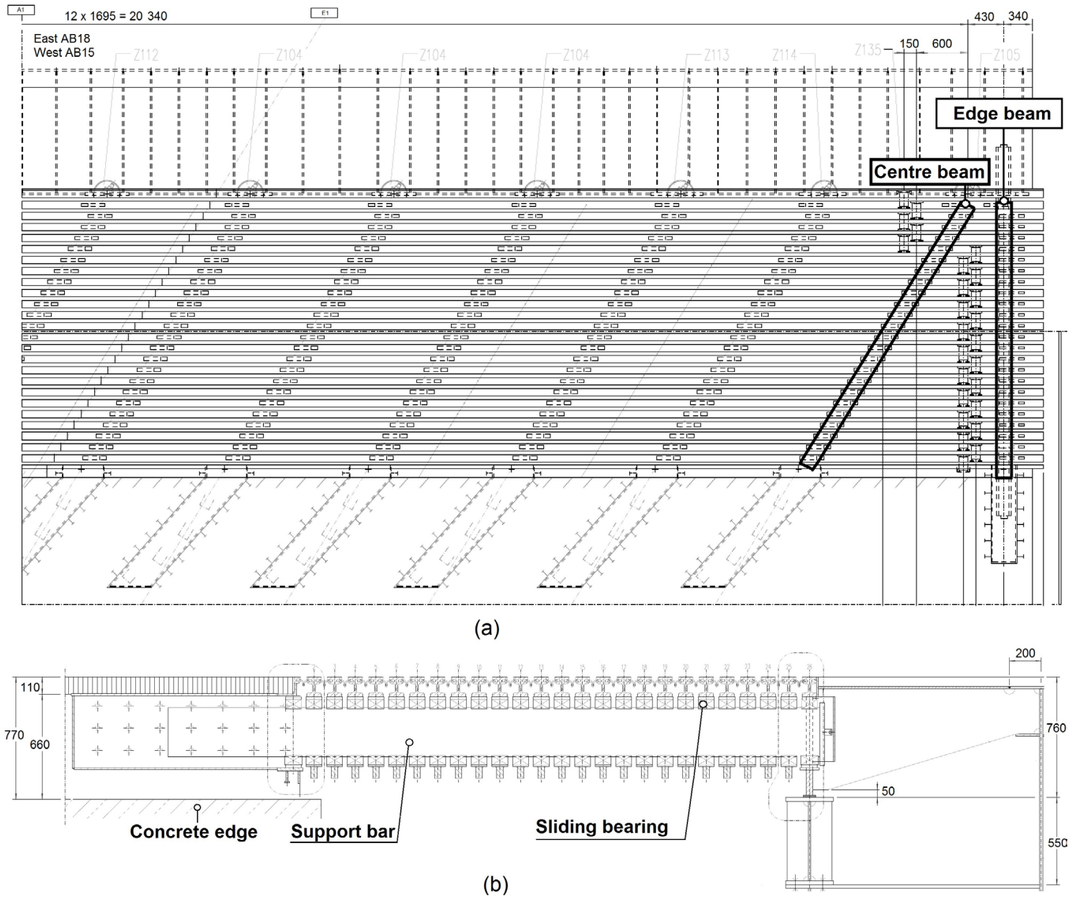

Figure 3: Great Belt Bridge expansion joint details

3. Measurement Location & DIC Setup

The DIC monitoring was carried on the expansion joint edge beam (Figure 4a). The camera providing information on the movement was set up perpendicular to the beam while the camera gathering data on the rotations was set up along the beam length. The field of view obtained from both cameras is shown on Figure 4b and Figure 4c. The DIC system allowed for simultaneously monitoring of all movements, deformations and rotations induced by the temperature difference. The DIC system was controlled remotely from Atkins office via LAN throughout the entire course of the monitoring period.

4. Results

This section presents the outcome of the long-term DIC monitoring (movement & rotation) performed on the expansion joint edge beam. The DIC data is presented together with the relevant temperature readings obtained from the Danish Meteorological Institute (DMI).

4.1. Edge Beam - Rotation & Movement

Figure 5 presents the combined movement and rotation measurement of the edge beam and the corresponding

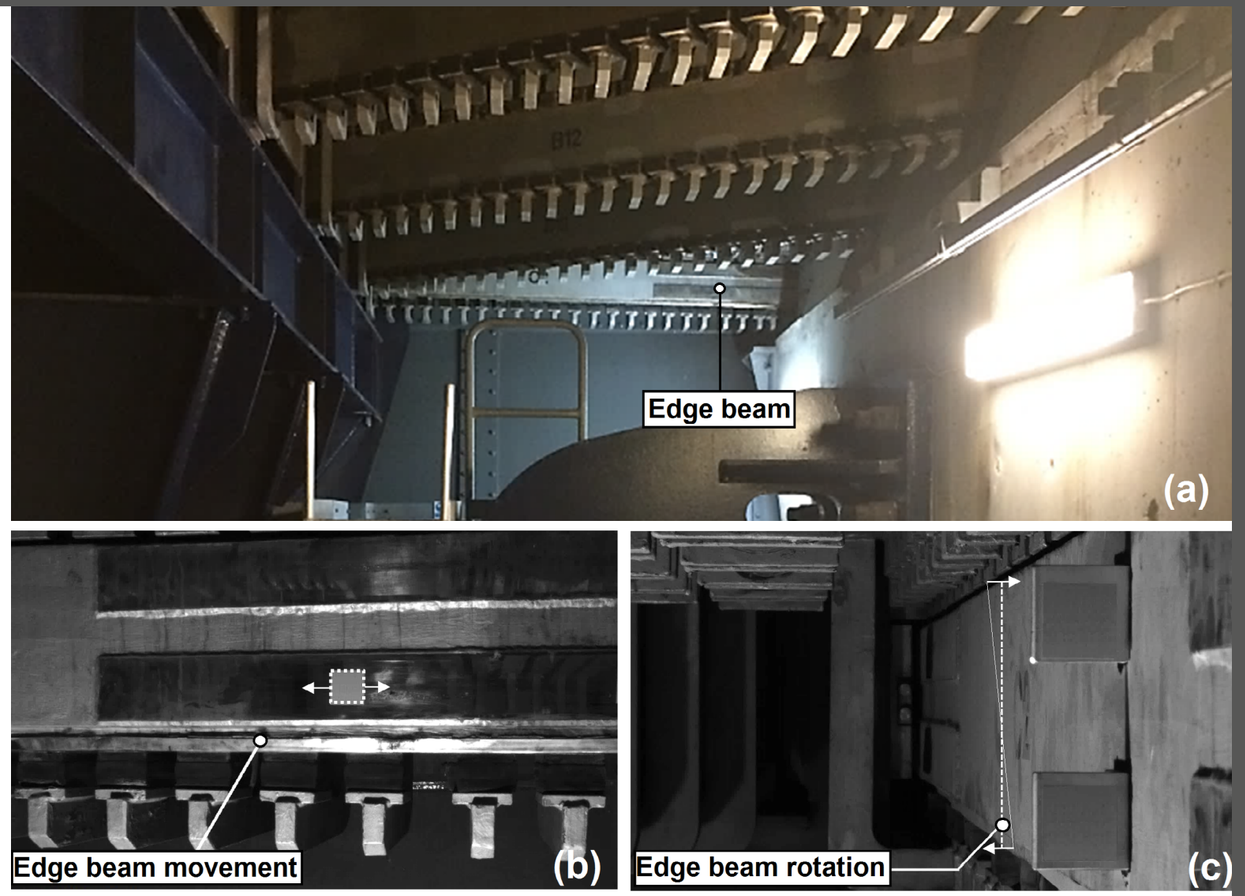

Figure 4: Measurement location (a), movement (b) and rotation (c) measurement using DIC

temperature data. It can be seen that a good agreement between the data obtained from the DIC system (Figure 5a) and the temperature data received from the DMI (Figure 5b) has been found. The rise and decrease in temperature within a day is followed by the movement of the expansion joint. A very high resolution of the DIC rotation measurement has been achieved and was reaching 0.01 deg. The DIC data show that edge beam is experiencing maximum daily rotation of up to 1.05 deg. The data also indicate that the edge beam is both moving and rotating at the same time.

5. Statistical Analysis and Probabilistic Considerations

The following section presents the statistical analysis performed on the monitored data with a view to establishing a mathematical model which relates the air temperature to deformations in the joint. The proposed model for the expansion joint beam movement depending on temperature is expressed using following equations:

$$M(t, \Delta t_{6h}) = m_\mu(t) + f(\Delta t_{6h}) \quad (2)$$

$$m_\mu(t) = 4.302 \cdot t - 33.61 \quad (2.a)$$

$$f(\Delta t_{6h}) = 4.99 \cdot \Delta t_{6h} - 0.161 \quad (2.b)$$

The model $M(t,\Delta t_{6h})$ is comprised of two different parameters: the mean movement trend m_μ (t) [mm] at a given temperature t [°C]; and a mean offset $f(\Delta t_{6h})$ [mm] from m_μ *(t)*.

The mean movement trend, m_μ *(t)*, is computed from one month of observations and it shows an approximate average movement at a given temperature. A linear equation was chosen as the difference between the goodness of fit R^2 of a 2nd order polynomial to a linear equation is small (R^2_{linear}=0.401 and R^2_{second}=0.406).

A statistical analysis is performed on the deviation between the actual measurements and the movement trend m_μ *(t)*. Figure 6 shows a histogram of the deviation together with the fitted normal distribution. If further probabilistic analysis is desired (e.g. Monte Carlo simulation for fatigue analysis), the random variable accounting for the deviation should be added to the mean trend m_μ *(t)*. The variable has a normal distribution with the mean value of 0 mm and the standard deviation of 12.16 mm.

The effect of temperature change on the measured movements in relation to the mean trend is analysed. Figure 7 illustrates the correlation between the temperature changes and the measured movement in relation to mμ (t) where Δt_{6h} was defined as the temperature change over 6 hours (the difference between the temperature at a certain hour and the temperature 6 hours earlier).

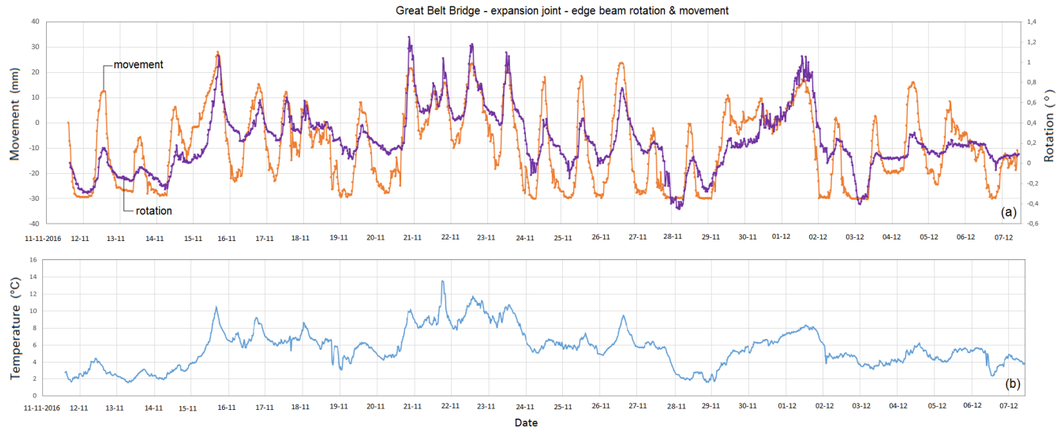

Figure 5: Movement and rotation of the edge beam acquired using DIC (a) and the corresponding temperature data (b)

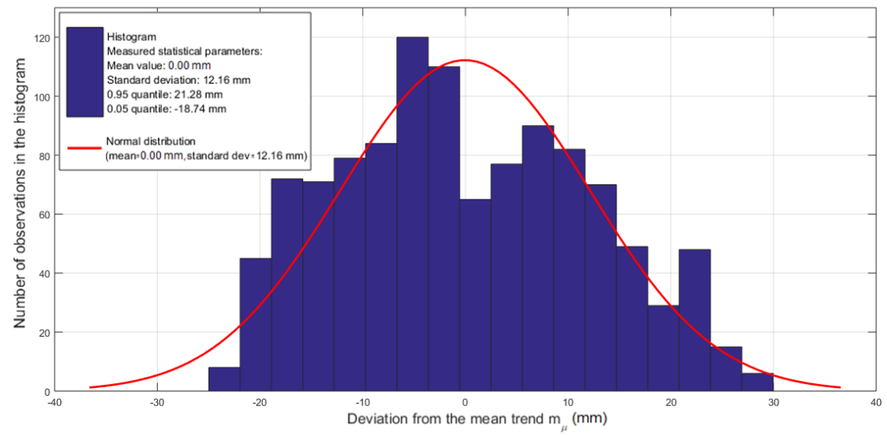

Figure 6: Analysis of the measured data offset in relation to m_μ *(t)*

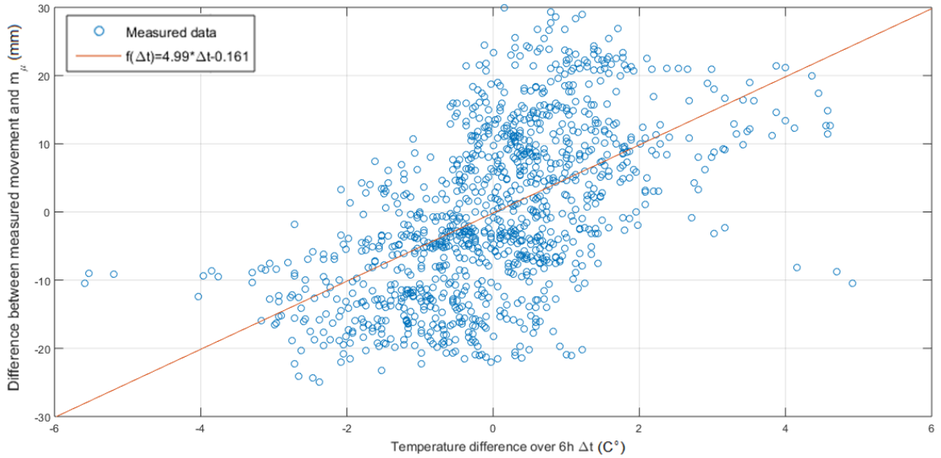

Figure 7: Correlation of temperature changes with the measured movement in relation to m_μ *(t)*

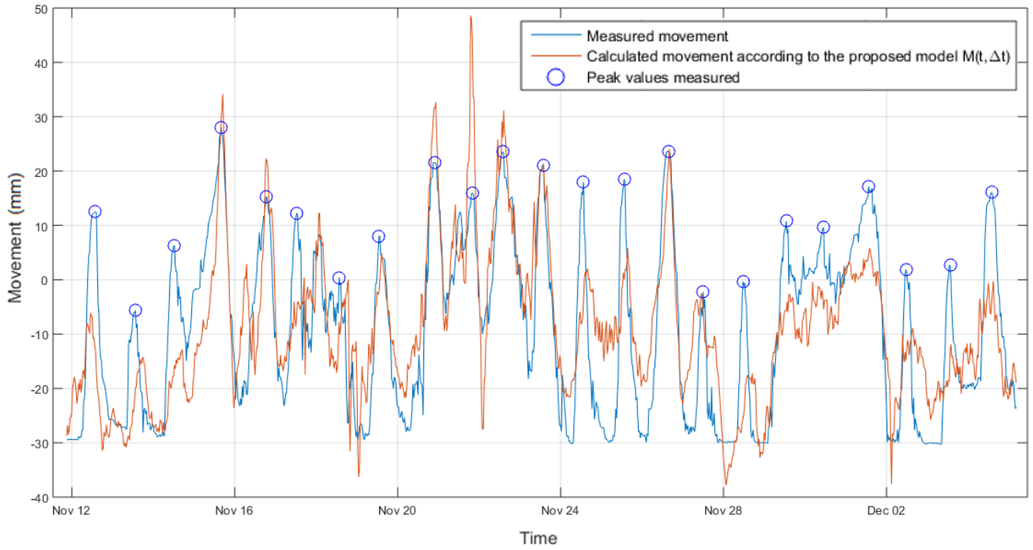

Figure 8: Proposed model $M(t,\Delta t_{6h})$ against measured data and peak movements

Figure 8 shows the proposed model $M(t,\Delta t_{6h})$ (plotted considering 95% confidence intervals) together with the monitoring data. The correlation between the model and the measured data is 77%. The daily peak movements were shown in Figure 8 and a stastitical analysis was performed. If an extreme value analysis is desired, the mean value of the daily extremes was estimated as 11.96 mm with the standard deviation of 9.29 mm. A Gumbel distribution (being independent of temperature) can be then assumed for modelling the daily peak movement.

6. Conclusion

In October 2016, Atkins was appointed by Sund & Bælt to provide long-term monitoring system to analyse the rotation and movement of the Great Belt Bridge expansion joint due to temperature change. DIC system was used as a cost effective data gathering tool providing information on movement and rotation of the expansion joint. The long-term DIC monitoring system was designed and set up within 2.5 weeks. The system was remotely controlled via LAN connection from the Atkins office. The monitoring project was delivered on time and on budget despite a very tight timeframe.

The outcome of the monitoring provided previously unavailable data, helped to better understand the behaviour of the expansion joint and informed next steps with respect to the maintenance strategy. The results of the monitoring showed good agreement between the data collected using DIC method and the temperature data received from the Danish Meteorological Institute. From the collected data a mathematical model was established, which relates the air temperature to deformations in the joint. Such a model forms basis for further probabilistic analysis and allows for real-time evaluation of monitoring data and for cost-efficient identification of problems in the functioning of the joint. To the authors knowledge this is one of the first applications of the DIC technology for long-term monitoring of a suspension bridge.

Awknowledgements

Originally published as: Winkler J, Hansen MD. Innovative Long-Term Monitoring of the Great Belt Bridge Expansion Joint Using Digital Image Correlation, Structural Engineering International, 2018 (28:3): 347-352, DOI:10.1080/10168664.2018.1461539

References

[1] Berfield, T. A., Patel, J.K., Shimmin, R.G., Braun, P.V., Lambros, J. and Sottos, N. R. 2007. Micro-and nanoscale deformation measurement of surface and internal planes via digital image correlation. Experimental Mechanics, 47 (1), 51-62.

[2] Jiang, R., Jauregui, D.V. and White, K.R. 2008. Close-range photogrammetry applications in bridge measurement: Literature review. Measurement, 41(8), 823-834.

[3] Jauregui, D.V., White, K.R., Woodward, P.E. and Leitch, K.R. 2003. Non contact photogrammetric measurement of vertical bridge deflection. J. Bridge Eng., 8(4), 212-222.

[4] Bales, F.B. 1985. Close-range photogrammetry for bridge measurement. Transportation Research Record, Washington, D.C., 950, 39-44.

[5] Li, J.C. & Yuan, 1988. B.Z. Using vision technique for bridge deformation detection, Proc., International Conference on Acoustic, Speech and Signal Processing, New York, 912-915.

[6] Johnson, G. W. 2001. Digital close-range photogrammetry - a portable measurement tool for public works. Proc., 2001 Coordinate Measurement Systems Committee Conf., Coordinate Measurement Systems Committee.

[7] De Roover, C., Vantomme, J. , Wastiels, J. and Taerwe, L. 2002. Deformation analysis of a modular connection system by digital image correlation. Experimental techniques, 26 (6), 37-40.

[8] Lee, J.J. & Shinozuka, M. 2006a. A vision-based system for remote sensing of bridge displacement. NDT&E Int., 39(5), 425–431.

[9] Lee, J.J. & Shinozuka, M. 2006b. Real-time displacement measurement of a flexible bridge using digital image processing techniques. Exp.Mech., 46(1), 105-114.

[10] Santini-Bell, E., Brogan, P., Lefebvre, P. Peddle, J., Brenner, B. and Sanayei, M. 2011.Digital Imaging for Bridge Deflection Measurement of a Steel Girder Composite Bridge. Transportation Research Board (TRB 90th Annual Meeting), Washington, D.C , USA.

[11] Chiang, C., Shih, M., Chen, W. and Yu, C. 2011. Displacement measurements of highway bridges using digital image correlation methods. Proc., SPIE – The International Society for Optical Engineering, 8321(1), 83211G-6.

[12] Yoneyama, S. & Ueda, H. 2009. Bridge Deflection Measurement Using Digital Image Correlation with Camera Movement Correction. Materials transactions, 53 (2), 285-290.

[13] Yoneyama, S., Kitagawa, A., Iwata, S., Tani, K. and Kikuta, H. 2007. Bridge deflection measurement using digital image correlation. Experimental techniques, 31(1), 34-40.

[14] Busca, G., Cigada, A., Mazzoleni, P., Zappa and Franzi, M. 2012. Cameras as displacement sensors to get the dynamic motion of a bridge: performance evaluation against traditional approaches. Proc., 6th International Conference on Bridge maintenance, Safety and Management (IABMAS 2012), Stresa, Italy.

[15] Kim, S. & Kim, N. 2013. Dynamic characteristics of suspension bridge hanger cables using digital image processing. NDT &E International, 59, 25-33.

[16] Sas, G., Blanksvärd, T., Enochsson, O., Täljsten, B. and Elfgren, L. 2012. Photographic strain monitoring during full-scale failure testing of Örnsköldsvik bridge. Structural Health Monitoring, 11(4), 489-498.

[17] Küntz, M., Jolin, M., Bastien, J., Perez, F. and Hild, F. 2006, Digital Image Correlation Analysis of Crack Behavior in a Reinforced Concrete Beam During a Load Test. Canadian Journal of Civil Engineering, 33(11), 1418-1425.

[18] Winkler, J., Fischer, G., and Georgakis, C.T. 2014, Measurement of local deformations in steel monostrands using digital image correlation. Journal of Bridge Engineering (ASCE), 19(10).

[19] Winkler, J., Georgakis, C.T., Fischer, G., Wood, S., and Ghannoum, W. 2015, Structural response of a multi-strand stay cable to cyclic bending load . Journal of Structural Engineering International 2/2015. (DOI: 10.2749/101686614X14043795570138).

[20] Winkler, J., Hendy, C., 2017, Improved Structural Health Monitoring of London's Docklands Light Railway Bridges Using Digital Image Correlation. Structural Engineering International, SEI 3/2017, DOI: 10.2749/sei.1353.

Asset Management and Condition Monitoring | 002

Brownfield and Beyond: Innovation is Needed to Develop Systems to Identify Problems Before They Occur

Carinne Plantin

Principal Process Engineer,
Oil & Gas,
Aberdeen, UK

Lisa Tayler

Senior Process Engineer,
Oil & Gas,
Aberdeen, UK

Peter Henderson

Process and Facilities
Team Lead,
Oil & Gas,
Aberdeen, UK

Abstract

Oil and gas operators face significant challenges to continue producing economically from their fields. Maintaining high standards of safety as well as production targets is key to successful operation but as assets age, more time and money is spent on firefighting repetitive issues.

When a problem occurs, there is a tendency to rush to an obvious solution, jump to conclusions or get after a quick fix. Unless the problem is properly understood, it is not possible to engineer the best solution and there is a risk that implementing the wrong solution leads to repetitive failures and an overall increase in maintenance costs for repair. This paper details the structured approach developed by Atkins, called design & operability review, which performs a robust, comprehensive root cause analysis and identifies the cause of, or contributory factors to, a problem. By adopting this rigorous approach, problems can be solved, action taken, and repeated failures avoided.

Problems typically become a priority issue to deal with once they have caused a production outage. Atkins look ahead is to prevent operations disruption by using advanced analysis tools to anticipate the problems.

Atkins' idea is to develop a Process Intelligent Engine which will use live data monitoring and perform analysis and calculations to provide a warning before a specified limit is breached.

Keywords

Design & Operability Review; Anticipate problems; Avoid repeated failures

1. Introduction

Oil and gas operators face significant challenges to continue producing economically from their fields. Maintaining high standards of safety as well as production targets is key to successful operation but as assets age, more time and money is spent on firefighting repetitive issues. The typical brownfield issues are illustrated in Figure 1.

There is a simple solution to prevent those repetitive failures which cause considerable loss in time and money as well as an increased safety risk: understand the root cause of the problem to identify the appropriate brownfield modification. This article proposes a rigorous method to perform the root cause analysis and presents an innovative solution to anticipate problems to avoid unwanted shutdowns.

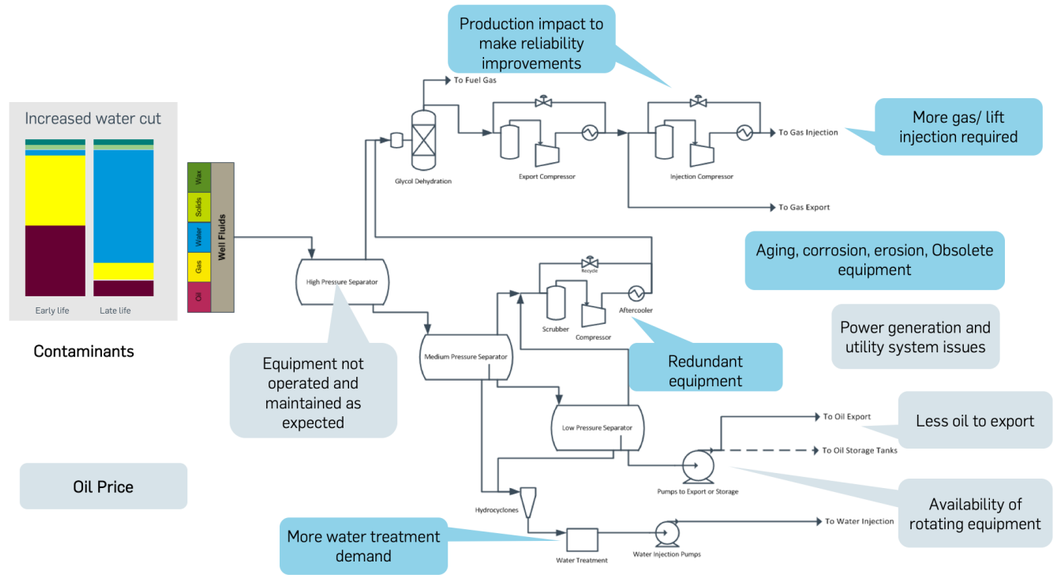

Figure 1: Typical brownfield challenges - Oil & Gas plant

Problem	Opportunity	Risk
Equipment failures/ breakdowns	New developments/ Tie-backs	Integrity risk
Capacity restriction	New wells/ production	Emission risk
Production/ performance issues	OPEX reduction	Personnel risk
	Rationalisation	Business risk
	Life Extension	

Table 1: Categories of brownfield challenges

2. What Challenges?

Brownfield challenges can be categorised into three sets of issues as illustrated in Table 1. Aging assets are expected to produce at the rates they were designed for, but over time, fluid properties, water cut, and contaminants change - leading to performance issues and capacity restrictions. Often, the original design intent for systems is not known or understood, and equipment is operated outside of the original operating envelope. In a low oil price environment, the pressure to reduce shutdown duration, maintenance spend, and manpower can lead to a focus on short-term problem solving of known risks rather than long-term future proofing of assets.

Opportunities to extend asset life exist in the form of developing new tie-backs and drilling new wells to replace declining production. New systems can be installed to improve reservoir performance, such as enhanced oil recovery systems, lift gas, and water injection. Operational costs can be reduced by rationalising redundant equipment. However, these opportunities rely on the existing processes and equipment continuing to run effectively and efficiently.

The status of the plant is crucial to planning for the future of the asset. Integrity issues can lead to loss of containment,

risk to personnel and releases to the environment. These are hazardous and costly, in terms of production losses, unplanned spend, and impact on reputation. Brownfield modifications are required to manage risks including asset integrity and equipment availability as well as taking opportunities to extend field life. It is important to define brownfield modifications carefully to select solutions that will provide the optimum balance between capital expenditure, operational costs, risk reduction and project benefits. This article will focus on front-end brownfield engineering, outlining a robust approach to problem solving, and utilising big data to pre-empt problems and reduce risk.

3. A Systematic Approach to Solving Problems

When a problem occurs, there is a tendency to rush to an obvious solution, jump to conclusions or get after a quick fix. Unless the problem is properly understood, it is not possible to engineer the best solution and there is a risk that implementing the wrong solution leads to repetitive failures and an overall increase in maintenance costs for repair. For example, it is not unusual for a corroded pipe to be replaced like-for-like without an assessment as to what may have changed in the system to cause or exacerbate the corrosion.

At Atkins we have devised a systematic approach, called a design & operability review, which performs a robust, comprehensive root cause analysis and identifies the cause of, or contributory factors to, a problem.

- Has the system been designed adequately?
- Is the system being operated as per design intent?

The review targets all parts of the system: fluids inside equipment/pipes; the equipment itself and environmental and external factors.

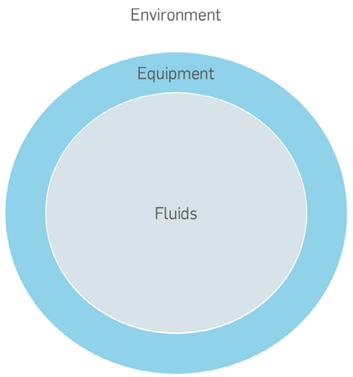

Figure 3: System boundaries

The rigorous approach uses a pre-set table (Figure 4) containing key words that are considered or ruled out as a cause of the problem.

We have devised a systematic approach, called a design and operability review, which performs a robust, comprehensive root cause analysis and identifies the cause of, or contributory factors to, a problem.

The design review is based on available design information and industry standards, guidelines and practices. Insights from operator's experience or examination of similar systems elsewhere can be invaluable.

The operability review is based on plant data to determine actual fluid properties and mode of operation. The objective is to determine if the plant is operated as per design intent and if not, if the changes could explain the problems. All modes of operations, including start-up and shutdown, are considered. A process simulation can be used to reflect actual operating mode and determine capacity limitations, such as separator gas-liquid separation performance, line hydraulic constraints, pipe vibration, and exchanger fouling.

Logs, maintenance reports, and inspection queries (IQs) are analysed to determine the frequency of failures and gain feedback from previous assessments. Engaging the operations team is key to ensuring the current mode of operation is understood.

This rigorous approach using pre-defined key words has the advantage of screening out a range of issues while reducing the risk of missing a potential root cause. The approach can be applied to all types of problems before solutions are considered. Ensuring that the root cause is identified upfront allows the optimum solution to be implemented. The assessment provides a better understanding of the system so that benefits or risk reduction achieved by a potential brownfield modification can be quantified, and additional risks or constraints identified.

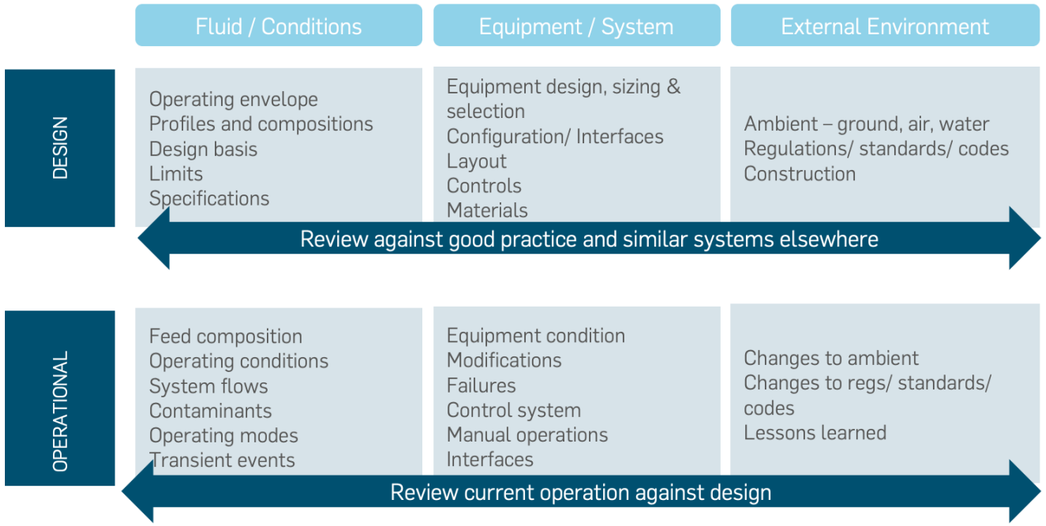

Figure 4: Design and operability review check list

3.1. Example Case: Exchanger Failure

The following example demonstrates the benefits of using the design and operability review on an exchanger failure, in this case a tube bundle failure of an oil heater (see Figure 5). The exchanger is crucial to operation, to lower the viscosity of the oil and allow the oil to be pumped to the downstream system. A high oil viscosity leads to increased pressure losses in the lines and potential blockage of the downstream system. The exchanger is a shell-and-tube type with oil on the shell side and heating medium on the tube side.

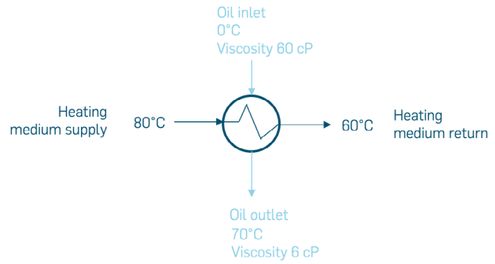

Figure 5: Oil heater

The operations team has experienced regular external tube failures due to corrosion and had to regularly replace the tube bundle. The cause of corrosion was not properly understood, and after each failure the tube bundle was replaced like-for-like. The tube bundle has failed repeatedly and incurred significant repair costs.

The design and operability review of the system has found the root cause of the corrosion. Each part of the system was reviewed using the pre-defined keywords. The contributory factors to the corrosion and subsequent tube failure has been highlighted as shown in Figure 6.

The review demonstrated that corrosion was caused by multiple factors. The exchanger design was such that stagnant zones were created inside the shell, leading to accumulation of water pockets despite the low water content in the oil. The operating enveloped differed from original design, with less oil being processed through the exchanger, leading to low velocities in the shell, which also contributed to creating the stagnant zones. The actual controls on the heating medium were such that the desired temperature was not met, leading to colder oil in the exchanger and formation of corrosive deposits. The exchanger was operated in batch mode and left for long periods, also contributing to stagnant zones and formation of corrosive deposits.

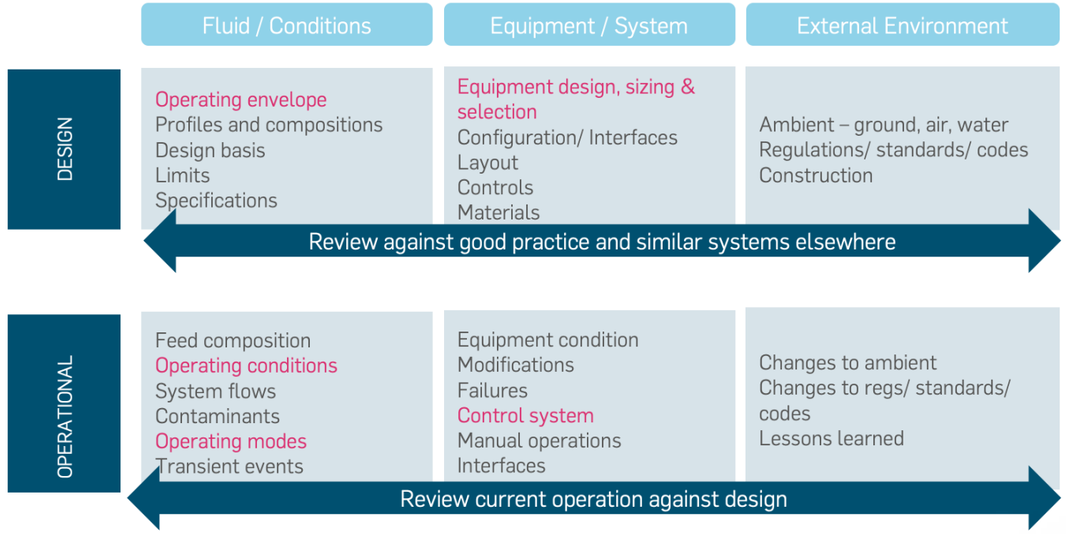

Figure 6: Application of design and operability review on an oil heater failure

Following the design and operability review, several targeted options were proposed to the reduce risk of stagnant zones and cold temperatures in the exchanger. Short-term operational modifications as well as long-term physical upgrades were proposed.

4. Looking Ahead: The Process Intelligent Engine

In our experience, brownfield modifications tend to be implemented to solve a problem that has already occurred and has caused an unplanned shutdown. It's currently difficult for operators to pre-empt problems due to the complexity of parameters involved. The business loss associated with unplanned shutdowns could be prevented if operators are made aware of the actual system limits.

We believe that this is feasible by developing and using an innovative system which makes an effective use of available data. This new system is a completely novel approach to brownfield engineering that would reduce the amount of safety and environmental incidents and improve facilities' uptime.

Our system requires a new specific analysis tool to be developed. This new tool would monitor complex systems where a combination of factors coincide to create a problem, such that issues can be identified before they affect production or compromise safety. As shown in Figure 7, our new analysis tool would be linked to the existing data historian to extract relevant data which will be computed into the new Process Intelligent Engine to perform calculations required for the analysis. The tool would then provide a user-friendly output that can be viewed by operators to show the trend of a specific parameter and warn of an impending problem.

Key to the success of designing and implementing the Process Intelligent Engine is to use a collaborative approach with constant client involvement. This new tool needs to be developed by a specialised team with necessary expertise in developing prediction and optimisation algorithms and calculations. Input from client technical experts and target end users will also help understanding the issues and requirements and provide suitable, reliable solutions that add real value to operations.

Results, predictions and suggested actions generated by the new tool would be viewed in a way suitable to the target end users. For onshore field engineers, a graphical user interface within the tool would show the relevant information, allowing them to review the results and decide what actions to implement for adjusting and optimising production. To avoid operator overload, the tool could be set up to only publish key data or an overall status, enabling them to choose the best time to review the actions identified by the tool without disrupting their activities.

Our idea is that the tool would use existing data by being connected to the existing production historian for extracting relevant data and publishing key metrics and results. This link would be securely established to ensure the overall security of the historian is not affected. A configuration with a data access layer, managing the interaction with the historian via a known channel would allow the component to be hosted in a secure environment. The Process Intelligent Engine would use this component to obtain the data required for analysis and optimisation.

We have the in-house capabilities to develop this tool and can develop a Process Intelligent Engine fit-for-purpose to answer specific issues.

4.1. Example of Benefits Using the Process Intelligent Engine

As this system has not yet been implemented in practice, let's look at a theoretical example of how it would work. The example shown in Figure 8 considers monitoring of a gas dehydration unit composed of molecular sieve beds. The molecular sieves are used to reach a very low water specification in the gas (less than 1 ppmv) as water may cause corrosion or hydrate issues in downstream systems, or form ice in cryogenic processes that could cause an unplanned shutdown. Once the molecular sieves are fully saturated with water, water will break through in the downstream system with large amount of water being carried over very quickly. It is therefore crucial to remain within the molecular sieves' capacity.

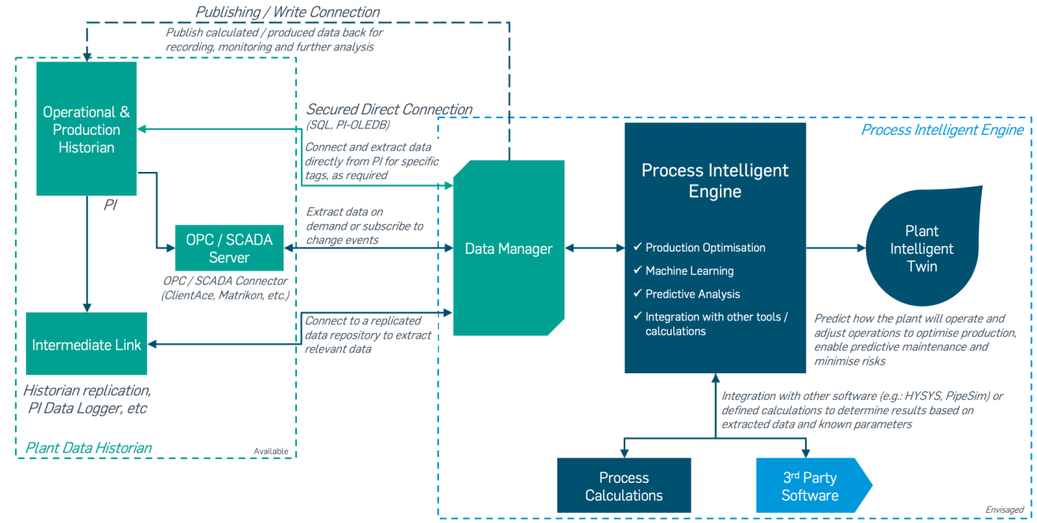

Figure 7: Plant live data integration

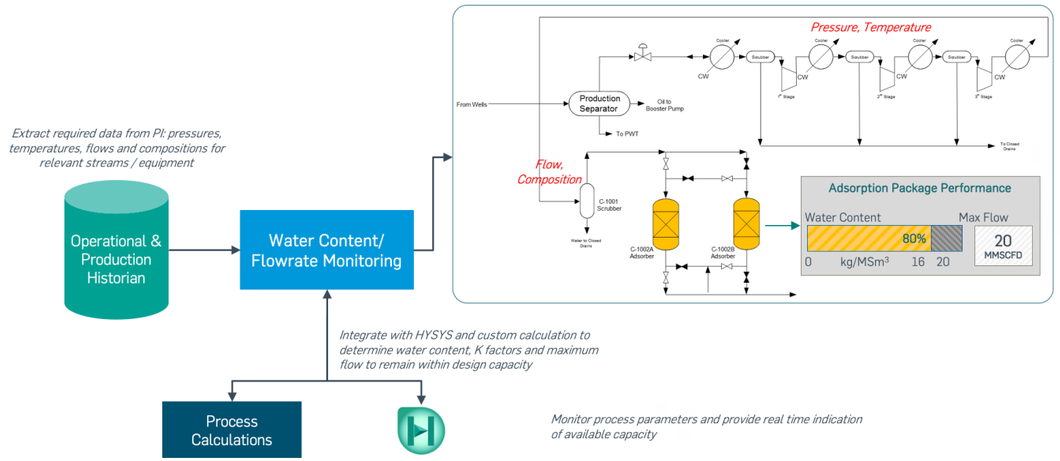

Figure 8: Capacity monitoring example

Determining the utilisation of the molecular sieves is not straight forward, it depends on a variety of factors. The water content in the gas feeding the dehydration unit may vary due to fluctuations in the actual operating conditions, change of feedstock composition over field life, change of operating mode or following upgrades done elsewhere on the platform. The water content calculation can be performed in the Process Intelligent Engine, that will take input data from the operational & production historian. Typical input data are gas composition (taken upstream of the dehydration unit), pressure and temperature. The Process Intelligent Engine could be linked to process simulation software to determine the water content of the gas at the molecular sieves bed inlet. The utilisation of the bed would be calculated using the water content of the feed gas, duration of the adsorption cycle, beds dimension, molecular sieve performance (kg of water adsorbed per volume of bed), and hydraulics within the bed.

The output is a simple percentage of utilisation of the molecular sieves which will help the operations team to visualise the actual molecular sieves utilisation for the actual operating conditions. As such, water breakthrough could be prevented by ensuring operation is always maintained well below molecular sieves capacity.

5. Conclusion

In brownfield engineering, considerable time and money is spent on repairs to failed or inefficient items. When a problem happens, there is a tendency to draw conclusions quickly without identifying the real cause of a problem. By adopting a rigorous approach, problems can be solved, action taken, and repeated failures avoided. Performing a design and operability review of the system ensures that the root causes are identified and the right solution is put in place.

Problems become a priority issue to deal with once they have caused a production outage. Advanced analysis tools could help prevent operations disruption by anticipating the problems.

By using live data monitoring and performing analysis and calculations in a Process Intelligent Engine, a warning could be provided before a specified limit is breached. Anticipating problems will avoid unplanned shutdowns and costly interventions as well as reducing associated safety and environment risks.

There is a real value to stop and think before rushing to a solution. This will ultimately save time, money, prevent unwanted production outage and reduce risks of repetitive failures.

Acknowledgements

Originally published in: Plantin C, Tayler L, Henderson P. Brownfield and Beyond: Innovation is needed to develop systems to identify problems before they occur. The Chemical Engineer, 2018 Jun; 924: 36-41.

Railway Embankment Stabilisation: Economical Asset Management

Simon J Holt

C Geol FGS CSci CEng
Principal Engineering Geologist
Engineering, Design and Project Management
Croydon, UK

Isaac W Griffiths

CEng MICE
Senior Geotechnical Engineer
Engineering, Design and Project Management
Croydon, UK

Ian Payne

CEng MICE CIHT
Senior Asset Engineer (Geotechnics)
Network Rail
London, UK

Abstract

Ashdon Way railway embankment in Basildon, Essex is an 8m high, 500m long embankment founding on the London Clay Formation and comprising predominantly of reworked London Clay fill. The embankment has a history of slope instability problems which have led to continued regular track maintenance requirements and associated imposition of temporary speed restrictions. This paper discusses how detailed slope monitoring, track performance data and site investigation were used to target and value engineer slope stabilisation measures at the site using soil nails and/or cess retention, making £5.8M savings compared to a traditional sheet piled wall solution. The slope monitoring was undertaken by borehole inclinometers (including automated inclinometers) which allowed detailed interrogation of slope movement before, during and after construction. A progressive failure mechanism was identified from the monitoring data. The slope monitoring allowed post construction assessments of the success of the scheme and management of the residual risk for adjacent untreated areas.

Keywords

Slopes – Stabilisation; Geotechnical Engineering; Railway Tracks

1. Introduction

The Anglia Route Collaboration (ARC) comprising Network Rail, Volker Fitzpatrick and Atkins was part of a framework to address the highest priority earthworks instability in the five-year Network Rail funding cycle Control Period 5 (CP5). The majority of the 1091km of earthworks in Anglia that needed most urgent attention were embankments, typically with over steep slopes and generally underlain by the London Clay Formation with Alluvium and glacial deposits occasionally the founding stratum. Network Rail has a responsibility to prioritise sites based on passenger safety and passenger disruption through temporary speed restrictions or line closures. Sites causing passenger disruptions are commonly addressed through near surface maintenance interventions but occasionally the problem lies within or beneath the embankment and site investigation and geotechnical specialist support is required to determine and optimise the necessary engineering intervention. Current asset management strategies are well summarised in the Network Rail Earthworks Asset Policy (2016) and by Glendinning et al. (2009) along with the challenges faced by infrastructure managers holding limited budgets and high requirements for user experience.

Early mitigation works in CP5 adopted full fix 120-year design life solutions such as sheet piled walls on embankment renewal sites that had limited monitoring data but needed urgent intervention. As CP5 evolved, the renewal portfolio undertaken on the ARC Contract framework was subject to budget constraints that meant a need to move towards more innovative risk based and focused mitigation to release funding to maximise the volume of improvements delivered across the wider region (Network Rail, 2016).

Ashdon Way embankment in Basildon, Essex was one of the highest priority sites with slope instability on the north side leading to periodic temporary speed restrictions that were needed prior to remedial works construction in Year 2 of CP5. This embankment for the busy Southend to London commuter railway is approximately 500m long and 8m high, surrounded by flat ground and is located approximately 150m west of Basildon Railway Station (Figure 1). This paper will aim to demonstrate through risk assessment, site investigation and detailed interrogation of slope monitoring trends, how more cost-effective targeted mitigation was possible at Ashdon Way and how residual risks were controlled.

The over-steep unengineered London Clay embankment slope at the site has led to high magnitudes and rates of slope movements. Progressive embankment failure trends will be explored in this paper together with a discussion of how the mitigation solutions were selected. The importance of automated monitoring during construction and how ultimately the success of the works was measured from post-construction monitoring will be discussed. Untreated areas of the site are subject to continued observational monitoring and their ongoing movement trends and possible future emergency works strategies are presented.

2. Failure of Rail Embankments

Assessing the causes of embankment instability can be challenging as the rail network has many embankments with similar characteristics (slope angle, height, fill composition, method of construction etc) but with very different performance and behaviour (O'Brien, 2013). Briggs et al. (2017) summarised three common rail embankment failure mechanisms; pore water pressure increase, seasonal shrink swell and progressive embankment failure. These failure mechanisms can be inter-related and can act together or in sequence.

Rail embankments are vulnerable to rainfall induced pore water pressure increases due to the high permeability of track ballast covering the embankment crest. It has been reported that five times as many rail delay incidents from geotechnical causes occur in winter months compared to summer months and this can be attributed to rainfall induced pore water pressure increases (Briggs et al., 2017).

Vegetation cover on embankment slopes can complicate embankment pore water pressures as vegetation cover can reduce infiltration, increase evapotranspiration and lead to seasonal pore water pressure variations. Seasonal deformation in embankment slopes has been linked to soil

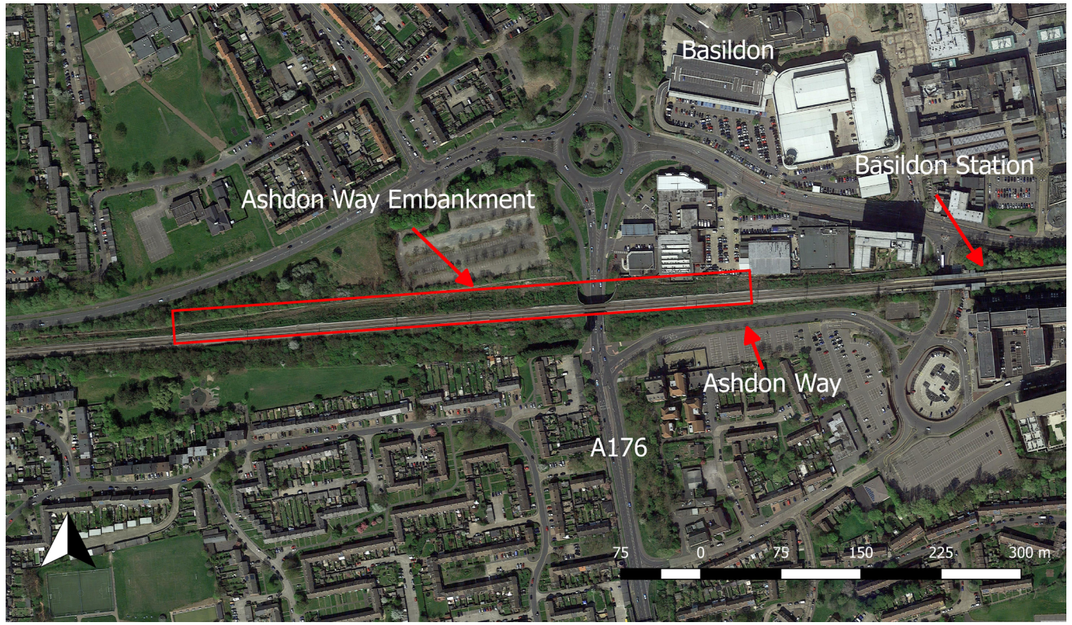

Figure 1: Site Location Plan © 2018 Google Map data

water content through soil moisture deficit calculations. Winter heave is observed during periods of low soil moisture deficit and summer settlement occurs during periods of high soil moisture deficit (Briggs et al., 2017). Prolonged periods of dry weather in Anglia results in significant localised temporary speed restrictions at the end of the summer.

The removal of high water demand trees from embankment slopes reduces the magnitude of seasonal pore water pressure changes but also leads to a reduction of deep seated suctions which can cause slope failure (Smethurst et al., 2015). Seasonal pore water changes have also been observed on less heavily vegetated slopes. Smethurst et al. (2006) observed summer soil moisture deficits on a grass covered cut slope in London Clay but soil suctions returned to zero in winter indicating that grass does not have a stabilising effect during winter. Elevated winter pore water pressures have also been observed in heavily vegetated slopes (Ridley et al., 2004).

Progressive failure of slopes was first reported by Karl Terzaghi (Terzaghi, 1947). Progressive failure can occur under non-uniform loading of a slope; part of the slope mass begins to fail and then failure develops along a rupture surface. As shear strain increases past peak along the rupture surface, the soil strength will begin to reduce towards a residual strength; soil strength will be non-uniform and strain dependant along the length of the rupture surface and at failure all of the failure surface will have been fully formed. Seasonal shrink swell of railway embankments can also lead to progressive failure mechanisms developing. A number of previous studies have undertaken detailed finite element analyses of the progressive failure of slopes, most notably Potts et al. (1990) accurately modelled the failure of Carsington embankment dam which failed progressively due to the development of high strains in the "boot" area of the dam. Potts et al. (1997) were also able to reproduce observed progressive failures in railway cutting slopes in clay using finite element analysis. There is a shortage of case studies from literature of well instrumented real time monitoring of slopes undergoing progressive failure (Briggs et al., 2017).

This case study will build on this past work by presenting detailed field monitoring records of a railway embankment that experienced the above failure mechanisms and actions undertaken to stabilise the failure.

Figure 2A: Cross Section view of the embankment showing the worst area of poor track condition and leaning overhead line. The photograph was taken in summer 2015 and shows the site after removal of large trees with some grow back of grass and small bushes evident.

Figure 2B: Evidence of toe bulge which has displaced troughing housing a HV Cable at the embankment toe. The age of the bulge is not known but it is believed to be relatively recent and associated with the current track problems.

3. Historical Instability Problems

The site has a history of instability problems with loss of line and level of the track (Figure 2A) and continued regular track maintenance requirements including re-ballasting. This resulted in thick ballast, a locally distorted troughing route and a steep ballast shoulder that spills out onto the crest of the embankment slope. Additional ballast and regular track lifting have created additional load on the embankment. Evidence of significant toe bulging including the buckling of troughing supporting a High Voltage electricity cable route at the toe (Figure 2B) was identified in one area indicating more recent rather than historic slope movements shortly after construction. Ultimately the associated track problems resulted in a temporary speed restriction periodically being put in place at this part of the site. Access to maintenance records together with discussions with the maintainer highlighted the key areas of concern over time. Such findings were also backed up by the digital technology tool Linear Asset Decision Support (LADS) which provided key earthwork assessment information principally on track rail deflections, frequency of maintenance interventions and Ground Penetrating Radar derived trackbed performance. The LADS data for the site between 2011 and 2014 indicated the occurrence of track twist faults at 23ml 68ch and the deterioration of the track condition and potential for the development of further twist faults (Figure 3). A high number of maintenance activities around 23ml 68ch were also evident.

No historic ground investigation (GI) and slope monitoring data was available for the site and the geotechnical desk study for the project recommended inclinometer boreholes typically at the crest, midslope and toe in the worst affected areas (Atkins, 2014). While no ground profile or slope monitoring data was available initially, it was apparent from geomorphological observations that the track problems were related to a more global earthworks problem. Prior to GI and slope monitoring at the Approval in Principle Form 001 stage (Atkins, 2015a), a robust solution was initially proposed to mitigate the whole site with a 500m long toe sheet pile wall and slope regrade; the cost of such a solution was subsequently considered to be uneconomical.

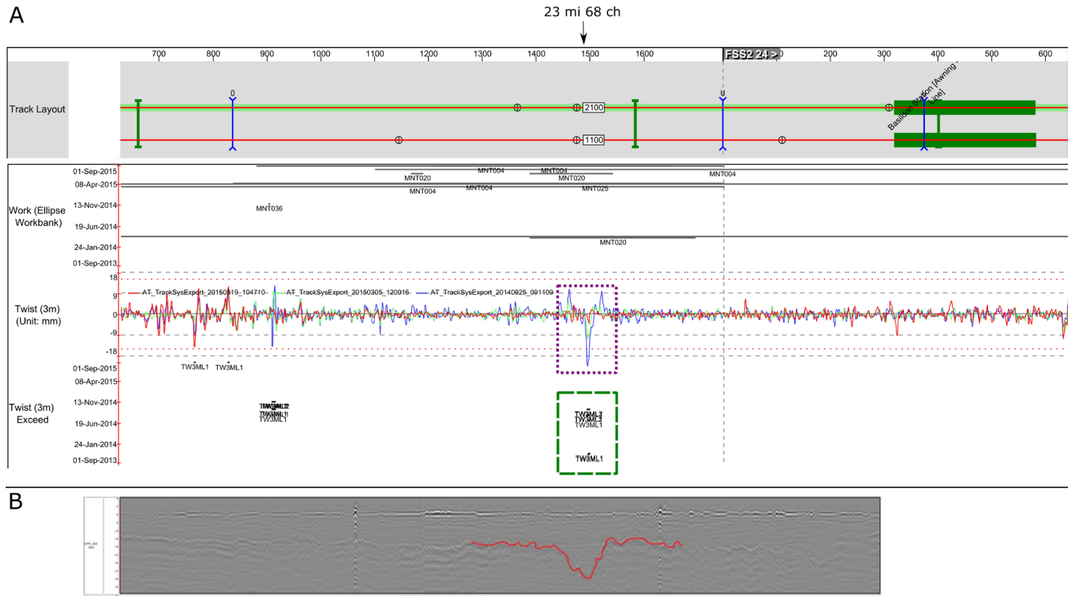

Figure 3: NR Linear Asset Decision Support (LADS) data for the site. The full LADS system provides a large number of data fields for interrogation. The figure presents (from top to bottom) Track Layout, Maintenance Workbank, Track Twist, Twist (3m) Exceedance and Ground Penetrating Radar (GPR) 400MHz. Twist exceedances (twists faults) can clearly be seen at 23ml 68ch (dashed highlight) and the development of a further twist faults can be seen at the same location (dotted highlight). A clear trough in the track formation can be seen in the GPR plot. A high concentration of workbank maintenance activities can also be seen concentrated in this area; the LADS system is interactive and allows full details of these activities to be viewed.

4. Ground Conditions and Geotechnical Properties

The key to being able to refine the mitigation options and extent was to establish a more detailed ground model at a few sections through the site using GI (GEL (Geotechnical Engineering Ltd), 2014 and Topdrill Ltd, 2015) combined with detailed topographical survey, geomorphological observations, LADS data and interpretation of slope monitoring data. Initially two key sections at 23m 68ch and 24m 04ch were targeted for assessing ground conditions and slope movements and the key section at 23m 68ch is shown in Figure 4A and 4B.

The ground conditions are relatively consistent across the whole site area with Made Ground (embankment fill) overlying the London Clay Formation. The embankment fill was predominately cohesive (reworked London Clay). It was described as a very soft to firm clay with high to very high plasticity containing small quantities of sand and gravel throughout. The upper 1m below track ballast was generally more granular comprising loose slightly silty, gravelly sand and ash. Reworked structureless chalk fill made up a proportion of the Made Ground and was identified in small localised areas. During the construction works, parts of the lower embankment slope were exposed with the chalk fill appearing to be forming regular spaced counterfort drains which may have been historical drainage and/or strengthening measures. Similar chalk filled drains were also found by Smethurst et al. (2015) in a London Clay embankment at Hawkwell, Southend.

The embankment fill consistently showed an increase in strength with depth but typically comprised soft to firm clays with occasional near surface ash and sand. Standard Penetration Test (SPT) N values were typically recorded

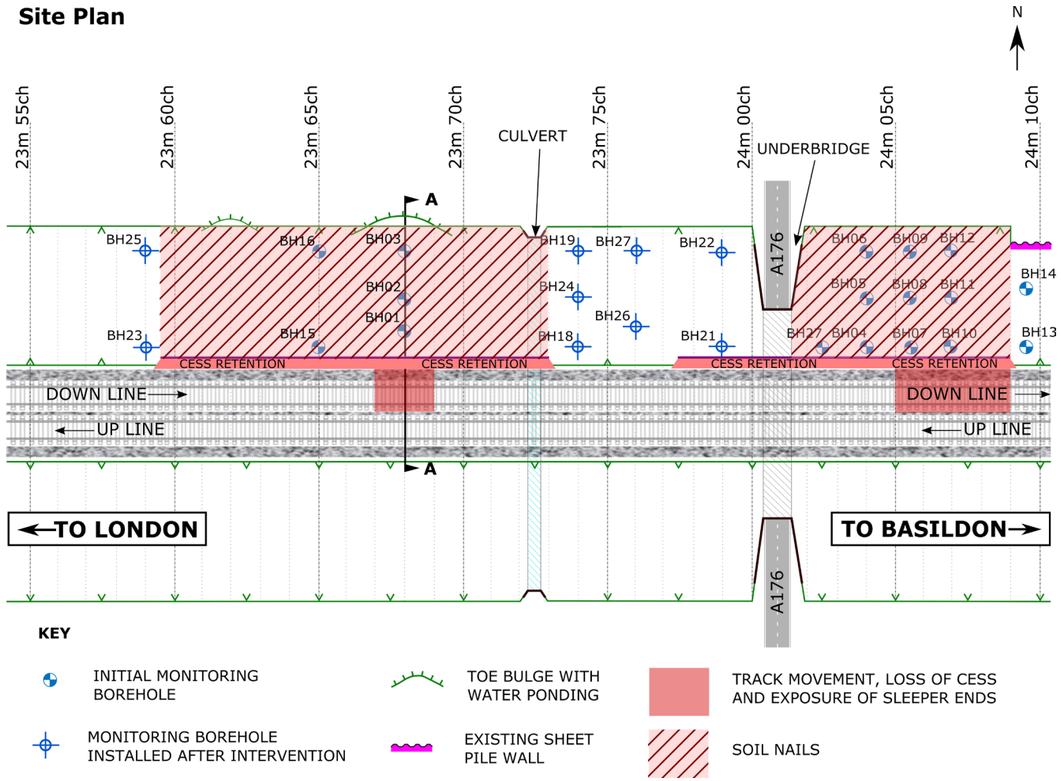

Figure 4A: Plan showing failure zones pre-intervention

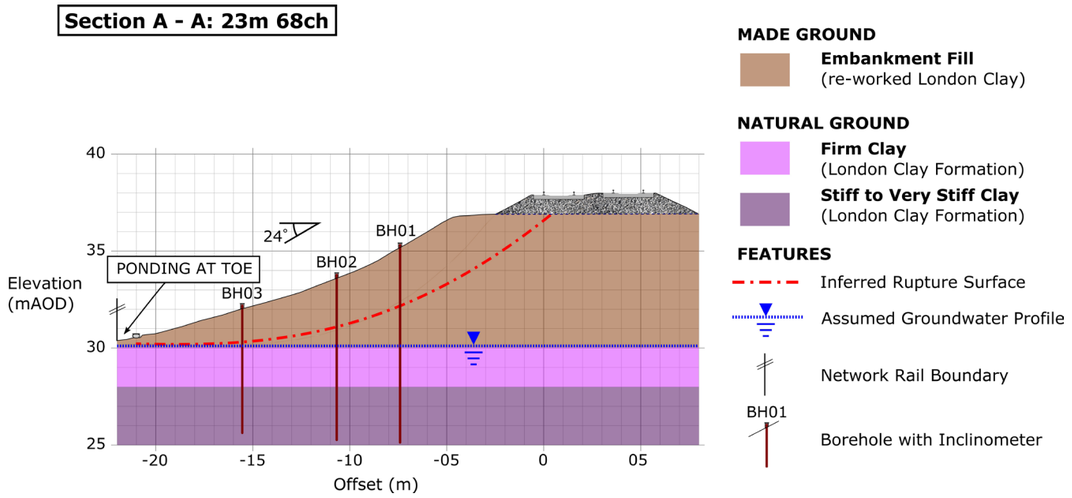

Figure 4B: Cross Section showing failure zone pre-intervention (23ml 68ch)

between 5 and 15. It was apparent that the embankment fill had a lower strength at the 23m 68ch section with SPT N values as low as 3 in very soft clay close to the toe.

The interface between the Made Ground and underlying London Clay was typically encountered at the base of the embankment as shown in Figure 4B. The London Clay Formation was described as firm to stiff (locally very stiff) sandy clay with high to very high plasticity. The London Clay was weathered brown and typically sandier in the upper 10m showing an increase in undrained strength with depth to more unweathered fissured grey clays. The inclinometers were installed into stiff to very stiff London Clay at depths of 6 to 10mbgl (depending on embankment height). Slope climbing rigs were used to complete the GI, allowing good descriptions from recovered windowless sample liners, Standard Penetration Tests and inclinometer installations. Undisturbed samples were not possible to determine undrained shear strength parameters and so laboratory testing was limited to classification and chemical testing.

The Atterberg Limit Tests carried out on reworked London Clay fill and the underlying natural London Clay showed relatively consistent results with liquid limit typically ranging from 70-80% and Plasticity Index (PI) typically ranging from 40-60%. Natural moisture content was typically 25-30%. Consequently, such soils have a high shrink swell potential according to BRE (1993) Digest 240 and this is discussed further in relation to the potential effects of devegetation and slope movements related to seasonal moisture variations.

Groundwater was not encountered during the GI but small areas of ponding in the area around the embankment toe close to 23m 68ch were observed on the geomorphological walkover survey. It was apparent that the moisture content within the embankment fill and underlying London Clay generally decreases with depth. There appears to be greater softening that has occurred at the toe around 23m 68ch and this may be related to the observed localised ponding. No active surface drainage was present at the site and the culvert at 23m 78ch was partially blocked. Historical maps indicated that a stream previously passed under the railway embankment at this location, however with the development of housing around the site this stream has become covered and no significant evidence of it could be seen further away from the embankment.

5. Failure Trends

Given the critical nature of the site and the need to intervene, only limited slope monitoring data was available prior to detailed design. Despite this, failure trends were apparent early on and the embankment slope at 23m 68ch showed evidence of active failure. Figure 5 shows the movement rates were around 60mm over 263 days and this rate of movement was relatively consistent in all three inclinometers. Given the rate of failure, after several months of manual monitoring, Network Rail installed automated instruments at this section to provide real time slope monitoring (Figure 6) so that an emergency situation could be identified quickly when trigger values were reached to allow further mitigations such as speed restrictions and even line closure to be put in place. The automated

instrument array used three C12-SIPI Smart In-Place Inclinometers supplied by Soil Instruments Limited, Uckfield, UK) with single instruments positioned at embankment toe, midslope and crest, with an additional crest camera and infra-red light camera used to view the site condition. Monitoring information was collected on a data logger and uploaded to an ftp site via GPRS modem before being extracted onto an online visualisation site.

The ground model at 23m 68ch showed the least favourable movement conditions. Other sections including 24m 04ch and 05ch generally showed slower rates of movement although evidence of progressive failure trends was apparent (see Figure 7). Over the same monitoring period prior to mitigation (263 days), at 24ml 05ch movement of 49mm was recorded at the toe, gradually decreasing in the midslope to 24mm with the lowest movements of 9mm at the crest as shown in Figure 7. While such movements were less critical, it was postulated that they may be showing early signs of failure that ultimately could lead to the level of movement evident at 23m 68ch. Progressive failure may not be the only failure mechanism present at the site. As summarised in Section 2, shrink swell, pore pressure increases and progressive failure mechanisms can often be interlinked. A large proportion of the embankment slope was historically covered by large mature trees which were removed prior to 2014 to allow more detailed investigation of the slope. It is likely that the mature trees were causing seasonal movement of the embankment given the high shrink swell potential as has been observed at other similar London Clay embankments nearby on the network. Seasonal shrink swell could have initiated progressive failure at the site and the removal of the mature trees would have reduced soil suction. Any instability problems may

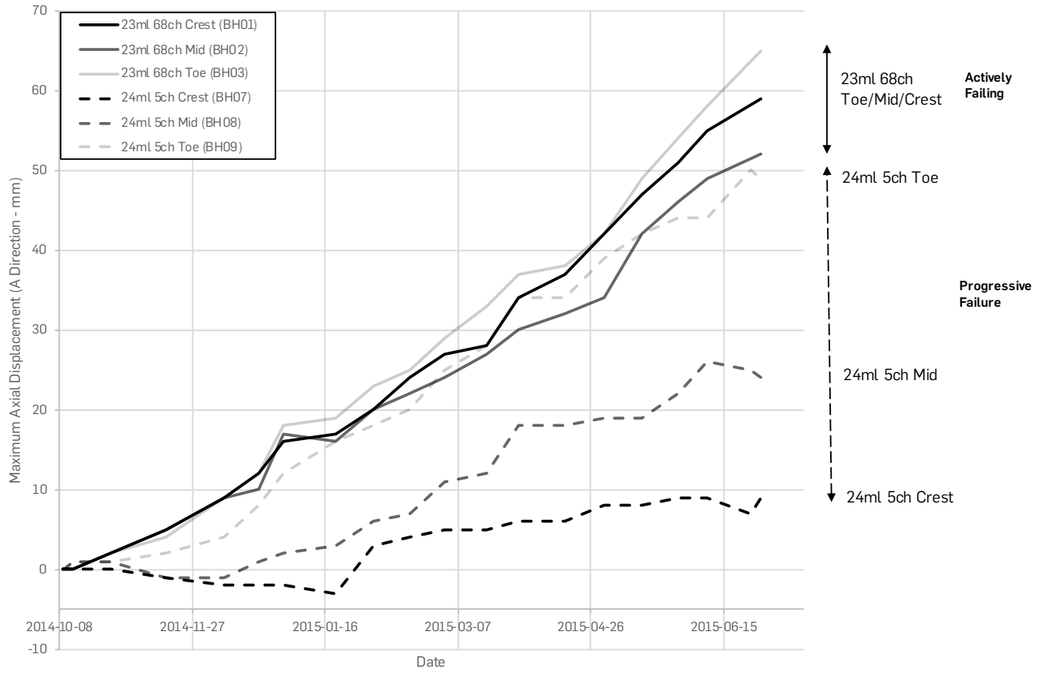

Figure 5: Mechanisms of slope movement at Ashdon Way Embankment. The plot shows maximum downslope inclinometer displacement at toe, midslope and crest at two locations of the site: 23ml 68ch and 24ml 5ch. At 23ml 68ch the slope appears to be in a state of "active" failure as the rate of slope displacement is similar and relatively high at slope toe, midslope and crest. At 24ml 5ch the slope displacement shows possible signs of progressive failure as the rate of movement is significantly higher at the toe than at midslope or crest, this suggests that a progressive failure mechanism could be developing and it is postulated that over time as failure progresses the mechanism could trend to an "active" failure as shown at 23ml 68ch.

Table 1: Geotechnical Design Parameters

Geological Formation	Thickness (m)	Unit Weight (kN/m^3)	Effective Angle of Internal Friction (degrees)	Effective Cohesion (kPa)
Ballast	0.40 to 1.30	18	35	-
Made Ground	0.70 to 5.85	18	22	1
Residual Strength Made Ground	Along failure plane	18	13	1
London Clay Formation	25+ (unproven)	19.5	23	2

have been exacerbated by the presence of the partial blockage to the culvert outfall contributing to elevating pore water pressures at the embankment. It is likely that these elements were related and have all contributed to the observed instability issues.

The inclinometer displacement data is plotted against daily precipitation readings in Figure 6. The precipitation data was taken from Writtle weather station and is considered to provide a reasonable record of precipitation at the site (Met Office, 2016). Prior to construction work, the rate of displacement recorded in all three boreholes at 23m 68ch was relatively constant. However, the rate of movement appeared to slow following heavy rainfall. A higher level of rainfall was recorded on 24th July 2015 and this was followed by 3 to 4 days of lower than average slope movement. The maximum movement prior to the rainfall event was typically 0.6 to 0.8mm/day but in the 4 days following the 24th July the maximum rate of movement was typically 0.2 to 0.4mm/day. The reason for this apparent decrease in the rate of movement is not known as typically high rates of rainfall are associated with an increased incidence of slope failures; for example, Briggs et al. (2013) demonstrate this indirectly by linking long periods of zero Soil Moisture Deficit to slope failures. There is also usually a lag betweeen a rainfall event and increased rates of movement but this was not apparent with such high rates of movement already being recorded prior to a rainfall event. This observed behaviour could warrant further study.

6. Risk Management and Optioneering

Whilst three of the four instrumentation sections showed signs of progressive failure at different stages, the actively failing area of the slope with consistently high movements was limited to close to the toe bulge section at 23ml 68ch. In addition to assessing ground conditions, walkover observations and monitoring data, a detailed interrogation of maintenance records and Linear Asset Decision Support (LADS) track monitoring data was undertaken. The site was subdivided into low, medium and high-risk areas against a set of failure criteria with the view that the higher risk and some of the medium risk areas only would be mitigated initially. Remaining areas were subject to further monitoring through existing and additional instrumentation set out by a future works strategy which is discussed later.

Various mitigation solutions were possible, and having considered budget restrictions, access, boundary constraints, the need to demonstrate sustainability and the HV cable at the toe, a solution comprising soil nails with a 60-year design life to satisfy global stability was selected and a typical cross section is shown on Figure 8. A king post cess retention system using Grundomat piles was also more widely used to provide local stability for the trackbed and enable reconstruction of a compliant cess area which accommodates the lineside infrastructure as shown on Figure 8. The optioneering process was accelerated by collaborative workshops by all framework partners. Solutions and various intervention extents were priced to balance risk and cost, taking due account of public safety. The selected extent of the mitigation and further observation locations were reported in the F002 Statement of Design Intent (Atkins, 2015b) and are shown in Figure 4. The budget savings were significant at approximately £5.8M compared with the sheet pile wall option, in line with the Earthworks Asset Policy (Network Rail, 2016) allowing release of funding for other critical earthwork sites. Whole life costs were taken into consideration and although future works may be required at the site, these were projected to still be well below the cost of a robust low maintenance sheet pile wall solution.

7. Stabilisation Design

Geotechnical analysis for the remediation works was undertaken in accordance with BS EN 1997-1:2004 (Eurocode 7) Geotechnical Design (including the National Annex) (BSI, 2007 and 2010a), Network Rail Geotechnical Design NR/L3/CIV/071 (Network Rail, 2011) and BS8006-1:2010 Code of practice for strengthened/reinforced soils and other fills (BSI, 2010b). The design life of the stabilisation measures was in line with the requirements of NR/L3/CIV/071 and a minimum 60-year design working life was specified. The values for rail traffic loading were taken from BS EN 1991-2 (BSI, 2010c). Allowance for a maintenance load was made in the permanent case and temporary construction loading was also applied. Geotechnical design parameters were derived from the GI information, published literature and back analysis of the failing slope (see Table 1). Multiple limit equilibrium stability analyses were undertaken to obtain a failure surface that corresponded well to the failure observed in the inclinometer data. Groundwater level was taken at the toe of the embankment consistent with the ponding observed in the critical area. A pore pressure coefficient, ru = 0.2 for the embankment fill was included in the analysis.

The soil nail and cess support systems were analysed separately. The cess support system comprised Grundomat piles supporting Armco type barriers and the Grundomat system was analysed as a series of laterally loaded piles using the Brinch Hansen method. Global stability failure was not considered as the Grundomat piles were intended to support the cess only and the soil nail system would stabilise the full embankment. The soil nail resistance was calculated in accordance with BS8006-1:2010 (BSI, 2010b) and the global stability of the soil nailed embankment was

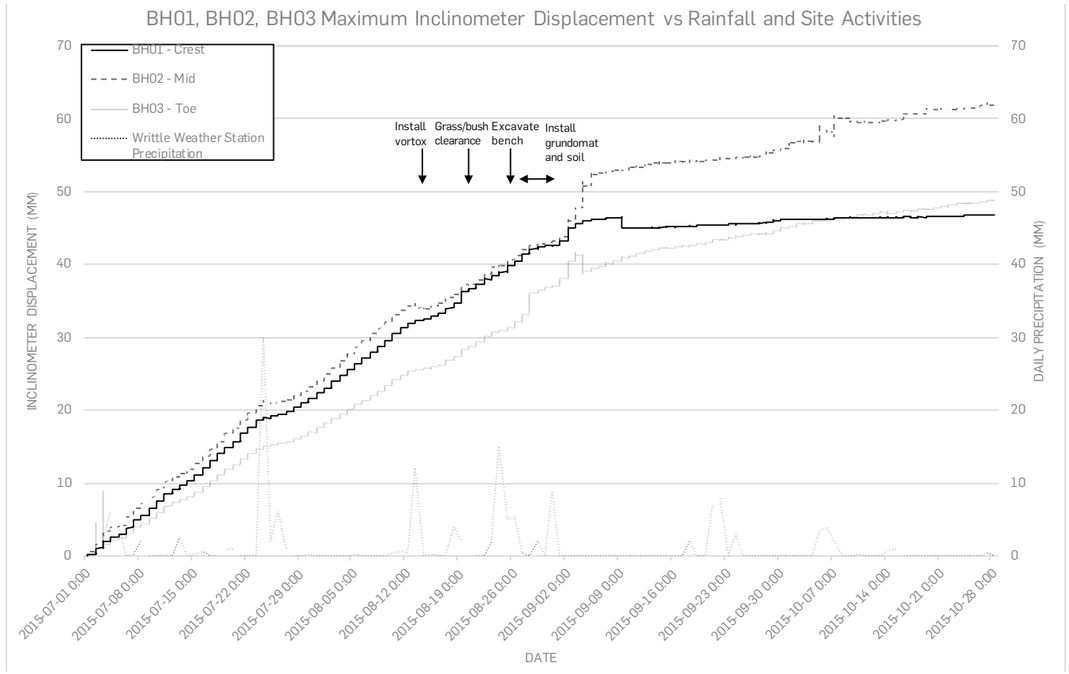

Figure 6: Automated inclinometer monitoring of slope movements before, during and after construction at 23 mi 68 ch. The plot shows the maximum downslope displacement recorded at each of the inclinometers against daily rainfall data from the Writtle weather station. The reduction in the rate of slope displacement following Grundomat cess retention piles and soil nail installation is clearly evident.

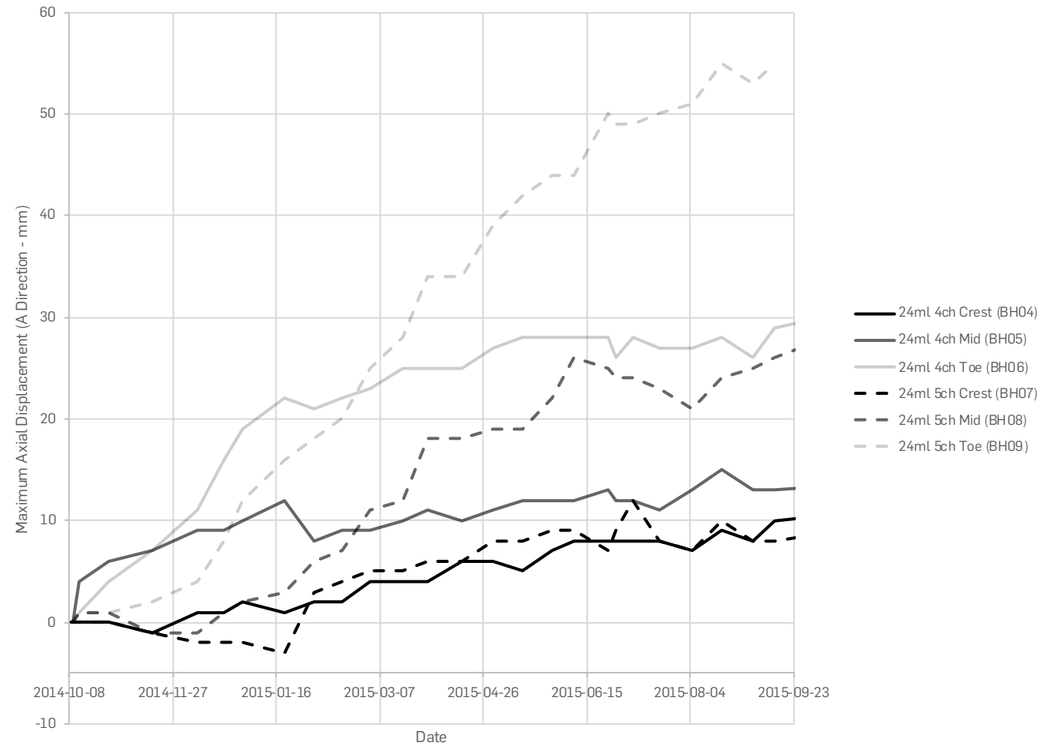

Figure 7: Inclinometer monitoring at 24ml 04ch and 24ml 05ch. The plot shows maximum downslope displacement from the crest, midslope and toe inclinometer. The observed displacement suggests the possible presence of a progressive failure mechanism as the rate of slope displacement is highest at the toe and lower at embankment midslope and crest.

checked by limit equilibrium slope stability analysis. Past authors have noted that the modelling of progressive failure is strain dependant and cannot be modelled accurately using limit equilibrium analysis (Potts et al., 1990). However, in the case of Ashdon Way embankment the inclinometer monitoring data suggested that the embankment was beyond progressive failure and was effectively reaching "active failure" in the most critical section whereby an almost full failure surface had developed and the full height of the embankment was undergoing movement. The failure of the embankment was considered in the limit equilibrium stability analysis by including a residual strength zone of the embankment fill material along the failure plane identified by the inclinometer data. Given the embankment fill is predominately reworked London Clay with a PI of 40-50%, Voight (1973) showed that London Clay with such a PI range typically had a residual effective angle of internal friction of 14° although a value of 13° was conservatively adopted in design. Using residual strength is a conservative approach given a residual strength failure zone would have led to a more rapid failure. When the slope is at an earlier stage of progressive failure, more detailed finite element analysis using a strain softening model may be considered to allow a more economical design. The final soil nail extent and layout is presented in Figures 4A and 8. The soil nail system comprised 32mm self-drilling soils nails at 2m vertical spacing and 1.5 to 2m horizontal spacing. Soil nails were installed at a relatively steep 35-degree angle to avoid passing the centre line of the embankment, this would allow future remediation of the opposite side of the embankment if required. Soil nail lengths typically varied from 9 to 11m to allow penetration into the underlying London Clay Formation.

8. Monitoring During Construction

Construction of the stabilisation scheme was undertaken during normal railway operational hours with the railway fully open to traffic throughout construction. Observational Track Monitoring (OTM) was utilised to ensure that any movement of the track was identified to safeguard passing trains. The OTM scheme involved the monitoring of 68 reflective survey targets installed in the cess and at 1.8m spacing along the length of the site. The OTM targets were surveyed three times daily and exceedance of trigger levels would initiate further inspection of the site. The OTM monitoring was complimented by an automated inclinometer monitoring system installed in three boreholes at the most sensitive section of slope instability at 23ml 68ch. The system provided hourly monitoring of slope movement throughout the construction period which allowed slope movement to be correlated against site activities (see Figure 6). The monitoring system automatically uploaded monitoring results along with a live camera feed to an online web portal for interrogation and transmitted an automatic text message warning when movement triggers were exceeded. The monitoring system and camera provided a useful mechanism for the Anglia Route Asset Manager to monitor onsite activities and identify large slope movements due to construction but is not relied upon as a mechanism for ensuring the safety of the line in the event of slope failure as there is no direct link to the signalling control centre.

The construction period commenced on 10th August 2015 with the installation of Vortox fencing adjacent to the track to delineate the site and was followed by vegetation clearance work on 20th August. No significant changes to slope movement were observed following these site activities. Temporary benching into the midslope and toe of the embankment slope for access occurred on 27th August with no noticeable immediate change in slope movement but the following day a relatively large movement of 2.9mm in one day was observed in the borehole at the toe of the embankment at 23m 68ch. Alternative plant was sought to install soil nails from the toe to avoid benching. No significant change in the rate of movement was observed in the midslope and crest inclinometer boreholes at this location.

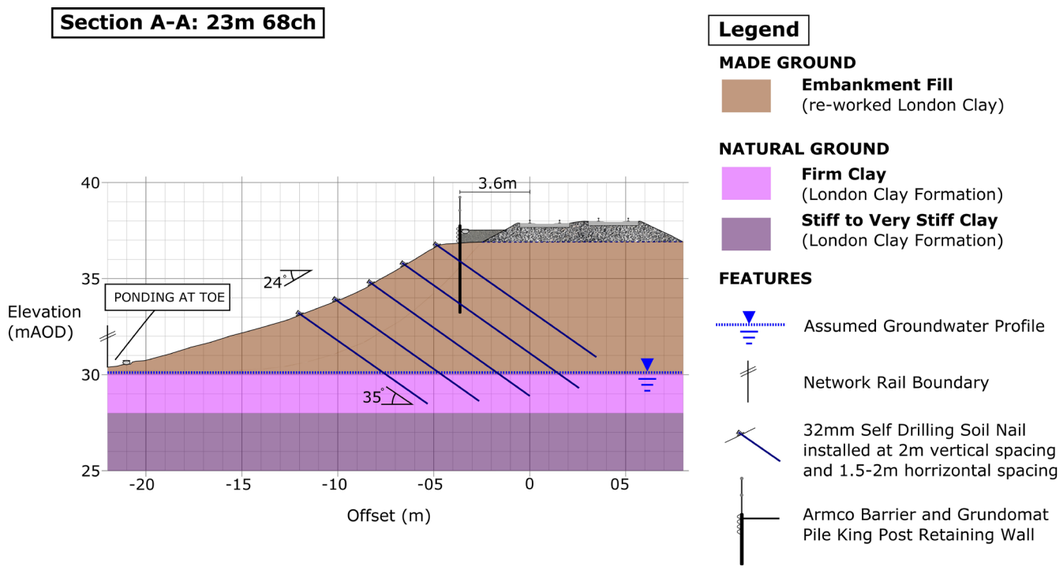

Figure 8: Cross Section showing intervention works (23ml 68ch)

The soil nail and Grundomat installations close to the automated instruments commenced on 27th August with initially large movements (between 1 and 3mm/day) observed in all boreholes up to 5th September, followed by a decrease in movement after the 5th September. The increase in movement is likely to be due to disturbance of the slope during the soil nail installation process. The drilling into the slope induces vibrations and creates voids which allows the surrounding soil to relax into the void space prior to grouting and the grout has low strength initially when it is injected into the borehole.

Installation of the Grundomat piles had a relatively quick effect on reducing upper slope movement. As the crest of the slope was constrained by the Armco sheets spanning between the piles, the rate of movement in the crest borehole reduced to almost zero (see Figure 9). The stabilising effect of the soil nails takes longer to occur as tensile strain must develop along the grout/soil interface and slope movements are needed to induce tension in the nails before the soil nails become fully effective. The rate of movement in the mid slope and toe inclinometers decreased gradually almost to zero following the soil nail installation (Figure 6) and a very small rate of movement continued as expected causing strain to develop in the soil nail.

It should also be noted that the soil nail facing mesh and head plates were not fully installed until after October 2015. It was expected that a steady decrease in the rate of movement in the embankment slope would occur as resistance on the soil nails increases. Following completion of construction work on site, the automated monitoring equipment was moved and re-used at another high-risk embankment site therefore no further automated readings were taken although manual readings were continued post construction and showed clear evidence of continued stabilisation.

9. Monitoring Post Construction - Future Work Strategy Plan

The stabilisation work at Ashdon Way embankment was successful with no emergency maintenance interventions, no speed restrictions and no reported issues at the site post construction. Movement of the slope was constrained in the intervention areas. The risk management approach targeted intervention at specific zones of the site which were observed to be at greater risk with continued monitoring undertaken in the remaining zones. Results of the continued inclinometer monitoring of the unstabilised areas showed limited displacement at most inclinometer positions. However, more significant displacement was observed in midslope boreholes at 23ml 74ch and midslope at 23ml 77ch (see Figure 10). Minimal displacement was observed at the crest inclinometers at these locations which suggests that the early stages of a progressive failure mechanism could be underway at these locations; vegetation removal for the works could also have been a trigger that initiated movement in these areas. It is possible that other areas of the earthwork could be affected by stability issues as the remainder of the earthwork has similar slope geometry, embankment fill material and underlying geology, however further monitoring will need to be undertaken to inform decisions on whether further works are required in the next Control Period CP6. The adjacent areas were not stabilised in the original works to limit the capital expenditure on the project to allow more work to be undertaken at other critical earthworks sites on the Anglia railway network. The limited movement currently observed in the majority of the unstabilised areas shows that this approach has been effective.

The residual risk posed by the targeted intervention at the site was managed by the development of a “Future Work Strategy Plan” which acted as an asset management manual for the earthwork asset (Atkins Limited, 2015c). The Future Work Strategy Plan summarised monitoring trigger levels based on inclinometer data, LADS data, Track Maintenance Engineer (TME) observations and OTM. Both amber and red trigger levels were developed with set actions required to inspect the site or investigate further if the triggers were met. The strategy plan also provided rapid response designs involving the use of fill material to stabilise the embankment in the event of sudden movement with an emergency toe berm intervention. Furthermore, the plan provided a longer term planned solution comprising further soil nails that could be readily applied in the future to the unremediated areas in the event of monitoring triggers being exceeded. Following completion of this project Network Rail (2017) have published a new standard on “Earthworks Monitoring Strategy Selection and Implementation” which covers many of the general concepts developed in the “Future Work Strategy Plan”.

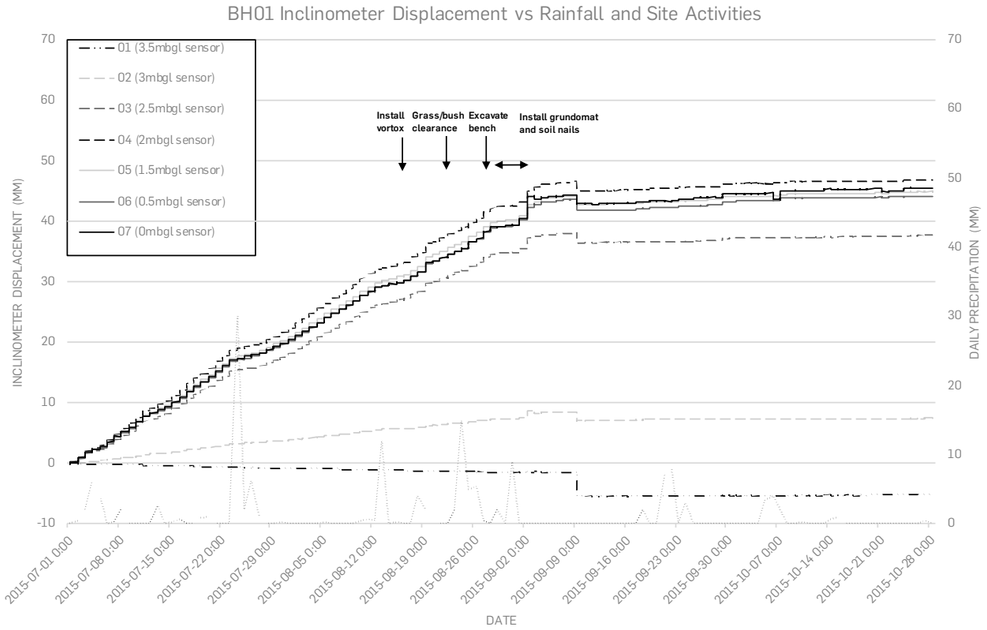

Figure 9: BH01 23ml 68ch Inclinometer Displacement vs Rainfall and Site Activities. The plot shows the maximum downslope displacement recorded at each of the sensors at BH01. This data is plotted against rainfall data from the Writtle weather station and key site activities.

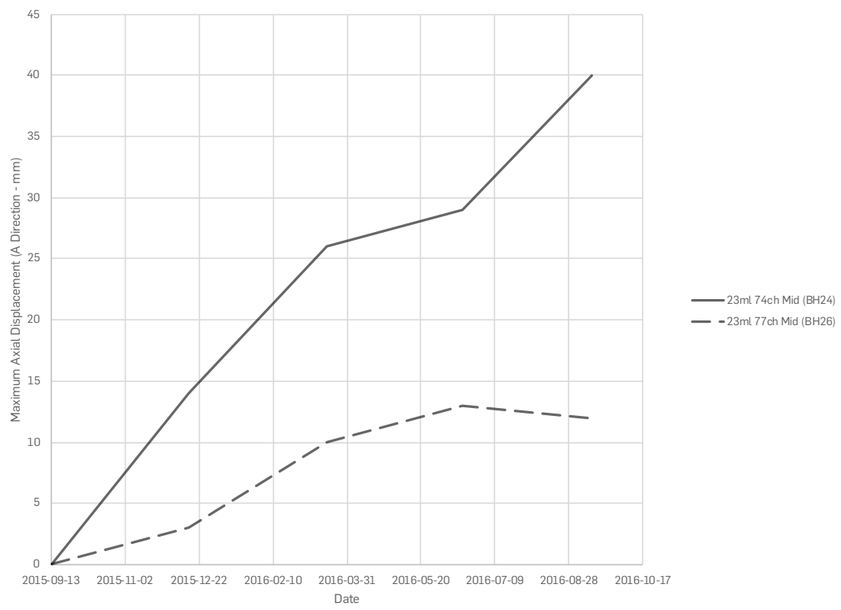

Figure 10: Inclinometer monitoring at "unremediated" areas at 23ml 74ch and 23ml 77ch. The plot shows maximum downslope displacement from each of the inclinometers. Displacement rates at these inclinometers are higher than at others in "unremediated" areas and could indicate potential future stability issues; further monitoring will be required to confirm this.

Conclusion

Detailed interrogation of the slope movement trends, track problems and development of a ground model enabled optimised mitigation for higher risk zones of the embankment slope, demonstrating sound asset management. Risks were controlled through observational monitoring of other areas with a Future Works Strategy Plan. The combination of soil nails and cess retention using Grundomat piles has halted slope movements at the areas treated and allowed continued safe operation of the railway. A robust quick fix solution such as sheet piles with a 120-year design life was not a sustainable option on the framework contract considering whole life costs. Close collaboration between client, contractor and consultant provided an alternative managed solution.

The combination of Network Rail maintenance information and observations with desk study findings and a geomorphological walkover survey enabled targeted GI. Installation of inclinometer arrays at key areas enabled understanding of the cause and behaviour of the slope movements that could put public safety at risk. Active failure was evident in the worst affected area of the site and visible signs were evident with the bulge at the toe, the track dip and dropped shoulder at the crest. While this area had greater softening of the embankment fill and underlying London Clay, the ground models were similar for all sections studied at the site and progressive failure was evident at different stages of development and continues to be monitored in adjacent untreated areas. There had been evidence of some historical drainage within the embankment fill and there appears to have been generally more movement either side of the partially blocked culvert.

Monitoring slope movements at various depths identified a clear failure surface to model and input into a back analysis which identified parameters to compare with those derived from GI and published material. Modelling a residual rupture surface was considered appropriate at the critical section, although there is potential to consider finite element strain modelling for the earlier progressive failure trends before they become active which may further optimise mitigation.

Investment in automated 're-usable' monitoring and OTM at the critical section enabled greater control for Network Rail in case of an emergency prior to and during construction works and trains could run to the normal timetable on a busy commuter line throughout. Real time slope monitoring during construction showed slope movements were sensitive to certain site activities such as pile and soil nail installation. The reaction on construction completion was quick, especially with the former which rapidly halted movement at the crest. The mid and lower areas of the slope showed slower reaction to the soil nails while the strain was developing and head plates installed, although the rate of movement has levelled out as predicted.

There was not a direct relationship between rainfall and slope movement, however there was an apparent reduction in slope movement rate immediately following rainfall. The instruments will continue to be monitored and such trends continually assessed to see whether they warrant further study.

The observational monitoring in the areas adjacent to mitigation has revealed some slope movements which could be expected. However, a Future Works Strategy Plan is in place including trigger values and designs which have enabled Network Rail to plan rather than being reactive to emergency works which is more cost effective. Areas within the site will continue to be prioritised against other sites in the Anglia region to ensure best value and optimising safety for the public.

Acknowledgements

Originally published as Payne I, Holt SJ and Griffiths IW (2018) Railway embankment stabilisation: economical asset management. Proceedings of the Institution of Civil Engineers – Geotechnical Engineering 171(4): 332-344, https://doi.org/10/1680/jgeen.17.00101.

The authors would particularly like to acknowledge Anthony Dewer and Jonathan Garelick (Network Rail), David Wright, Steve Revill, Richard Dowling and David Addy (Atkins) and Bob Brickwood (Contractors Engineering Manager), Lee Clifton (Construction and Project Manager) and Stuart Fielder (Atkins) for assistance in compiling the figures for this paper. The input of a wide range of staff from Contractors, instrumentation specialists (ITM) and Network Rail is also acknowledged.

References

Atkins Limited (2014) CP5 Critical Earthworks Risk Management - Geotechnical Desk Study for Ashdon Way. Doc Ref: 137959-ATK-REP-EGE-000023 Rev1, Croydon, UK.

Atkins Limited (2015a) CP5 Critical Earthworks Risk Management - Ashdon Way Form 001: Approval in Principle. Doc Ref: 137959-ATK-F01-EGE-000023 RevA02, Croydon, UK.

Atkins Limited (2015b) CP5 Anglia Critical Earthworks Risk Management Sites Package 1 - Ashdon Way Embankment F002: Statement of Design Intent. Doc Ref: 142456-ATK-F02-EGE-000001 Rev01, Croydon, UK.

Atkins Limited (2015c) CP5 Anglia Critical Earthworks Risk Management Sites Package 1 - Ashdon Way Embankment Future Works Strategy Plan. Doc Ref: 142456-ATK-REP-EGE-000002 Rev2.0, Croydon, UK.

BRE (1993) Digest 240 Low Rise Buildings on Shrinkable Clay Soils, Part 1.

Briggs KM, Loveridge FA and Glendinning S (2017) Failures in transport infrastructure embankments. Engineering Geology 219: 107-117, https//doi.org/10.1016/j.enggeo.2016.07.016.

Briggs KM, Smethurst JA, Powrie W and O'Brien AS (2013) Wet winter pore pressures in railway embankments. Proceedings of the Institution of Civil Engineers – Geotechnical Engineering 166(5): 451-465.

BSI (2007) NA to BS EN 1997-1: 2004 National Annex to Eurocode 7: Geotechnical Design – Part 1: General rules.

BSI (2010a) BS EN 1997-1: 2004. Eurocode 7: Geotechnical Design – Part 1: General rules.

BSI (2010b) BS 8006-1:2010. Code of practice for strengthened/reinforced soils and other fills.

BSI (2010c) BS EN 1991-2: 2003. Eurocode 1: Actions on structures – Part 2: Traffic loads on bridges.

GEL (Geotechnical Engineering Ltd) (2014) CP5 Infrastructure Projects, Ashdon Way Factual Report on Ground Investigation. Doc Ref: 29715 Version B, Gloucester, UK.

Glendinning S, Hall J and Manning L (2009) Asset-Management Strategies for Infrastructure Embankments. Proceedings of the Institution of Civil Engineers - Engineering Sustainability 162(2): 111-120.

Met Office (2016) Writtle Weather Station Daily Precipitation Data 2015 - 2016. Met Office, Exeter, UK.

Network Rail (2011) NR/L3/CIV/074. Geotechnical Design Issue 4. Network Rail, London, UK.

Network Rail (2016) CP5 Earthworks Asset Policy. Network Rail, London, UK. Issue 6, 27 April 2016.

Network Rail (2017) NR/L2/CIV/086/Mod06. Module 6 Earthworks Monitoring Strategy Selection and Implementation Issue 1. Network Rail, London, UK.

O'Brien AS (2013) Assessment of old railway embankments - time for a change? Partial Saturation in Compacted Soils: Geotechnique Symposium in Print 2011: 19-32.

Potts DM, Dounias GT and Vaughan PR (1990) Finite element analysis of progressive failure of Carsington embankment. Geotechnique 40(1): 79-101.

Potts DM, Kovacevic and Vaughan PR (1997) Delayed collapse of cut slopes in stiff clay. Geotechnique 47(5): 953-982.

Ridley A, McGinnity B and Vaughan P (2004) Role of pore water pressures in embankment stability. Proceedings of the Institution of Civil Engineers - Geotechnical Engineering 157(4): 193-198.

Smethurst J, Briggs K, Powrie W, Ridley A and Butcher D (2015) Mechanical and hydrological impacts of tree removal on a clay fill railway embankment. Geotechnique 65(11), 869-882.

Smethurst JA, Clarke A and Powrie W (2006) Seasonal changes in pore water pressure in a grass-covered cut slope in London Clay. Geotechnique 56(8), 523-537.

Terzaghi K (1947) Theoretical Soil Mechanics. London: Chapman and Hall.

Topdrill Limited (2015) CP5 Anglia Critical Earthworks Site 23 Ashdon Way. Doc Ref: TOP1890 - 137959 Ashdon Way FR01 Rev01, Milton Keynes, UK.

Voight B (1973) Correlation between Atterberg plasticity limits and residual strength of natural soils. Geotechnique 23(2): 265-267.

Improved Cable Condition Monitoring with Recovery Time Using the Advanced Portable Polymer Tester (APPT)

Narendra Sachdev

Specialist, I&C Engineer
Nuclear
Mississauga, ON, Canada

Fabrice Guerout

Research Scientist
Canadian Nuclear
Laboratories
Chalk River, ON, Canada

Abstract

SNC-Lavalin Nuclear has developed a patented next-generation portable cable indenter for measurement of indenter modulus in accordance with international standard IEC/IEEE 62582-2 and for measurement of recovery time. The tool is based on a prototype initially developed by Atomic Energy of Canada Ltd. with enhancements to the usability and ergonomics of the instrument. Recovery Time (RT) shows more sensitivity to cable degradation than Indenter Modulus (IM) for several cable jacket and insulation materials, including irradiated PVC, thermally aged CSPE, and irradiated/thermally aged XLPE.

SNC-Lavalin collaborated with Canadian Nuclear Laboratories to qualify the tool and have developed a cable database. Operating experience (OPEX) from a field trial at a Nuclear Generating Station was incorporated into the design. The Advanced Portable Polymer Tester (APPT) features single user operation, touch screen control, consistent automated cable clamping and temperature control, measurement of IM and RT, improved human factors and immediate preliminary results information post-test.

Keywords

Condition monitoring; Indenter modulus; Recovery time; Polymer testing; Electrical cable

1. Introduction

Electrical cables are used extensively in Nuclear Power Plants (NPP), particularly in the control and safety systems. These cables must function through their service life during both normal and postulated accident conditions. If the jacket or insulation on these cables becomes degraded, problems with the function of the cables can occur. This is especially true in a design basis event which can place additional stresses on the cable material (insulation or jacket).

Elongation at Break (EAB) of the insulation material has been used as a measure of the condition of the insulation. A 50% absolute EAB is normally defined as the end-of-life condition based on a conservative estimate of aged cable to survive design basis accident conditions (IAEA-TECDOC-1825, 2017).

A measurement of EAB is a destructive test that can only be performed in a laboratory environment. Non-destructive tests have been developed and correlated to the EAB values to allow for field testing (in-situ; on-power) of electrical cables in NPPs.

For a range of polymers commonly used for electrical cables, measurement of Indenter Modulus (IM) and Recovery Time (RT) gives a good correlation to the EAB values and, for this reason, these monitoring parameters give a good indication of cable ageing. RT shows a stronger response to ageing and closer correlation to EAB than IM (U.S. Department of Energy, 2016) (Guerout and Boor, 2015) for some materials such as irradiated or thermally aged XLPE insulation which is a material with a notoriously weak age versus IM response.

Measurement of IM is generally performed in accordance with the IEC/IEEE international standard (IEC/IEEE 62582-2 ,2016). RT is a new monitoring parameter for which no standard has yet been developed.

2. Refurbishment of CANDU® NPP

® Registered trademark of Atomic Energy of Canada Ltd. (AECL) used under exclusive license by Candu Energy Inc.

Electrical cables are long-lived and critical components that need to be evaluated on an on-going basis with a solid ageing management program in place to ensure the safety and reliability of the cables, particularly as they affect the safety and reliability of the plant.

Additionally, as many of the CANDU type NPPs undergo refurbishment to extend their operating lifespan, the condition of the electrical cables in the plants and assessing their ageing is one of the most important aspects of ensuring the instrumentation and control systems are capable of functioning throughout the extended life of the plant (IAEA-TECDOC-1825, 2017).

3. APPT Development

In 2010/2011, a prototype field version of a Portable Polymer Tester (PPT) was developed. The main objective of the prototyping activities was to develop a highly controllable, portable, non-destructive tool using state-of-the-art technology to identify the indentation parameters that are most prone to tracing the degradation of polymer-based components.

The prototype tool incorporates the classical measurement of IM via the linear drive of a probe tip into the material to be tested (the probe having been slightly preloaded onto the sample surface). The IM is derived from simultaneous acquisition of the probe reaction force and probe displacement during the indentation phase. It is the ratio between the changes in the applied force and the corresponding displacement of a probe driven into the sample. The tool also makes provision for the measurement of post-indentation parameters, such as force relaxation and deformation recovery via the measurement of RT.

In 2012 and 2013, the prototype PPT was used to prove the feasibility of performing tests at nuclear sites. The overall performance and reliability of the prototype field version was deemed satisfactory and resulted in the completion of a condition assessment for several cables.

There has been a growing interest at the Canadian utilities and internationally for cable indenter testing services and for the technical advantages offered by the PPT technology.

In 2015, SNC-Lavalin Nuclear initiated a project to improve the prototype PPT. The focus of the improvements was on reducing the weight and size of the instrument and improving the operability. However, many other changes were made to the design.

4. APPT Features

The improvements on the prototype PPT concept have resulted in the APPT, see Figures 1 and 2. The APPT is an instrument designed to measure IM and RT. The APPT instrument is based on the methods described in the IEC/IEEE standard 62582-2, 2016. However, to improve the accuracy and repeatability of the results obtained, the APPT has several advancements compared to the current first-generation indenter instruments common in the industry.

The APPT will measure the IM value over the force range of 1-4N as specified in the standard; however, the primary IM reported by the APPT is the IM over the distance between 50% and the full indentation depth. By controlling and measuring the indentation over a fixed depth rather than a fixed force, the APPT gives a more reliable indication of the change in the cable condition as a cable ages (Guerout and Boor, 2015) (IAEA-TECDOC-1825, 2017).

IM and RT are measured at a consistent cable surface temperature. A consistent temperature for performing the tests normalizes the results since both IM and RT values vary with the temperature of the test cable (Guerout and Boor, 2015). As the ambient temperature where cables are located can vary for different areas within an NPP, a heating system is incorporated into the head of the APPT to control the tested cable area to a reference test temperature, thereby ensuring a more accurate measurement.

Cable clamp force in the APPT is controlled via an automatic clamping system. The IEC/IEEE standard specifies the clamp force to be “the minimum force required to keep it (the cable) in place.” Other indenter instruments have manual clamping mechanisms or open loop powered mechanisms which result in variations in the clamp force achieved or unknown clamping forces. Variations in clamping force increases variability in the IM and RT results.

The APPT incorporates direct measurement of the probe tip position which results in greater accuracy of measurement than first-generation indenter instruments.

In addition to the improvements made to the APPT to increase the quality and repeatability of the IM and RT measurements, other improvements have been made to the functionality and usability of the instrument. These improvements include:

Figure 1: SNC-Lavalin Advanced Portable Polymer Tester (Complete Unit)

1. Preset test configuration files for field work. The required test parameters for a cable are prepared prior to field work occurring. In the field, the operator simply needs to select the file for the cable being tested. This reduces the burden on the operator, and operator dose, and reduces the likelihood of operator error.
2. The testing sequence is automated to reduce operator workload and the operator is provided with on-screen feedback during testing so that they can monitor the progress of the testing.
3. The APPT has been designed to test cables in the size range of 2 mm to 60 mm. This size range is greater than other indenter instruments and will enable monitoring of most low voltage cables in the plant.
4. The size and weight of the APPT have been optimized to permit enhanced portability and enable single user operation.
5. Enhancements have been made to the APPT's usability to improve human performance.
6. The APPT is controlled via a touch screen mounted in the tool head providing all functions of the instrument in a location convenient for the operator.
7. The APPT provides immediate preliminary result information post-test to the operator via the touch screen. These preliminary results allow the operator to gain a sense of the consistency of the test results from a test location. The results are further analyzed by a team of experts with the help of an extensive database of cables of different jacket and insulation materials and their IM and RT values for different levels of accelerated ageing – both thermal and radiation.

Figure 2: SNC-Lavalin Advanced Portable Polymer Tester

5. Testing and Qualification Methodology

Following the development and incorporation of the design changes to the APPT based on the field trials at a Nuclear Generating Station, further functional testing of the APPT was performed to verify the tool behavior and confirm all feedback/OPEX identified in the field trials had been addressed. This functional testing included testing the APPT in field-like conditions in SNC-Lavalin laboratories.

In addition to the functional testing of the APPT, a qualification test program has been performed to verify the results from the APPT are consistent with other indenter instruments, particularly with the prototype PPT instrument on which the APPT is based.

Throughout the qualification testing, SNC-Lavalin Nuclear has collaborated with Canadian Nuclear Laboratories (CNL) to qualify the methodology used for operation and testing of the APPT and ensure that the results obtained with the APPT accurately predict the cable ageing characteristics.

A typical APPT test sequence consists of three parts: a preload and indentation phase, followed by a force relaxation phase, and then a deformation recovery phase. Typical APPT force and displacement signatures obtained during preload, indentation, force relaxation, and deformation recovery are shown in Figure 3.

Preload consists of bringing the probe in contact with the polymer surface and preloading it in a repeatable manner with a predefined depth. The indentation phase consists of driving the probe at a pre-set indentation speed into the polymer material to a pre set indentation depth that can vary from 50 µm to 500 µm (approximately 0.002 in to 0.020 in), depending upon the thickness and stiffness of the sample being tested. A typical indentation depth is 127 µm (0.005 in). Force and displacement signals are measured simultaneously during indentation and are used to derive the specific compressive stiffness of the material, also called "Indenter Modulus."

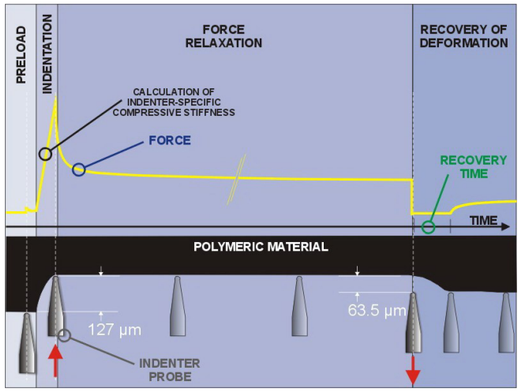

Figure 3: Typical APPT Test Sequence

The force relaxation phase consists of holding the indenter at the maximum depth reached at the end of the indentation phase. The reaction force typically peaks immediately upon completion of the indentation phase and then decreases over time. This maximum depth position is held for 60 seconds to allow for relaxation of a large portion of the force initially generated. This phase is a conditioning step prior to the deformation recovery phase that occurs upon retraction of the probe tip.

The recovery phase starts at the end of the force relaxation phase. At this stage, the probe is retracted quickly to a predetermined position and then the time required for the compressed polymer surface to resume contact with the probe tip is measured. At the time of contact, a force is again detected by the load cell. This time interval is defined as the polymer deformation RT. Without force relaxation prior to retraction of the probe tip, the polymer surface tends to spring back very quickly, whether the material is aged or not. However, if the force is allowed to relax prior to retraction of the probe tip, an aged sample is usually much slower to recover than an unaged sample.

6. Parameters Sensitive to Cable Degradation – IM and RT

Laboratory studies show that IM and RT are two output parameters that can be used in combination to characterize degradation in a broad variety of cable insulation and jacket materials. These materials include PVC, CSPE, Ethylene Propylene Rubber (EPR), XLPE, XLPO, and SiR (IAEA-TECDOC-1825, 2017) (Guerout and Boor, 2015).

IM is known to be sensitive to increased cable insulation/ jacket degradation resulting from thermal ageing of PVC, EPR and CSPE and from irradiation of XLPE, EPR and CSPE (IAEA-TECDOC-1825, 2017) (International Atomic Energy Agency, 2000). However, IM does not change significantly with increased irradiation dose in PVC - even for high doses - and does not change significantly with increased thermal ageing in XLPE (IAEA-TECDOC-1825, 2017). IM tends to increase with increased thermal ageing in PVC, EPR and CSPE. IM tends to increase with increased irradiation dose in XLPE, EPR and CSPE.

RT tends to increase with increased thermal ageing duration and/or increased irradiation doses in PVC, CSPE and XLPE. An example is given in Figure 4 for irradiated PVC insulation. The graph shows that RT increases with increased cumulated irradiation dose whereas IM (S) remains unchanged (Guerout and Boor, 2015).

For some XLPE formulations, RT has been shown to decrease with thermal ageing duration as shown in Figure 5 for a Rockbestos XLPE insulation (IAEA-TECDOC-1825, 2017). Again, in this case, IM does not change significantly with increased thermal ageing duration.

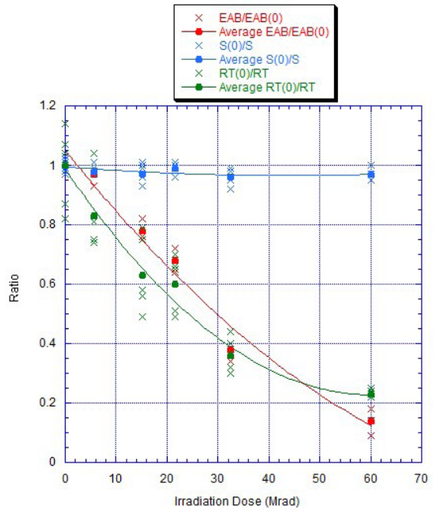

Figure 4: Irradiated PVC Insulation: Change in EAB, Recovery Time, and Indenter Modulus from Unaged Value

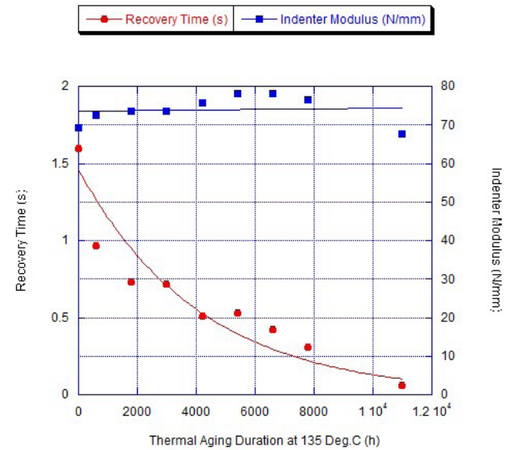

Figure 5: Recovery Time and Indenter Modulus Data for XLPE Insulation Thermally aged at 135°C

Test results from testing of irradiated XLPE insulation samples are shown in Figure 6. Here again it can be seen that RT (70% ratio drop) shows very good correlation with the EAB (80% ratio drop) whereas IM (S) shows significantly lower ratio drop at 20% (Guerout and Boor, 2015)

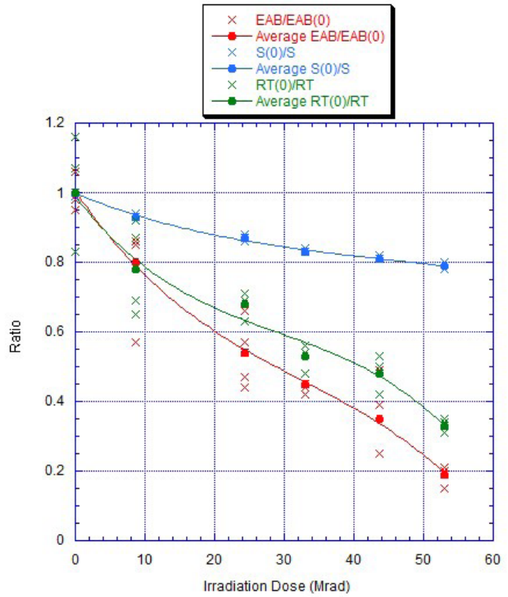

Figure 6: Recovery Time versus IM for Irradiated XLPE

7. Factors Affecting Variability in Cable Indentation Parameters (IM and RT)

There are several factors that can contribute to the variability in the cable indentation test parameters. Some of them are discussed below.

7.1 Temperature

Based on the type of cable material tested, indenter test results can be largely dependent upon test temperature. An example is shown in Figures 7 and 8 for IM and RT measured for PVC at temperatures ranging from 13°C to 42°C. Correction factors could be used to determine the IM or RT at various temperatures. However, these correction factors will differ for various cable materials used in nuclear plants. Therefore, for on-site measurements taken in rooms where the temperature may vary from one testing campaign to another, it is desirable to control the tested portion of the cable to a constant reference temperature. APPT incorporates a heater and temperature control to provide a consistent temperature of the tested portion of the cable resulting in consistent and accurate values of IM and RT.

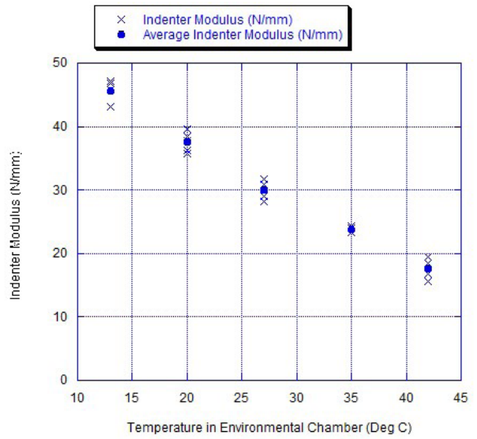

Figure 7: Indenter Modulus versus Environmental Temperature for Unaged PVC Jacket

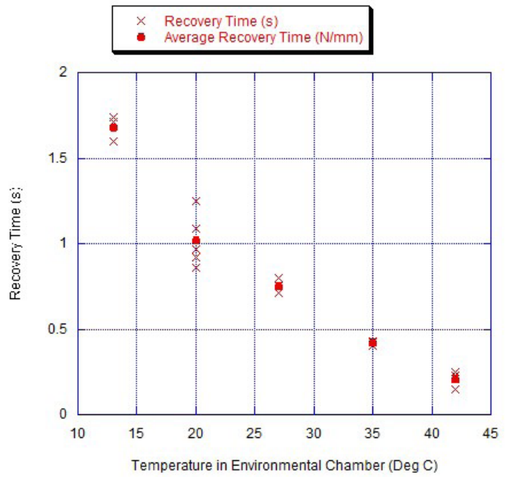

Figure 8: Recovery Time versus Environmental Temperature for Unaged PVC Jacket

7.2 Clamping Force

Clamping force has been found to be a factor that influences the IM measurements (IEC/IEEE 62582-2, 2016) (IAEA-TECDOC-1825, 2017). Testing by SNC-Lavalin has shown that it also influences RT. APPT incorporates automatic clamping force control resulting in consistent values for indentation parameters IM and RT.

8. Cable Ageing Reference Database

As the OEM for the CANDU reactor and the licensee of the CANDU technology, SNC-Lavalin Nuclear knows the cable types and configurations used in CANDU 6 NPPs and other reactors of the CANDU type. Using this knowledge base, SNC-Lavalin Nuclear has tested a sample set of cables covering a large variety of cables used in CANDU style NPPs. The cables were tested in various stages of ageing to generate a reference database of IM and RT results. This database of results is used by our team of technical experts as a basis for comparison with results obtained in the field in NPPs as a reference to assess the extent of the ageing that has occurred.

9. Actual Deployment of APPT

SNC-Lavalin recently (February 2019) successfully deployed the APPT as part of a contract with a Nuclear Generating Station to perform cable condition monitoring.

SNC-Lavalin is offering a turn-key solution to utilities for cable ageing monitoring. Within this solution SNC-Lavalin Nuclear will perform field inspections of cables selected for monitoring by the utility using the APPT and then perform the analysis of the test results, comparison with reference information as applicable, and report to the utility on the condition of the cables. Offering the cable condition monitoring as a service benefits the utilities as it ensures that the instruments being used in the field benefit from any upgrades made to the product; it eliminates the need for the utilities to train staff on the operation of the APPT and the inspection standards; and the results from testing will be stored in a centralized repository database, ensuring that the results are securely stored and recalled for comparison with the results from future tests. Establishing a cable ageing program and monitoring cable health (i.e. Condition Monitoring) helps prevent unplanned downtime and, in case of life extension, may prevent unnecessary expense for replacement of cables if the cables are shown to be in good condition.

Using the expertise of a group focused on supporting the utilities with their cable ageing management programs, SNC-Lavalin Nuclear can help utilities comply with best practices and latest regulatory requirements in cable ageing management, including: CNSC REGDOC- 2.6.3 – Ageing Management, 2014; IEC/IEEE 62582-2; IAEA guidelines; and USNRC Guide 1.218.

10. Conclusion

SNC-Lavalin has a developed state-of-the-art next-generation indenter APPT that offers many advantages over the current generation of indenter instruments, in particular the ability to measure the RT of the electrical cable material. Access to RT allows for assessment of material degradation that could not be detected if using IM. Using the APPT, SNC-Lavalin Nuclear can provide cable monitoring services to utilities in support of their ageing management and asset management programs, thereby saving the plant time and money from unplanned outages or premature cable replacement.

References

IAEA-TECDOC-1825, 2017, “Benchmark Analysis for Condition Monitoring Test Techniques of Aged Low Voltage Cables in Nuclear Power Plants”

IEC/IEEE international standard, “Nuclear power plants – Instrumentation and control important to safety – Electrical equipment condition monitoring methods – Part 2: Indenter modulus”, IEC/IEEE 62582-2, 2011+A1:2016.

IEEE Transactions on Dielectrics and Electrical Insulation (Volume: 22, Issue: 5, October 2015), Development of indentation techniques in support of cable condition monitoring programs, Guerout, F.M., Boor, R.G.

International Atomic Energy Agency, “Assessment and Management of Ageing of Major Nuclear Power Plant Components Important to Safety: In-Containment Instrumentation and Control Cables”, Volume 1, IAEA-TECDOC-1188, 2000 December.

U.S. Department of Energy, M3LW-16OR0404022 PNNL-25432, 2016, “Evaluation of Localized Cable Test Methods for Nuclear Power Plant Cable Ageing Management Programs”

Data-Driven Design | 005

The Potential Use of Wi-Fi Data in the Development of Agent-Based Pedestrian Models

Francesco Angelelli

Consultant
Engineering, Design and Project Management
London, UK

Jason Morrow

Technical Director
Engineering, Design and Project Management
London, UK

Abstract

The use of agent-based pedestrian models for the assessment of future conditions in public realm environments is normal practice, especially where conditions are particularly complex and flows significant.

This paper presents the work undertaken for the pedestrian survey and modelling of Oxford Circus and its surrounding streets, some of the busiest and complex public spaces in the UK. The work included the adoption of Wi-Fi survey technology for the survey of pedestrian movement, as well as the deployment of more traditional survey methods to act as control and validation checks.

The approach undertaken shows some of the advantages and limitations of using the Wi-Fi survey technology and provides the initial approach for potential inclusion of Wi-Fi surveys as standard practice in the development of larger urban agent based pedestrian models.

Keywords

Pedestrian modelling; Public space; User experience

1. Introduction

Agent-based pedestrian models are commonly used to simulate pedestrian conditions in various environments including the public realm. The standard approach is to survey pedestrian flows to inform a base year model which simulates existing conditions to a reasonable level of validation [1]. The validated model can be used to test the impact of changes in demand or spatial layout, thus making this tool essential for the assessment of pedestrian safety and experience.

As models increase in size and complexity, one of the biggest limitations is the availability of data that inform and validate these models. As new technologies enter the pedestrian surveying market, it is important that the pedestrian modelling industry embraces such innovation [2].

This paper presents the innovative methodology undertaken for the pedestrian survey and modelling of a large public realm in London where Wi-Fi data have been used to inform the base year model. The approach undertaken shows advantages and limitations of this technology and explores the potential for inclusion of Wi-Fi surveys as standard practice in pedestrian simulations.

2. Methodology

2.1. Microsimulation Software

The agent-based simulation tool adopted in this study is Legion SpaceWorks. Agents in Legion follow the least effort path to their destination. Local agents avoid collisions with other agents following an algorithm focused on preserving their personal space. Legion algorithm is proven to provide a reasonable level of validation for simulating local pedestrian behaviour [1].

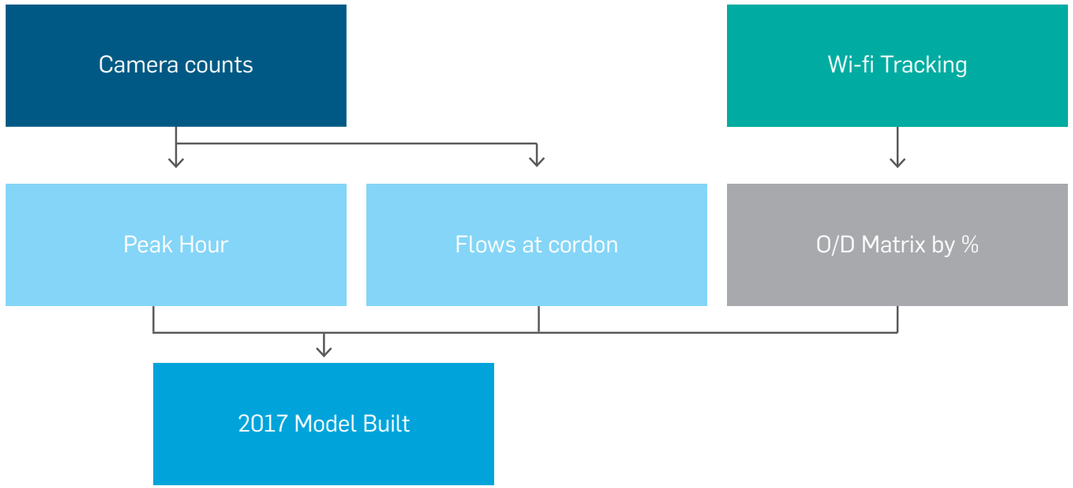

Figure 2.1: Demand derivation

2.2. Survey Objective

Traditional survey methods such as camera counts provide an accurate measure of pedestrian flow dimensions. However, such information must be completed and validated with the use of other datasets to gain a thorough understanding of pedestrian movements and demand trends (Figure 2.1).

2.3. Technology Overview

Wi-Fi enabled devices regularly scan for Wi-Fi networks to associate with. By doing so they produce a signal containing their MAC Address, which is unique for each device.

The survey technology uses Wi-Fi nodes to capture MAC Addresses alongside signal strengths and timestamps at a frequency that depends on the type of device, the manufacturer and the activity level. The frequency is generally between one second to 60 seconds [3].

In recent years device manufacturers started using MAC Address randomisation techniques aimed at protecting the privacy of users. Although the survey technology adopted allows tracking of a relevant portion of devices, with the evolution of mobile devices and operating systems, the level of protection could impact the future deployment of this technology. As of today, there are techniques that can bypass randomisation and allow tracking of 100% of devices [4].

According to EU's General Data Protection Regulation MAC addresses should be considered Personal Information and their collection must be subject to the individuals' consent. However, truncating MAC Addresses would make the identifier non-unique and the relative data not personal, thus not subject to individuals' consent [5]. The possibility to capture multiple devices with the same truncated identifier are expected to be limited if a small area and a short period are considered.

2.4. Installation

The hardware deployed consisted of Open Mesh nodes (OM2P-HS) that could capture signals from Wi-Fi devices and transmit data in real time to a cloud server. Each Wi-Fi node required connection to the electricity supply and to the internet. Internet connectivity was used to stream data to a cloud server in real time. Using a remote server has several advantages including security and real-time data monitoring. Nodes were attached to floodlights on building cornices for electricity supply. At the same time, a TP Link wireless router was used to connect the node to the 3G/4G mobile network. As recommended by the supplier [6] the nodes should be installed at a height of 3-5 m and should be clear from obstructions. Figure 2.2 shows an example of an installed box and how the network is capable of tracking known devices.

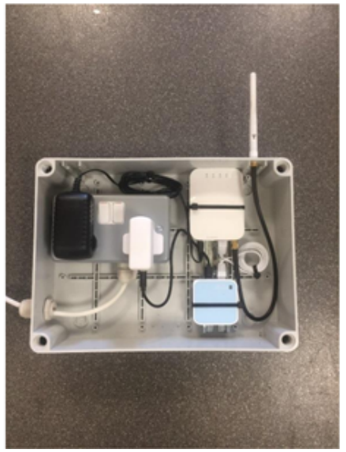

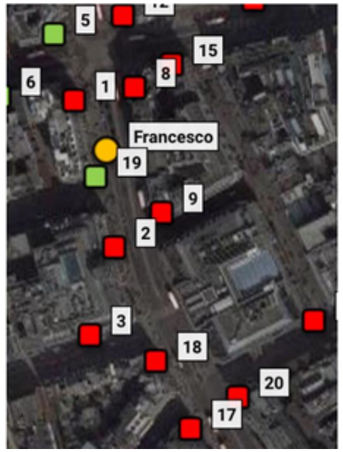

Figure 2.2: Wi-Fi kit, node installed on building cornice, tracking of known device

The cloud server and dashboard were provided by technology provider Accuware [3]. The live dashboard showed density map, map of tracked devices in real-time, daily/hourly profiles for each node/area. The daily dataset was provided at the end of each day and could be downloaded for the analyses. It should be noted that live data provide only an indication of demand in the area. Post processing of data is fundamental to obtain in depth insights and statistics.

Figure 2-3 shows the study area and the distribution of Wi-Fi nodes. A total of 19 nodes were installed, with four experiencing connectivity issues (electrical/internet) that had to be excluded from the analyses.

Survey days were August 8th - August 23rd and September 29th - October 15th.

2.5. Comparison of Weekday and Weekend Profiles

The Wi-Fi survey showed a weekday profile having three peaks: morning, lunch, afternoon. The weekend profile was instead smoother with a peak around 4 PM (Figure 2-4).

According to the RODS 2016 data [7] and Arup's report [8], the busiest periods for the area were 14:00 to 19:00 on weekdays and 12:00 to 16:00 on weekends.

The Wi-Fi survey confirmed the two peak periods for both weekdays and weekends. The weekday afternoon peak showed higher activity than the weekday peak.

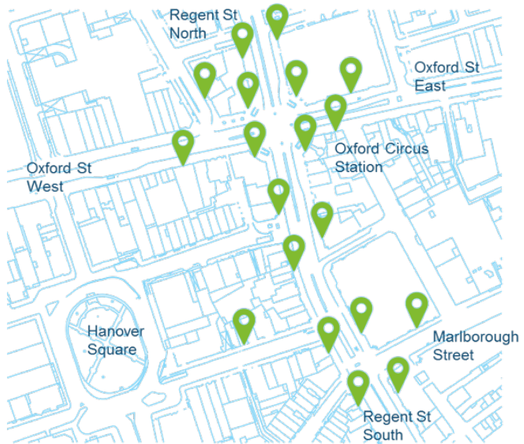

Figure 2.3: Study area and distribution of Wi-Fi nodes

2.6. Peak Hour

The Wi-Fi data showed a consistent daily pattern for weekday movements, as shown in Figure 2.6..

The drop in demand on the morning of August 11th was caused by the emergency evacuation of Oxford Circus Station due to a train on fire with its consequent closure [9]. This shows the benefit of this technology as it allows for the continuous monitoring of pedestrian movements including exceptional conditions, as opposed to traditional survey technologies.

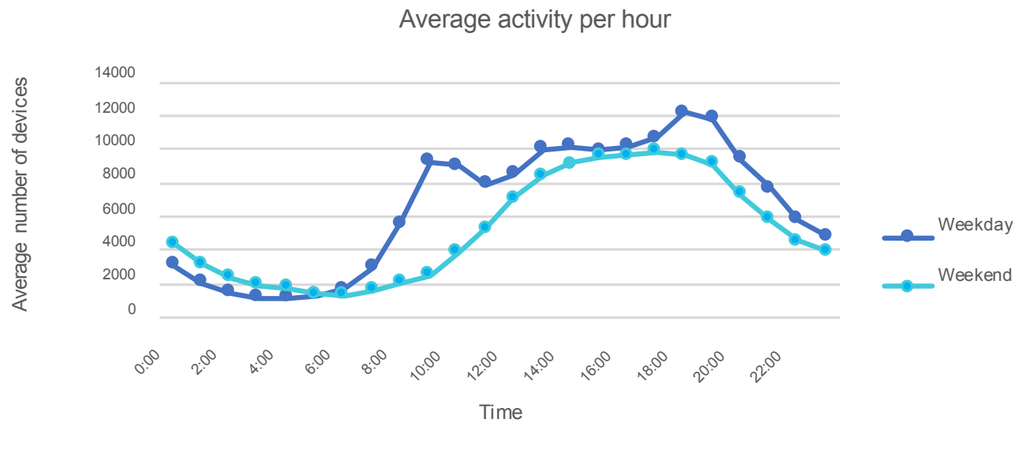

Figure 2.4: Average number of devices on weekday and weekend (Saturdays only)

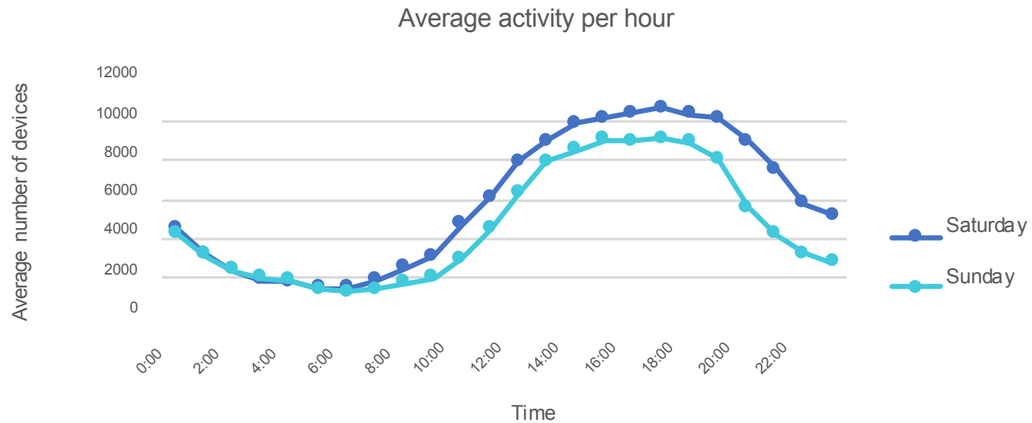

Figure 2.5: Average number of devices on Saturdays and Sundays

This data confirmed that the weekday peak hour is between 18:00 – 19:00, which is the same as in the pedestrian counts performed in May 2017.

2.7. Movements Between Nodes

As weekday pedestrian counts were performed on a Thursday, August 10th 2017 was chosen to derive the O/D matrix for consistency between the two datasets.

To avoid the fragmentation of routes at the control period boundary the control period for the O/D matrix was extended to four hours (16:00 – 20:00).

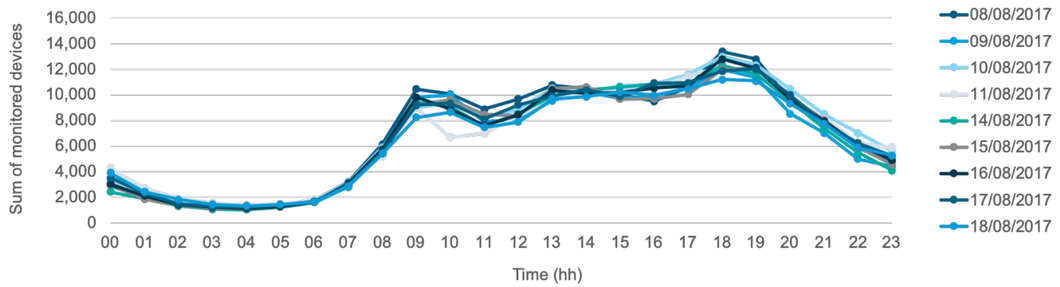

Figure 2.6: Hourly volume of devices monitored on different days. August 11th data was influenced by the emergency evacuation of Oxford Circus station due to a train on fire.

When more nodes captured a device simultaneously, it was assumed that the device would be in proximity of the node that showed the highest signal strength.

Intermediate locations were not included in the derivation of the O/D matrix. Hence, only the first and last location during the control period were considered.

The following movements were excluded from the derivation of origin-destination movements patterns:

- Movements that had the same initial and final location within the control period;
- Movements that are generated in intermediate locations within the study area (i.e., shops, offices) because these locations are excluded from the model and not relevant for the definition of O/D proportions.
- Static activity throughout the control period; and
- Journey times longer than 60 min.

The above-mentioned process allowed to determine 11,530 unique movements between the installed nodes.

2.7.1. Consistency of the Dataset

The matrix in Table 2.2 was compared with matrices from other weekdays. By comparing the proportion of devices monitored in each node of origin for Thursday, August 10th and the average proportion obtained for the whole period, the maximum discrepancy for each node was 3% (Figure 2.7).

A similar value was obtained when comparing destination nodes (Figure 2.8). Hence, Thursday, August 10th was assumed to be representative of PM peak condition.

2.8. Pairing of Nodes and Locations

The movements between nodes at the boundary were used to derive the origin and destination proportions to be adopted in the model.

Node IDs had to be paired with geographical locations. Some areas were covered by multiple nodes while some areas were only covered by a single node. The assumed pairing is shown in Table 2-1.

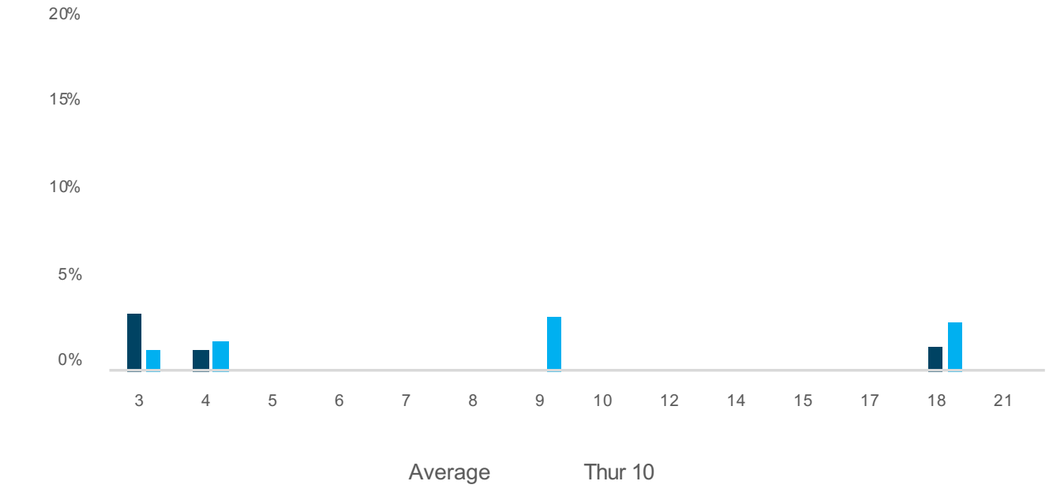

Figure 2.7: Comparison of origins obtained on sample day with other days.

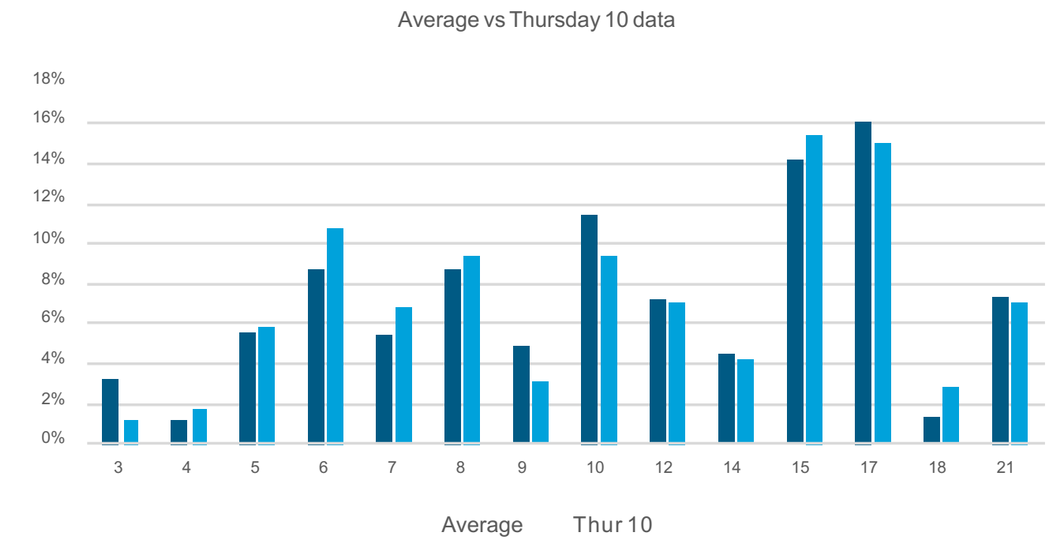

Figure 2.8: Comparison of destinations obtained on sample day with other days.

TABLE 2-1: PARING OF NODE IDS AND GEOGRAPHICAL LOCATIONS

Area	Node 1	Node 2	Node 3
West	6		
South	9	18	
East	15		
North	21		
Tube	5	8	12
Marlboroufh	10		
Hanover	3		
John Princess Street	4		

The resulting origins and destination proportions were then compared with proportions obtained from monitored flows at these locations. Figure 2.9 and Figure 2.10 show good correlation between origins and destination proportions obtained with the two survey types.

2.9. O/D Matrix

The pairing of nodes and locations resulted in an O/D Matrix with 5,947 movements. Successively, movements between internal nodes were excluded. The matrix obtained had 5,266 movements. The matrix was then translated into a non-dimensional weight matrix showing proportions from each origin to each destination. Proportions were multiplied with the origins obtained from the camera counts. This resulted in a new O/D Matrix inclusive of 39,073 movements. Finally, the Furness Method was used to reach convergence between destinations from the matrix and the camera counts. Convergence was reached in three iterations.

Finally, the matrix destinations have were split to account for the presence of footways on either side of the street. The so defined matrix accounted for 39,076 movements.

2.10. Walk Speeds

The Wi-Fi survey has been used to monitor speeds along major footways in an innovative way. Due to the long distance between the Wi-Fi nodes installed on Regent Street, the speeds recorded between them have been used as a sample to determine the speed profile of pedestrians in the area. As walk speeds can be monitored using the Wi-Fi survey, this therefore provides walk speeds that directly correspond to the main origin-destination information held within the same dataset.

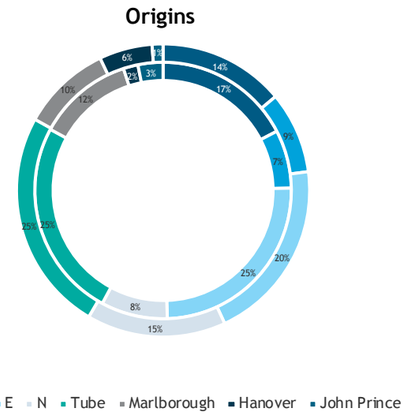

Figure 2.9: Proportion of origins obtained with Wi-Fi and camera counts

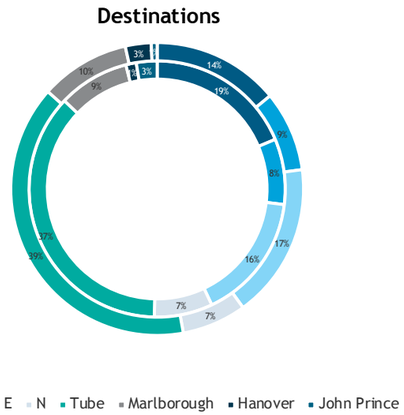

Figure 2.10: Proportion of destinations obtained with Wi-Fi and camera counts

In addition, speeds have also been investigated for pedestrians walking along Argyll Street, which runs parallel to Regent Street, but is pedestrianised. The comparison of the two datasets enables consistency across the two samples to be verified and to ensure that the data is not influenced by vehicular traffic. Figure 2.11 below shows the two speed profiles obtained from the Wi-Fi data. Both datasets show similar patterns. Hence, it should be excluded that vehicular traffic influences the Regent Street dataset.

Some high values were monitored in both streets. This tail is understood to be noise produced by a few devices that are reporting with low frequency. In this case it is possible that for some devices the detected distance is less than the real one, thus overestimating their speed.

When higher values are excluded, the profile shows a normal distribution with an average speed of 1.2 m/sec. The resulting distribution is consistent with industry standards and literature [10].

The speed profiles used in the model are consistent with Legion's default speed profiles that were utilised in the model.

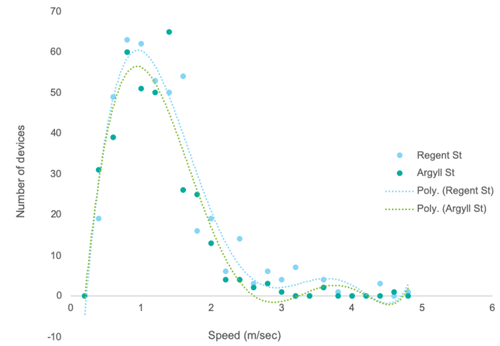

Figure 2.11: Walking speeds monitored in Regent St and Argyll St

2.11. Proportion of Commuters and Tourists/Shoppers

Following this analysis of RODS data [7], 53% of pedestrians were classified using the Legion default user group "UK Commuters," whilst the remainder were classified as "Tourists." The "Tourists" also include all shoppers in the area. "Commuters" are assumed to be familiar with the environment whilst "Tourists" are not. Speeds and size of users on walkways and stairs are the default values from Legion.

In addition, the number of devices that was captured for the first time during the afternoon peak was compared with the number of devices that had already been monitored at least once in the morning peak. This showed that the returning devices, presumably carried by commuters, was approximately 50% of total devices, thus validating the previous assumption.

2.12. Model Development

The adoption of further assumptions was required to build the model.

The model simulates movements between 18:00 and 19:00, with the addition of 15 minutes preload period and 15 min clearance period.

The demand profile at the model origins is derived from camera counts. A uniform distribution within each 15-min period is assumed.

The methodology followed for the definition of available space, the definition of crossing behaviour and of crossing times follows the prescriptions included in Street Level Modelling with Legion Best Practice Guidance (2009) from Transport for London.

Auto-navigation and routing by final destination is used for route assignment. Both are based on the shortest path assumption. For some routes it was necessary to prevent agents to use less crowded paths although these represented the shortest path to their destination.

On Oxford Circus it was observed that only pedestrians who were familiar with the environment would use the diagonal crossing. Hence, only agents pertaining to the "Commuters" were allowed to use the diagonal crossing.

According to 2016 RODS data [5], the "Journey Purpose" of 12% of the total number of people exiting the station is shopping. A few stores are included in the model, including Nike Town, Tezenis, United Colors of Benetton, Topshop, Apple, and H&M. Based on spot observations, the average delay (time spent within a store) is assumed to be five minutes. Such value was validated by the observed number of shoppers in stores.

3. Results

When comparing input and output matrix extracted for the simulation period between 18:00 and 19:00 the maximum difference for each origin and destination was 5% which could be considered acceptable considering the size of the model.

In addition, monitored and simulated flows on internal footways were compared using GEH and R-squared statistics, both widely used in traffic simulations. It is generally considered that a GEH less than 5 is acceptable if it is achieved for most values (85%). The R-squared value shows a good fit if it is close to the unit.

86% of flows resulted to have a GEH less than 5, and a value of R-squared for the entire set of 0.97 (see Table 3-1 and Figure 3.1). These results were considered acceptable.

TABLE 3-1: SIMULATED VS COUNTED FLOWS ON INTERNAL FOOTWAYS [PPL/H]

Area		Simulated	Counted	Difference	GEH
1	Argyll Street	6514	7905	-18	16
2	Marlborough Street	7807	7642	2	2
3	Regent Street SE	4572	4846	-6	4
4	Regent Street SW	4036	4300	-6	4
5	Hanover Street	1905	2167	-12	6
6	Princes Street	1185	1221	-3	1
7	Oxford Street SW	5936	5615	6	4
8	Oxford Street NW	5092	5198	-2	1
9	John Prince's Street	696	717	-3	1
10	Regent Street NW	3613	3550	2	1
11	Regent Street NE	5199	5182	0	0
12	Oxford Street NE	6597	6300	5	4
13	Osford Street SE	8183	7812	5	4
14	Little Argyll Street	1543	1458	6	2

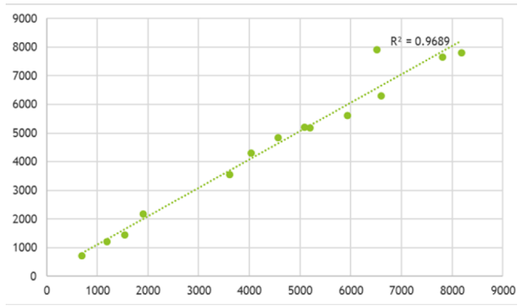

Figure 3.1: Simulated vs counted flows [ppl/h]

The model output includes density maps where density is mapped following Fruin's definition of Level of Service for walkways [7] as shown in Figure 3.2.

Figure 3.3 shows the cumulative mean density experienced over a certain period (in this case, 15 minutes, 18:15-18-30) in the 2017 Base model.

When visually compared to on-site observations, the model appears to replicate the site existing conditions on footways. Queues accumulating at Oxford Circus corners resemble in size and density the ones observed. The map shows high densities on the south-east corner of Oxford Street (1). This is also validated by the image of Figure 3.4 which was taken on a typical weekday at peak time.

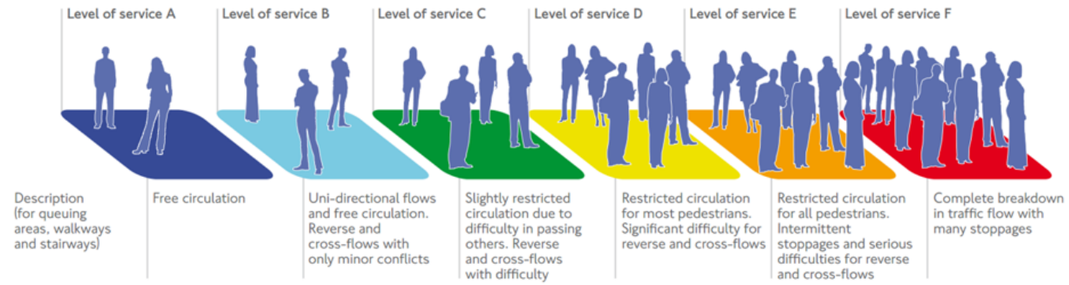

Figure 3.2: Fruin's definition of Level of Service for walkways

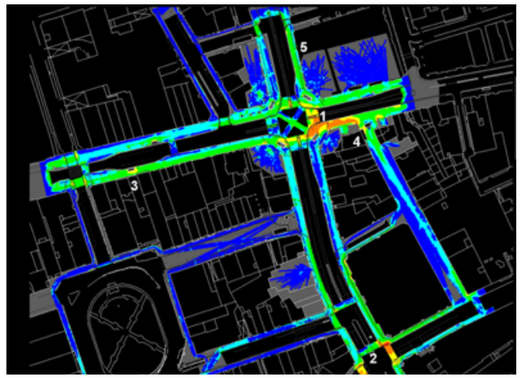

Figure 3.3: Fruin's Level of Service for walkways for the peak 15 min (18:15-18:30)

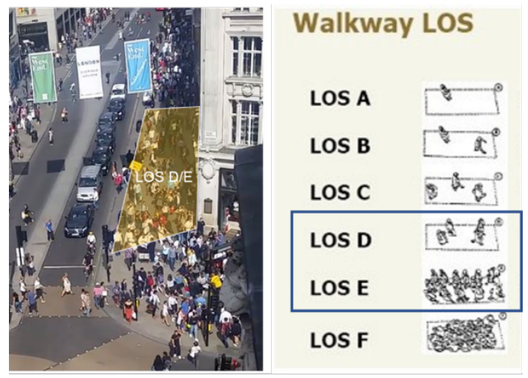

Figure 3.4: Visual validation of busiest footway

On Regent Street South queues at crossings result visually validated as well (2).

As observed, the pinch point produced by the reduced footway width and the presence of the bus stop on Oxford Street West – South footway generates higher densities (3). Similarly, at the north Argyll Street access the pinch point caused by the combined presence of active frontage and the central stand produces higher densities as well (4). Busy conditions were also observed on Regent Street North – East footway and are shown in the simulation (5).

4. Conclusions

The methodology used for the derivation of the O/D matrix introduced an innovative data collection method into the pedestrian modelling industry. The Wi-Fi survey provided valuable information for the generation and validation of model assumptions such as: weekday and weekend comparison, peak times, O/D matrix, pedestrian speeds and proportion of commuters.

The combination of traditional and innovative data collection methods was successful in the calibration of the 2017 base model (R-Squared of above 0.96 and GEH < 5 for most measured flows). Visual validation of simulated densities was also considered acceptable.

It can be concluded that the combination of camera counts and Wi-Fi surveys provide the modeller with an improved understanding of the movements within the study area with the possibility to investigate variations of several parameters over a longer period. This in the pedestrian modelling industry is crucial to include for demand variations and special events. For example, the survey highlighted the impact of a station on fire event and the relative dataset could be used to plan for such events. Therefore, the availability of more data can make assumptions more robust thus increasing the chance of obtaining more accurate future predictions. Hence, this is the goal the industry should work towards.

The work undertaken is a first step towards the inclusion of innovative technologies into the industry's standard approach. Future deployment and testing will be crucial to achieve the standardisation of the approach related to the data gathering, the data processing and the modelling with these technologies.

Acknowledgements

We thank the Crown Estate for funding this research and especially Peter Bourne for his constant support which was crucial in enabling this work.

We thank Lindsey Briggs and Eka Hintaran from Atkins for assistance with the data analyses and Chris Greenwood and Alex Pye from Atkins for their comments that greatly improved the manuscript.

We would also like to show our gratitude to Paul Neve from IDWE and his team for their patience during overnight installations and Francesco Hofer and Daniele Sala from Accuware for their prompt technical assistance.

Originally published as: Angelelli F, Morrow J, Greenwood C. The potential application of Wi-Fi data in the development of agent based pedestrian models. Proceedings of the 46th European Transport Conference, 10-12 Oct 2018, Dublin, Ireland © AET. Used with permission.

References

[1] P. K. Still, Crowd Dynamics, University of Warwick, Department of Mathematics, 2000.

[2] L. A. Alvarez P, Big data helps pedestrian planning take a big step forward, CIHT's Sustainable Transport, Network Management & Operations and Urban Design panels, 2015.

[3] Accuware Inc, 2017. [Online]. Available: https://www.accuware.com/.

[4] J. Martin, T. Mayberry and C. Donahue, "A Study of MAC Address Randomization in Mobile Devices and When it Fails," US Naval Academy, 31 March 2017. [Online]. Available: https://arxiv.org/pdf/1703.02874.pdf.

[5] P. Fuxjaeger and S. Ruehrup, "Towards Privacy-Preserving Wi-Fi Monitoring for Road Traffic Analysis," 22 February 2018. [Online]. Available: https://www.researchgate.net/publication/305877717.

[6] Open Mesh Inc, Open Mesh, 2017. [Online]. Available: https://www.openmesh.com/.

[7] LU, RODS data or Oxford Circus Station, 2016.

[8] Arup, The Impact of Crossrail on Visitors Numbrrs in Central London, London, 2014.

[9] R. Hartley-Parkinson, "Metro," Associated Newspapers, 11 August 2017. [Online]. Available: https://metro.co.uk/2017/08/11/oxford-circus-and-bakerloo-lines-closed-because-of-tube-fire-6844879/.

[10] J. J. Fruin, Pedestrian Planning and Design, 1971.

Safety by Design - The New Intake at John Hart Generating Station Project

Alexei V. Maiorov

M.Sc. Department
Head - Civil/Structures
Clean Power, Vancouver, BC, Canada

Arif. Kartawidjaja

M.Eng, M.Sc Sr. Civil-Structural Engineer
Clean Power, Vancouver, BC, Canada

Katarzyna Gdela,

Ph.D. Structural-Civil Engineer
Clean Power, Vancouver, BC, Canada

Abstract

The new 135 MW hydroelectric generating station has replaced the 70-year-old plant at BC Hydro's John Hart facility adjacent to a provincial park on Vancouver Island in British Columbia, Canada. InPower BC (entity owned by SNC-Lavalin) was selected to design, build, partially finance and maintain for 15 years the BC Hydro owned and operated new facility.

Initial design of the intake considered penetrating the dam at location with reservoir depth of 24m. Review of the concept as part of its design-build mandate concluded shallow water construction will be safer and more economical. The new intake was re-located upstream of a shallower monolith of the dam, which was strengthened to meet the dam safety requirements. The work had to be carried out in an existing reservoir with strict controls against contaminating the water. The design-built approach included development formalization and strict enforcement of a detailed construction sequence.

The paper describes the design-build process encompassing safety-by-design leading to successful construction and commissioning of the new intake.

Keywords

Safety by design; Intake; Design stages; Construction sequence

1. Introduction

Safety by design concepts allow design professionals to participate in enhancing site safety while ensuring a safe design of the structure itself. Designers should always consider how their design will affect the health and safety of those who will interact with the structure throughout its life. This means thinking about design solutions for reasonably foreseeable hazards that may occur as the structure is built, commissioned, used, maintained, repaired, refurbished or modified, decommissioned, demolished or dismantled and disposed of. Safety by design becomes even more important when the design work involves modification of existing structures without interrupting their operations as was the case in the John Hart Generating Station Replacement Project.

Built from 1946 to 1953, located approximately 6 km from the City of Campbell River downtown area, on Vancouver Island in British Columbia, Canada, the 126 MW John Hart Generating Station was nearing the end of its life cycle when BC Hydro decided to replace it. InPower BC (a wholly owned entity of SNC-Lavalin Inc.) was selected to design, build, partially finance and maintain for 15 years the new facility which is about 135 MW. The existing generating station included the main concrete dam, a power intake, above ground penstocks and a surface powerhouse. The replacement project involves construction of a new intake, a power tunnel, and an underground powerhouse, as well as removal of existing surface powerhouse and penstocks (Figure 1).

This paper describes the design of the new intake which involved a three-phase safety by design process aimed at remediating risks related to structural integrity of the new structure, as well as those pertaining to the safety of the existing dam, the geotechnical conditions, the construction methods and capacities, and the project management.

2. The New Intake and Outline of the Design Process

As per the owner's requirements, the new intake was required to be equipped with the following facilities:

- A trash rack, to prevent large debris such as logs from entering the turbines
- A maintenance gate (INMG), to allow servicing of the power intake operating gate
- An environmental flow release system (EFRS) and a low-level outlet (LLO)
- An operating gate (INOG), normally open during operation and only closed during tunnel maintenance, but capable of closing in an emergency during operation

All these structures/requirements had to be integrated with the project's existing head-work structures, particularly the concrete gravity dam. A three-phase approach was employed to conceptualize, design and construct the new intake while ensuring the safety of the existing structures.

In the pre-design phase (Phase 1), the owner's design concept was examined in detail. Historical information, including the as-built design documentation, was obtained and reviewed, and the as-built conditions were assessed through site visits. Face to face interviews with operation and maintenance personnel were conducted. Preceding years' dam safety reports and dam stability review reports were studied, and the instrumentation data was analyzed.

Subsequently, in the conceptual and schematic design phase (Phase 2), alternative schemes for layout of the new intake were developed and designed preliminarily. The alternatives were first discussed internally, and then with the contractor. The constructability review, the cost of construction, hazard identification and hazard analysis were performed. This was followed by a number of risks workshops involving the owner of the dam, the Canadian Dam Association (CDA) dam safety officers, and the power plant operation and maintenance team. Layout details, construction steps, and potential hazards were discussed. Rigorous consideration was given to possible ways of eliminating or minimizing the identified hazards.

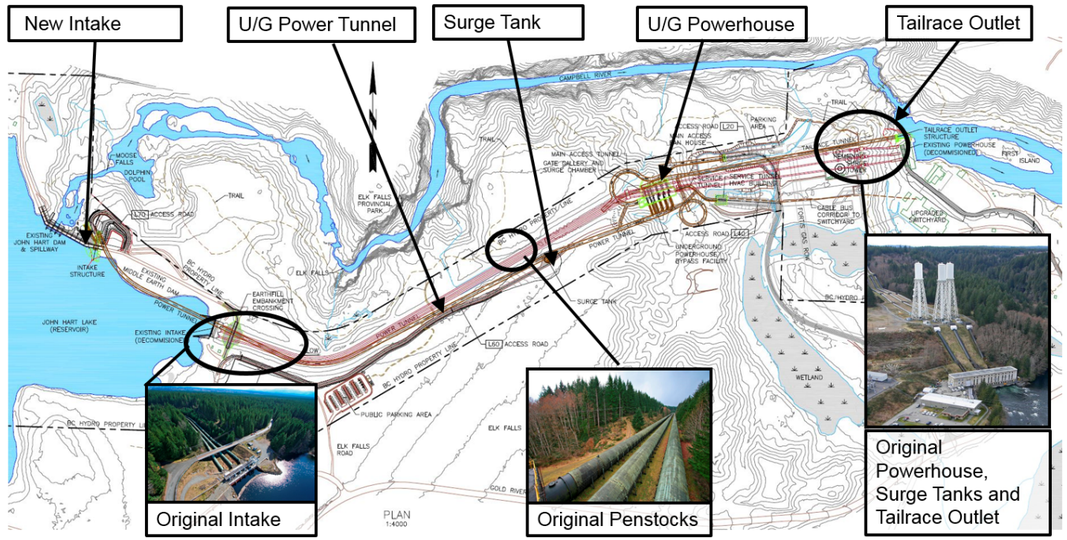

Figure 1: John Hart Generating Station - original and new layout

Finally, in the design and construction implementation phase (Phase 3), the intake construction sequence methodology was elaborated together with the contractor, establishing a high level of clarity for the construction-design team. The construction methodology was formalized in the form of drawings and agreed upon with the owner. The contractor was mandated to follow the agreed construction sequence, which included eight distinct construction stages considered by the designers. Each stage required addressing in the design the stage-specific safety risks.

During construction, the team was well aware of the construction procedure and risks involved. Any deviation from the design-assumed conditions found during the execution was communicated to the designer and the owner, and it was ensured that design modifications driven by site conditions did not increase risk.

The three design phases are described in detail in the following sections.

3. PHASE 1: Pre-Design

The existing concrete dam, which forms part of the John Hart facility, was built in the early 1940's and is an extreme consequence dam (as per Canadian Dam Association guidelines). Any uncontrolled release of all or part of the water impounded by the dam, whether caused by a collapse of the dam, is considered unacceptable. Consequences of failure related to any changes to the dam must therefore be carefully evaluated. This was an important consideration as the new intake was to be built close to, and integrated with, the concrete dam.

In the pre-design phase, our design and construction teams reviewed the constructability, safety and reliability aspects of the owner's proposed design concept which considered the new intake to be integrated with dam block #6 (Figure 2). The intake was proposed to be constructed at the bottom of this block (24 m below water level) with the gate structure placed on the upstream face. The water passage was to be excavated partly through the dam body and partly in the foundation rock. The proposed water passage dimensions would have left only a marginal wall thickness of the original block at its sides. Stability of the block was suggested to be secured by anchoring the intake water passage invert slab to the rock. The tunnel was proposed to be lined with concrete and secured to the dam concrete. All work was visualised to be done from within a 7.5 m radius caisson-like large watertight chamber stapled to the existing dam face and open at the top for access. Built-up steel sections were to be used to assemble the half circular segments which formed the arching cofferdam.

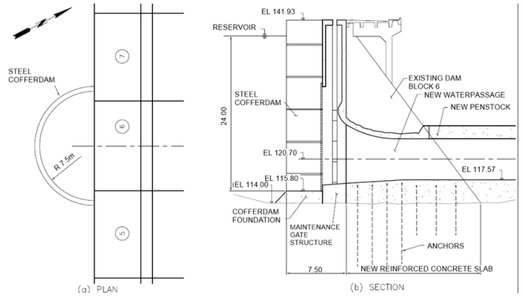

Figure 2: The owner-proposed intake design concept -plan and section.

In the pre-design phase, the owner-proposed design was subjected to a rigorous evaluation. The available historical information was obtained, and current site conditions were assessed through site visits. All the available dam safety related information was compiled and analysed, along with the latest instrumentation data. Further insight was gathered from the operation and maintenance personnel.

All the available information was synthesized and a detailed assessment of the owner-proposed design of the intake was undertaken. The assessment included dam safety aspects, design and construction considerations, construction cost and related risks. It was concluded that it would be safer and more economical to relocate the new intake to a lower height dam block which would allow for construction in shallower water. Dam block #2, with a height of 8 m, was selected, which also offered better access (Figure 3)

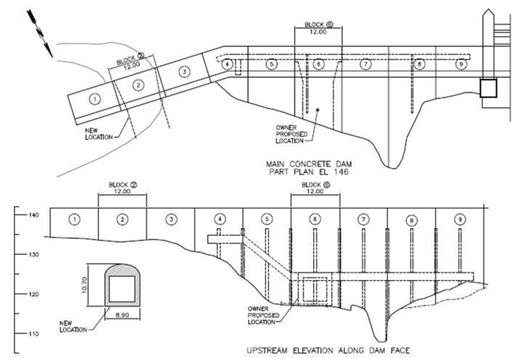

Figure 3: John Hart Generating Station existing main concrete dam with indicated initial and final locations of new intake.

4. PHASE 2: Conceptual and Schematic Design

The conceptual and schematic design phase was started by a detailed assessment of conditions around block #2. The available documents did not provide conclusive information about the exact level of rock foundation. Two scenarios were therefore considered: complete removal of block 2 or excavating a tunnel underneath. The second scenario was more attractive from a safety point of view, as it allowed the structural addition to first be built to the face of block 2, installing gates and then completing the tunnel. This scenario also ensured that the reservoir water was constantly blocked by two protective barriers throughout the construction of the intake.

Due to the safety rating of the dam and the owner's requirements, parts affected by construction activities were to comply with the minimum seismic design criteria at maximum design earthquake (MDE = 0.66g). To meet the requirements, the dam blocks 1, 2, and 3 were upgraded providing adequate structural performance during construction as well as operation.

Figure 4 shows the final concept, with the results of safety by design consideration implemented. In this concept, the new intake was to be built under the protection of a temporary steel pipe cofferdam erected upstream of the main concrete dam blocks 1, 2 and 3. The intake consisted of the following components: the intake maintenance gate structure, the intake tunnel, the intake operating gate structure, and the upper bend structure of the power tunnel shaft. Other permanent works included modifications to the existing concrete main dam, and construction of an abutment wall linked to block 1.

This phase was concluded by developing a specific construction sequence which formed the basis for detailed design of the structure.

5. PHASE 3: Detailed Design and Construction

The detailed design focused on enhancing structural, construction and operational safety. The design process was iterative and interconnected with fine-tuning of the construction sequence; close interface and collaboration of the construction team was crucial and was ensured at all times. The resulting construction methodologies gave the contractor a head start on how to de-risk construction activities and were carefully followed during the lifespan of the project. At the same time, the structures were designed to suit the construction sequence, taking cognisance of the

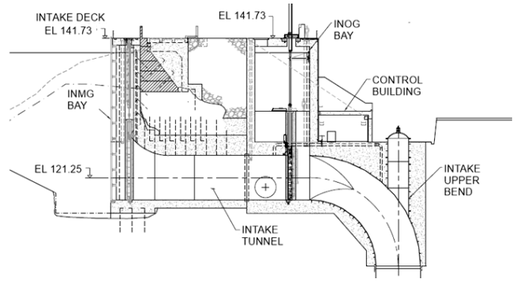

Figure 4: Final concept of the new intake.

risk associated with each construction phase.

5.1 Design Development

5.1.1 Steel Pipe Pile Cofferdam

The cofferdam was designed to be constructed upstream of dam blocks 1 to 3 to provide a dry space during the construction of the intake including the Maintenance Gate (INMG) bay structure. The cofferdam was also required to act as the first barrier against uncontrolled release of water from the reservoir during construction of the intake. The following risks and design considerations were identified and addressed within the detailed design process:

- Loss of water tightness and leakage into the work area through the interlocking piles or the rock sockets
- Structural failure of the steel structure or rock supports under the hydrostatic load
- Structural failure during design basis earthquake (DBE) event
- Constructability and access to accommodate contractor's needs
- Risk of contamination of the reservoir water (which would have affected the city's drinking water supply) during all construction stages.

The cofferdam was designed and constructed using interlocking hollow steel pipe piles driven into bedrock and a steel bracing system installed at the top of the pile wall, above the water level. The structure created a temporary dry enclosed area, allowing adequate space for construction activities associated with building the maintenance gate structure upstream of block 2. The cofferdam was equipped with 2 sealing cells at both ends, adjacent to blocks 1 and 3 and connecting to the dam, to prevent water leakage at the interfaces. Design of the bracing system considered construction access requirements and was optimized without compromising construction safety and ensuring structural stability of the cofferdam and the adjacent earth

fill dam. Finite element (FE) based structural analyses were used to design the cofferdam and the bracing system for all anticipated construction stages. These analyses also allowed the designers to benchmark deformation measurements for safety monitoring during dewatering and the construction period. An example of the FE analysis of the cofferdam model is shown in Figure 5.

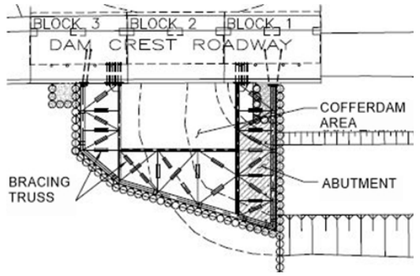

Figure 5: Intake cofferdam layout and FE element model.

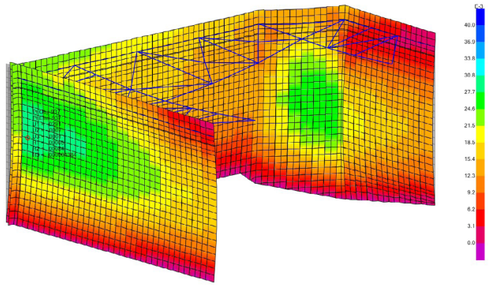

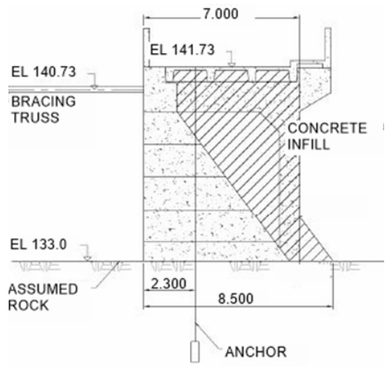

Figure 6: Block 3 dam modification.

5.1.2 Main Concrete Dam Modifications

Dam blocks 1, 2 and 3 were modified to enhance stability during normal operating conditions (after modifications) as well as for the construction period. The following risks were identified and addressed during the detailed design:

- The need for improvement of the capacity of the main deck to accommodate heavy construction vehicles
- Risk that at the start of construction, excavation of downstream backfill might disturb dam stability
- The possibility of unfavorable, lower than assumed rock foundation elevations

The dam blocks were modified by placing mass concrete infill below the deck level on the inclined downstream face (Figure 6). The increased weight improved stability safety factors and enhanced the deck's live load capacity, allowing for operation of heavy construction equipment. The bracing frame was proposed to be anchored in the newly placed infill of the blocks.

In addition, a post tensioning system was designed to improve stability of block 1 and 3 during construction while the intake cofferdam was in place and dewatered and transferred loads directly onto the upgraded blocks. After completion of construction and removal of the cofferdam, the anchors were proposed to be distressed and grouted to act as passive anchors for the MDE conditions.

Drilling and coring though the existing concrete of blocks 1 and 3 also allowed an assessment of concrete quality and verification of the rock-concrete interface. The data received was vital to advance the detailed design of the intake as the feasibility for tunnel excavation below block 2 was confirmed.

5.1.3 Intake Abutment

The intake abutment was designed in front of the dam block 1 as a concrete gravity structure, built inside of the cofferdam and 1 m from the edge of the intake approach channel (Figure 7). During the conceptual phase, it was identified that a permanent retaining structure that will support the adjacent earth dam after decommissioning of the cofferdam is required to improve structural, public and operational safety of the project. The risk was that the adjacent earth dam might collapse into the intake approach channel and lead to uncontrolled water release from the reservoir. Additional safety concerns incorporated in the detailed design were related to a possibility that intake channel rock excavation overbreak might undermine the intake abutment foundation. The rock foundation level of the abutment was confirmed during pipe pile installation of the cofferdam. Rock anchors are used to provide stability of the

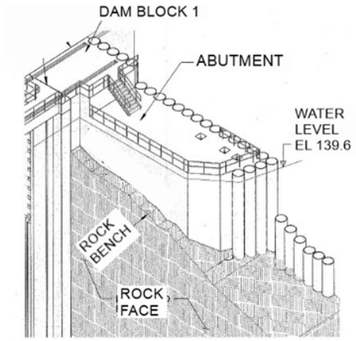

Figure 7: Intake abutment isometric view.

abutment for the considered design basis earthquake (DBE) during construction and MDE during operation.

5.1.4 Intake Maintenance Gate Bay Structure and Intake Tunnel

The Intake Maintenance Gate Bay structure (INMGB) was designed at the upstream face of block 2. The stability requirements imposed on the existing structures affected by construction activities introduced the necessity of structurally integrating the existing block 2 with the new INMGB structure. It was further discovered that, to ensure stability of this composite structure, the intake tunnel located directly behind the INMGB structure needed also to be integrated. The detailed design additionally addressed the following safety issues and structural integrity concerns:

- Possibility of large deformations due to MDE, hindering operation of the gates
- Uncertainty if the rock remaining between block 2 foundation level and the tunnel soffit would be competent enough to support the dam's weight
- Possibility of dam block settlement during tunnel excavation
- Accessibility of space for rebar placement at interface with INMGB and tunnel liner
- Consideration that rock plug removal explosion waves might damage the gate and concrete structure.

The composite structure was designed based on results of 3D finite element analysis aimed to ensure structural adequacy while accounting for and elaborating safety concerns and constructability (Figure 8).

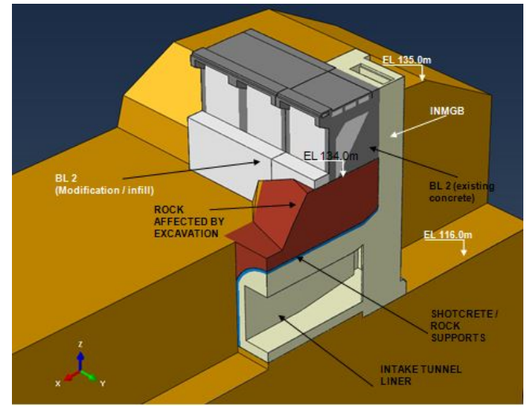

Figure 8: FE model of composite structure: INMBG.

5.1.5 Intake Operating Gate Bay Structure and Intake Control Building

The reinforced concrete gate tower structure houses the operating gate (INOG) and provides a foundation for the hydraulic gate hoist; it is equipped with access stairs and maintenance platforms. The intake operation control room was securely positioned between tower buttress walls supporting the INOG Bay structure on the downstream side. The detailed design considered the following safety issues:

- The possibility that the gate may not close if extensive deformation occurs after MDE
- The possibility that water may leak through the chamber wall
- The risk that rock elevation might be lower than assumed

The reinforced concrete structure was designed to remain elastic during MDE to ensure that the permanent deformation would be small and the gate can close after an MDE event.

5.1.6 Upper Bend

The Upper Bend structure was located on the downstream side of the INOG Bay structure. The design risks and design considerations for the Upper Bend were identified as follows:

- Power tunnel water filling via cracked gate will introduce a high velocity water jet that could result in premature concrete erosion in the long run.
- Concrete formwork installation and removal located at the top of the 90 m depth intake shaft will cause a safety hazard.

> Emergency water passage closure and rapid dewatering of the tunnel to be considered in structural design.

To address safety issues, it was decided to install steel liner in the transition section of the water passage (from rectangular to circular) and the power tunnel shaft bend. The steel liner was designed as a “stay-form” feature equipped with drainage holes to prevent buckling during rapid dewatering. The reinforced concrete encasement structure was confined in rock excavation and was designed to withhold the dewatering loads.

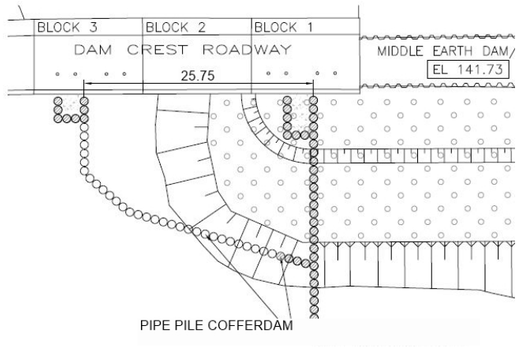

Figure 9: The cofferdam pipe pile layout.

5.2 Construction Progress

5.2.1 Installation of Silt Curtains and Erection of Pipe Pile Cofferdam

The first activity in the construction of the new intake was to install the cofferdam. Pipe piles were to be driven into the rock (Figure 9).

Prior to any other work a silt curtain was installed to contain any contamination of the water during pile construction and to prevent any hazard to public safety until completion of the intake construction. The new location of the intake allowed for a bigger footprint of the cofferdam, thus reducing risks associated with work in a confined space. Additionally, the newly selected location allowed safer and easier access from the dam crest and the abutment. During this construction stage specific site data was used to validate and, if necessary, to update the design.

5.2.2 Main Dam Modifications

The second milestone was to upgrade blocks 1, 2 and 3, improving their stability and allowing for their use as anchor block and as a support for the cofferdam bracing system. Dam blocks 1 and 3 were outfitted with post-tensioned

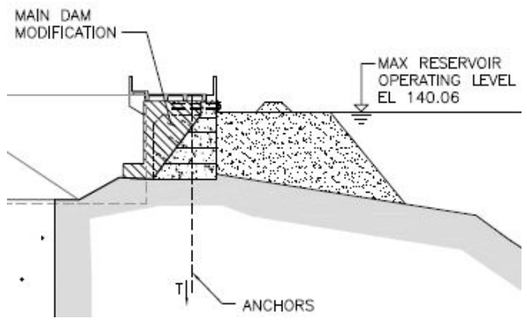

Figure 10: Main dam block 1 and 3 modification.

anchors (Figure 10). Concrete cores obtained during the installation of the anchors allowed for verification of design parameters such as strength of concrete, cohesion at the concrete lift joints and rock elevation underneath the dam blocks. The mass concrete infill placed below the bridge deck of blocks 1, 2 and 3 (Figure 11) also increased the live load rating of the bridge deck. At this stage, the reservoir was still retained by dam blocks 1, 2, and 3 as the cofferdam was not dewatered. The interlocked pile wall was not subjected to unbalanced load conditions yet.

5.2.3 Dewatering of the Cofferdam and Abutment Wall Construction

This stage of construction involved dewatering the cofferdam interior space, excavation of the overburden material, and the construction of the Intake Abutment structure.

Prior to these activities, the design cofferdam steel bracing frame was installed (Figures 5 and 12) The bracing frame was designed so that the dewatered cofferdam structure could support the unbalanced reservoir water and pressure from the adjacent earthfill dam during the remainder of the construction (Figure. 13).

5.2.4 Rock Excavation for Intake Operating Gate Bay Structure and Approach Channel

At this stage of construction, rock was excavated under protection of the cofferdam (Figure. 14). The sensitive rock excavation was performed at a slow rate. Three times the standard number of shearline drillings was done to avoid any overbreak that would undermine the abutment foundation and affect rock plug integrity. With a little delay, the rock was excavated at the downstream side also.

Figure 11: Dam blocks 1, 2 and 3 mass concrete placement is in progress.

Figure 12: Installation of the cofferdam brace.

Figure 13: Dewatered cofferdam area.

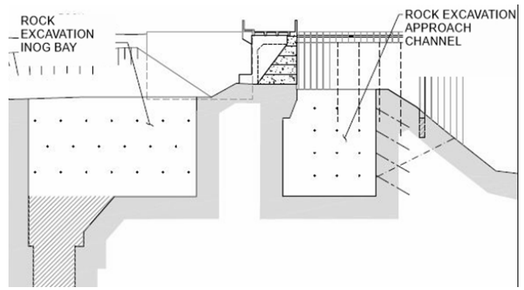

Figure 14: Approach channel rock excavation.

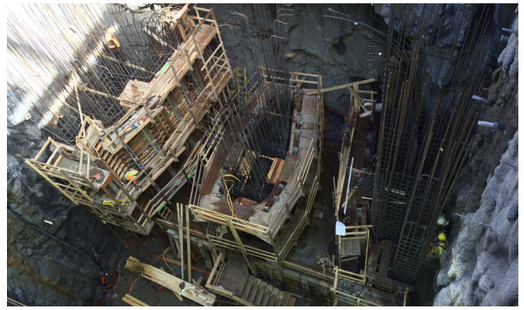

Figure 15: Construction of INMG bay.

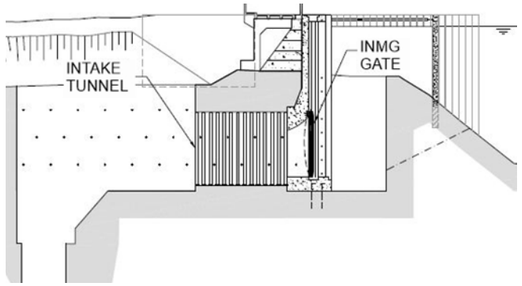

Figure 16: Completion of the intake tunnel and upper bend shaft excavation.

5.2.5 Construction of INMG Structure in Front of Block 2

During this stage of construction, the maintenance bay gate structure was built in front of the dam block 2, adjacent to the abutment block constructed earlier. Gate guides and trash rack embedments were installed and the second stage concrete was placed to secure gate guides and trash rack embedments.

The tunneling started from the downstream side of the dam under the protection of two water isolation barriers - the cofferdam and the rock plug below block 2. The backhoe ramming technique prevented risk associated with rock blasting under the existing concrete dam.

Figure 17a: Excavation of the intake upper bend shaft excavation and construction of intake tunnel

5.2.6 Completion of Intake Tunnel and Excavation of Intake Shaft Upper Bend

The maintenance gate was installed at this stage to provide a second barrier from the reservoir (Figure 16). In the closed position, this gate was meant to prevent an uncontrolled release of reservoir water in the unlikely event of a cofferdam breach during/after an MDE event.

Tunneling for the intake water passage was completed (Figures 16, 17a, 17b). Steel sets were installed along the excavated passage as a safety back up feature to complement the already provided rock bolting. The water passage was lined with reinforced concrete.

Figure 17b: Excavation of the intake upper bend shaft excavation and construction of intake tunnel

Figure 18: Intake structure before cofferdam removal.

5.2.7 Cofferdam Removal, Intake Channel Rock Plug Blasting, Construction of INOG Bay Structure, Upper Bend and Intake Control Building

During this stage of construction, the cofferdam area was watered up (Figure 18). The top brace steel frame was removed, and the divers cut the pipe piles to suit rock level and hydraulic profile of the intake approach channel (Figure 19). Blast protection was installed in the front of the trash rack. The intake channel rock plug upstream of the Maintenance Gate Bay Invert was eventually blasted. Simultaneously of the INOG Bay structure, Intake Shaft Upper Bend and Intake Control Building, and EFRS and LLO valve house were constructed downstream of the dam.

After the completion of the INOG Bay structure, the downstream side of block 2 was back-filled with rockfill to provide access from the Main Dam crest and Intake Maintenance Gate deck to the INOG deck. Platform and stairs were installed. The intake operating gate was installed at this stage to provide a second barrier from the reservoir. Debris boom was installed at the upstream side of the intake structure.

6. Remarks

As a result of the safety by design process, the overall risks of the intake design were minimised by eliminating hazards or applying the right hazard controls. Early project collaboration between designers and construction team allowed for the design to systematically and comprehensively identify, assess and eliminate or mitigate hazards to people, environment, project assets and reputation of the project.

When it comes to achieving safe design, responsibility rests with all groups, or individuals, who control or manage design functions. These include:

- Architects, designers, and draftspersons, who carry out the design
- Individuals who make design decisions during any of the lifecycle phases of a project such as project managers, engineers, manufacturers, suppliers, installers and builders
- Anyone who alters a design
- Building service designers, or others designing the fixed plant such as hydro mechanical equipment, balance of plant, ventilation and electrical systems

Safe design can be achieved more effectively when all the parties who control and influence the design outcome collaborate on incorporating safety measures into the design.

Figure 19: Silt curtain performance after cofferdam removal, INOG structure under construction.

Acknowledgements

The authors would like to thank the owner of the John Hart Generating Station, BC Hydro for the support and permission to share the gained expertise and work described in this paper.

The authors would also like to thank the John Hart Generating Station Replacement Project team and the join venture partner for their contribution in safe delivery of the project.

This paper was presented previously at International Commission on Large Dams (ICOLD) 2019 Annual Meeting and Symposium, Ottawa, Canada and published in the proceedings of the symposium: Sustainable and Safe Dams Around the Word – Tournier, Bennett & Bibeau (Eds) ©2019 Canadian Dam Association, ISBN 978-0-367-33422-2. Used with permission.

Mechanical and Electrical Design | 007

Mechanical Waste Gathering System (MWGS), Alternate Retrieval of Hanford Tank Waste

Doug Reid

Mechanical Engineer
Washington River Protection Services
Richland, WA, USA

Kayle Boomer

Senior Technical Advisor
Washington River Protection Services
Richland, WA, USA

Thom Myer

Washington River Protection Services
Richland, WA, USA

Jeffrey Rambo

Technical Program Manager for Tank Retrievals
U.S. Department of Energy (DOE), Office of River Protection

Gordon Crawford

Chief Engineer
Nuclear
Richland, WA, USA

Andrew Barr

Managing Director
Barrnon Ltd
UK

Abstract

Hanford has 149 underground single shell tanks, of which several have known or suspected leak sites. Sluicing with large volumes of solution in compromised leaking tanks is not desirable due to the risk of environmental release. To address the complex retrieval of hardpan nuclear waste in Hanford's single shell tanks, a Mechanical Waste Gathering System is being developed and tested, which breaks up the waste and moves it to the surfaces without the introduction of liquid to the tank bottom. To improve the removal of hardpan tank waste, Washington River Protection Solutions (WRPS) has leveraged industry knowledge and previous experience to identify a solution. This technology will provide another option for the technology toolbox at Hanford.

Keywords

Nuclear Waste; Retrieval; Innovative Technologies; Environmental Cleanup

1. Introduction

At the Hanford site, there are 149 underground single shell tanks (SSTs). Waste retrieval from these tanks pose many complex challenges due to the fact that the waste exists in multiple phases. The waste varies from liquid to sludge to hard concrete-like solids such as salt cakes and hardpan, each requiring their own removal strategy. In addition, many of these SSTs are known to or suspected to have leak sites. Some Hanford underground storage tanks have leaked (HNF-EP-0182, 2018) and there are concerns about actual or potential leaking of tank contents as the result of traditional waste retrieval methods, including sluicing.

The current practice for sludge and solids retrieval from the SSTs involves sluicing with either large volumes of supernatant or water. This approach is ineffective for hardpan coated tanks and is undesirable for leaking tanks as the addition of large volumes of liquid to leaking tanks has the potential to lead to an environmental release. A retrieval system capable of removing hardpan waste without the addition of liquid to the tanks is needed.

To improve the removal of hardpan tank waste at the Hanford site, without the introduction of liquid to the tank bottom, Washington River Protection Solutions (WRPS) has leveraged industry knowledge and previous experience to identify a solution. In 2017, at the annual Department of Energy (DOE) Grand Challenge competition, a technology was proposed as a solution to Hanford Tank Farms Mission Need as an idea to improve efficiency of tank retrievals known as the Mechanical Waste Gathering System (MWGS).

This technology uses a rotary cutter (referred to as rotocutter) to break up hardpan waste, a vacuum system to remove it from the tank floor, and an innovative self-contained sluicing system to convey the waste to the surface.

Atkins and Barrnon Ltd have developed many innovative remote solutions to waste retrieval problems at the Sellafield nuclear complex and at other commercial nuclear reactor sites in the UK. Atkins and Barrnon Ltd collaboratively developed the MWGS to a proof-of-concept level and it is being subsequently matured with DOE and WRPS financial and technical support.

In selecting the hardpan retrieval method, various technologies were studied including many that had been tried in nuclear waste tanks and many that had not. In evaluating these retrieval technologies, there are generally two key components:

- The end effector - used to locally free the hardpan from the bulk material
- The deployment system - used to position the end effector throughout the tank

Typically, these end effectors include:

- A variety of different mechanical cutting systems
- Sluicing techniques
- A toolkit approach where a variety of end effectors could be deployed from a single platform to suit different conditions within the tank

Typically, these deployment systems included:

- A compact Remotely Operated Vehicle (ROV) suitable for deployment through risers up to 42-inch diameter (the largest liner to date that has been cut centrally in an SST)
- A large ROV suitable for deployment through larger risers which may possibly be off-center in SSTs
- A small folding ROVs for deployment through the smaller original liners in SSTs
- Mast type deployment through large risers of around 42-inch diameter

The development team determined that to best meet stakeholders' expectations for an SST hardpan waste retrieval system the answers to the following four questions should be "yes":

1. Does the system avoid water introduction and therefore minimize the impact of environment impacts to the surrounding environment?
2. Can the deployment system handle end effector reaction forces?
3. Is the overall system robust enough to operate in the hostile SST environment?
4. Is the system compact enough to fit through a 42-inch riser?

The logical approach followed described above is illustrated in Table 1, which demonstrates that a mechanical cutting system sized for the 42-inch riser placed on a compact ROV conceptually answers all of these questions. All other system permutations reviewed do not satisfactorily answer one or more of these questions.

Table 1: Down Selection

Technologies		Does system avoid water introduction?		Can system withstand large reaction forces?		Is system robust?		Is system compact (fits through a 42-in. riser)?	
End Effector Type	**Deployment Configuration**	**Yes**	**No**	**Yes**	**No**	**Yes**	**No**	**Yes**	**No**
Mechanical Cutting		x		x		x		x	
Tool Kit (Commercial Excavator)		x		x		x			x
Sluicing			x	x		x		x	
	Compact ROV	n/a	n/a	x		x		x	
	Large ROV	n/a	n/a	x		x			x
	Mast System	n/a	n/a		x	*	*	x	
	Folding ROV	n/a	n/a	x			x	x	

ROV = remotely operated vehicle.
* = A mast system of this size capable of supporting large cutting forces has not been tested

2. MWGS Development Overview

A rudimentary demonstration was performed of such a system - a rotocutter on an ROV that was shown to successfully break up asphalt and unreinforced concrete substrates. From this demonstration, it was deemed that such a waste retrieval concept may be viable and numerous enhancements to the technology were proposed.

Maturation of this combined rotocutter/ROV system is being performed in accordance with the principles of DOE Order 413.3B to ensure that the critical technology elements (CTEs) of the MWGS are defined and matured. Some of the key CTEs include:

- Rotocutter tool geometry, tool tip design
- System cutting parameters – rotocutter speed versus ROV travel speed
- Bladecutter® - internal sluicing system
- Sluicing control proportional-integral-derivative (PID) loop
- Sensors to protect damage to tank

Accordingly, the technology is being developed in a phased approach to mature the technology to be suitable for eventual deployment in Hanford SST, as follows:

Phase I: Proof-of-principle testing of MWGS in UK

Phase II: Refinement of MWGS systems and endurance testing in UK of rotocutter

Phase III(a): Recombination of MWGS into a composite system including full umbilical management system and further refining elements with final testing in UK

Phase III(b): Full recombination of MWGS including a deployment system and full-scale cold testing and nuclearization in US

After Phase III(b) is satisfactorily completed the system is ready for full active fabrication and deployment.

3. MWGS Description

The MWGS is a robust tracking device (ROV that fits through a 42-inch diameter riser) with a rotating cutting chain with tungsten carbide teeth to break up the waste material. The debris is then vacuumed into a waste receiving vessel. Barrnon Ltd's proprietary Bladecutter® technology further reduces the size of the waste and slurries it up where it is then pumped out of the tank. Figure 1 illustrates the configuration and main components comprising the MWGS.

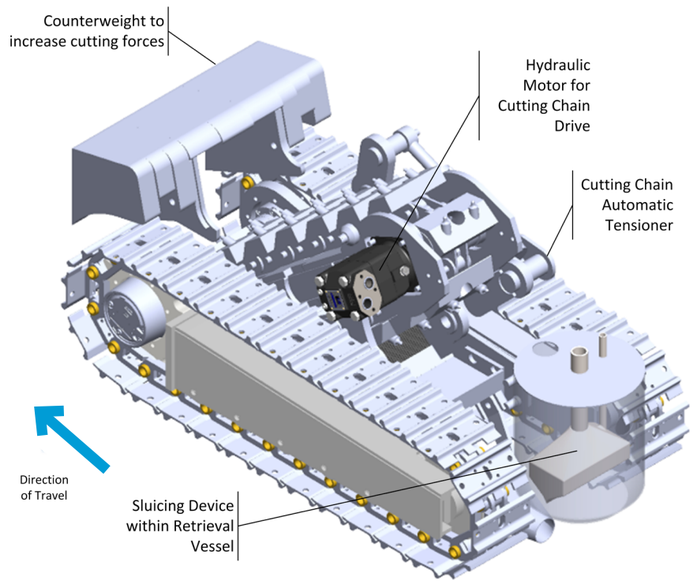

Figure 1: MWGS Phase 1 prototype schematic showing major components

The goals of this project are:

- Leverage industry knowledge and experience
- Demonstrate MWGS effectiveness to mobilize and retrieve simulated waste
- Identify and develop supporting systems that:
  - Convey mobilized waste out of the tank
  - Maneuver around in-tank obstructions (e.g. airlift circulator and miscellaneous debris bound up in waste)
  - Demonstrate full-scale integrated MWGS system effectiveness in a cold simulated waste environment

4. Phase I - MWGS Proof-of-Principle Testing

Prior to Phase I, Barrnon Ltd had performed some rudimentary testing of a rotocutter mounted on a ROV and demonstrated in principle the ability of the technology to break up asphalt and unreinforced concrete. Atkins and Barrnon Ltd therefore determined that this technology was likely suitable for breaking up hardpan wastes in Hanford SSTs.

Phase I was independently funded by Atkins and Barrnon Ltd to demonstrate a proof-of-principle working prototype system capable of breaking up and collecting 60MPa sandstone and unreinforced concrete substrates.

In Phase I, a system was designed and constructed comprising the following key components:

- A ROV with two parallel tracks capable of independent motion
- A rotocutter mounted on the ROV capable of being raised above the floor or lowered into a cutting location
- A vacuum crevice tool mounted on the ROV underneath the rotocutter
- A substrate collection vessel fed by the vacuum crevice tool and mounted on the ROV
- An off-board commercial vacuum connected to the substrate collection vessel
- A proprietary Bladecutter® inside the substrate collection vessel to further reduce the size of the spoils from the vacuum crevice tool using water jets and to subsequently sluice these spoils out of the vessel

- A water infeed and outfeed system to provide a balanced flow of sluicing water in order to allow solids to settle in three tanks in series and return the water for reuse
- A hydraulic power and control unit
- A rudimentary umbilical system
- Overhead and onboard closed-circuit television (CCTV) cameras
- Tank floor detection system
- An operator control station to control the ROV and rotocutter and to view the CCTV camera outputs. This control station was screened off to prevent the operator from directly viewing the rotocutter
- Three 2 m x 4 m test beds with three different substrates, which were chosen to be beyond bounding in terms of strength and toughness:
  - Local (St. Bees) 60MPa sandstone
  - 7:1 Sand to Portland Cement Mix
  - 5:1 Sand to Portland Cement Mix

During Phase I, the following issues were encountered:

- Manual control of the water level in the substrate collection vessel was problematic and on occasions caused overflow of sluice water into the vacuum crevice tool which caused wetting of dry materials and blockage of the vacuum pipe.
- Vacuum crevice tool had no height compliance causing:
  - The tool to be sometimes too high relative to the pulverized substrate below the rotocutter, making effectiveness of the vacuum poor (up to 50% of spoils not picked up).
  - The tool to be sometimes too low relative to the floor, causing the rotocutter to lift and the crevice tool to become damaged.

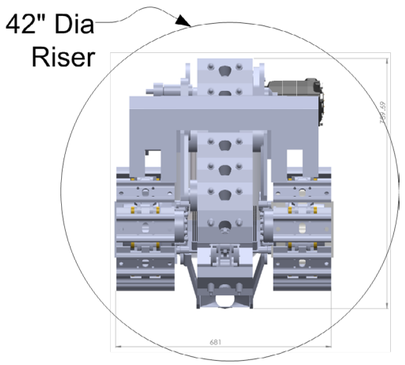

Figure 2: MWGS Phase I prototype lowered through a 42" diameter tube

5. Phase II – MWGS Prototype System Testing

Phase II goals were to incorporate lessons learned from Phase I and focus on refining the design of CTEs, including the waste collection system, the vacuum/sluicing vessel, the remote viewing system, the tank floor protection sensors, and the overall control system. A key decision made during this phase was to decouple the two primary system functions – the rotocutter and the retrieval (vacuum/sluicing) system to allow optimization of each without compromising the other. In particular this allowed a compliant vacuum crevice tool optimization in an open framework without obstruction by the rotocutter. The aspects of the CTEs developed were:

- Establish rotocutter tool life (endurance test)
- Improve vacuum collection system (VCS) pickup efficiency
- Evaluate the capability of MWGS to break up representative substrate simulants
- Test dual metal detecting sensors to ensure the tank floor is not damaged during operation
- Develop the control system
- Develop a PID loop to control water level in the substrate collection vessel
- Demonstrate the ability to remotely operate MWGS via a range of CCTV cameras and remote controls
- Modify the Human Machine Interface to display when either sensor detected metal

One enhancement to the rotocutter ROV in Phase II was the addition of a second tank floor sensor ensuring that the orientation of the ROV did not prevent the sensing of the steel floor. Figure 4 shows these sensors, enveloped in protective nylon shrouds, directly below the ROV counterweight.

Figure 3: MWGS Phase I testing at Barrnon Ltd, UK

Figure 4: MWGS Phase II rotocutter ROV

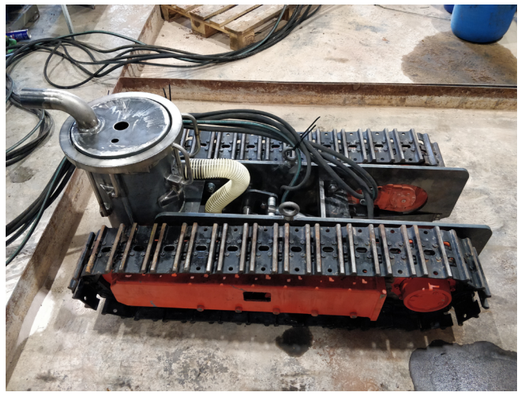

Figure 5: MWGS Phase II vacuum collection system (VCS) ROV

Figure 6 shows a schematic of the enhanced VCS ROV used on Phase II.

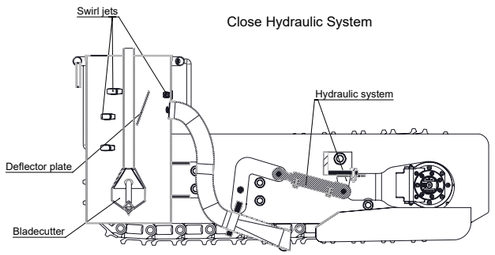

Figure 6. Schematic of Enhanced VCS

Vacuum collection was improved by the use of a compliant mount on the crevice tool, allowing it to ride just above the floor surface and deflector plates between the two tracks to direct the spoils towards the crevice tool (see Figure 7). A number of enhancements were also incorporated into the substrate collection vessel including swirl jets to keep solids suspended and a PID level control to prevent either an overflow from the vessel or loss of pump priming due to the emptying of the vessel.

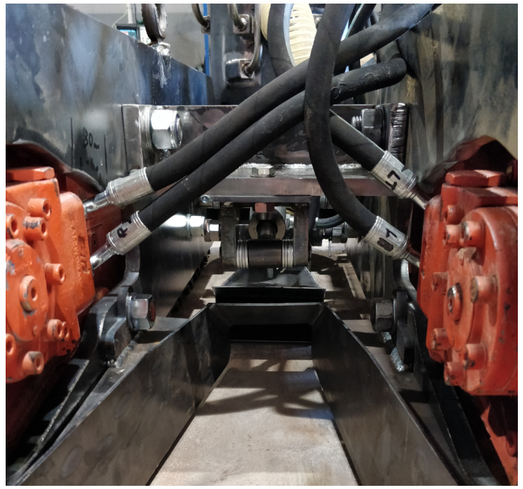

Figure 7: Vacuum collection system (VCS) nozzle and diverter plates.

The vacuum and sluicing systems were shown to be capable of prolonged operation with minimal human intervention. The vacuum material recovery improved from 50% to 80% by weight on a single pass.

Also improved was the sluicing conveyance of recovered material with particle sizes up to 20 mm (0.78 inches) being recovered.

New ROV track hydraulic motors were procured at the start of the test to replace the prior motors that were near end of life. Due to lead times and the limited testing window, it was necessary to procure hydraulic motors with a smaller gear ratio and hence higher output speed. To compensate for this, the oil flow to the motor was reduced to a flow rate that subsequently was found to have a deleterious impact on the motor performance. Even at this lower flow rate, the ROV traverse speed was greater than the rotocutter could break up the waste, causing the creation of particles larger than the vacuum system was able to sweep up. To somewhat compensate for this, the operator was required to "toggle" the drive joystick repeatedly between the drive and neutral position to try and reduce the effective drive speed. Some attendant issues including blockage of the vacuum crevice tool was determined to be mostly as a result of the rotocutter not suitably pulverizing the substrate due to the high ROV speed. After some persevering with this problem, it was decided to procure two new motors with much higher gearing ratios. These new drives performed much better and allowed operation at higher and more practical oil flow rates. With these new drives, the lower traverse speed ensured much more pulverization of the waste by the rotocutter.

Simulants were designed based on available knowledge of tank waste and Pacific Northwest National Laboratory (PNNL) processed knowledge from other waste development work (PNNL-11685, 1997; PNNL-26037, 2016; PNNL-26206, 2017). Figure 8 shows the test bed configuration used in Phase II testing. Recipe 1 was recommended by PNNL for testing. Recipe 2 was

Tray 1	Tray 2	Tray 3
Recipe 1 12.5% Portland Cement 87.5% "Sharp" Sand Water to achieve appropriate "slump"	**Recipe 2** 19% Kaolin 52.5% Plaster of Paris 28.5% Water	**Recipe 2** Includes a small amount of debris - e.g. metal fasteners and metal packing tapes **Recipe 3** 80% Kmag 20% Water

Figure 8: Phase II simulants and test beds configuration

Figure 9: Preparation of test bed 3 with K-mag island

representative of lower strength tank waste (300kPa). Recipe 3 was representative of a bounding high strength tank waste (10-20 MPa). Figure 9 shows the preparation of test bed 3.

6. Phase IIIa MWGS

Phase IIIa testing began in fiscal year 2019 and will further develop the technology readiness level (TRL) of the MWGS. The DOE technology readiness approach is being applied to this work. This next phase of work will include many new design features, enhancements, and testing. An umbilical management study will evaluate methods to effectively manage the challenge of umbilical routing within the tank space. Upgrading of the hydraulic system to allow sustained use of the system is also a goal. The MWGS will be recombined into a single ROV containing both the rotocutter and VCS. Further refinement of the sluicing PID control is another important goal for this next phase of work. Demonstrating the ability to sluice waste simulants to a height of 60 feet is very important in representing the hydraulics of SSTs. Development of an inline macerator to exclude large particles from blocking piping systems is also important. Many other tasks are planned, including evaluating tank sensor systems and using a combination of alarm and interlocked systems that auto-stop the rotocutter on tank sensing.

7. Conclusions

By leveraging industry knowledge and following a disciplined process of increasing the system TRL in carefully planned steps, the WRPS team is developing the MWGS as a promising solution for dry waste retrieval campaigns from leaking Hanford SSTs. This technology will provide another option for the technology toolbox at Hanford. In less than one year, our integrated system testing efforts have led to the combination of several commercial off-of-the-shelf components into a system adapted for the Hanford tank dry waste retrieval mission. At the end of Phase IIIb, the entire system will be at least a TRL 6 and will be ready for turn over to the Retrieval Operations group to begin final testing for deployment.

Acknowledgements

The work described in this paper was performed in support of the U.S. Department of Energy (DOE), Office of River Protection, and Washington River Protection Solutions (contract number DE-AC27-01RV14800).

Originally presented and published as: Reid D, Boomer K, Myer T, Rambo J, Crawford G, Barr A. Mechanical Waste Gathering System (MWGS), Alternate Retrieval of Hanford Tank Waste (19188). Proceedings of the WM2019 Conference, March 3-7, 2019, Phoenix, Arizona, USA

References

1. HNF-EP-0182, Waste Tank Summary Report for Month Ending January 31, 2018, Rev. 361, Washington River Protection Solutions, LLC, Richland, Washington.

2. PNNL-11685, 1997, Retrieval Process Development and Enhancements Waste Simulant Compositions and Defensibility, Rev 0, Pacific Northwest National Laboratory, Richland Washington.

3. PNNL-26037, 2016, Alternate Retrieval A-105 Application Assessment Report, Rev 0, Pacific Northwest National Laboratory, Richland Washington.

4. PNNL-26206, 2017, Evaluation of A-105 Waste Properties and Potential Simulants for Confined Sluicing Testing, Rev 0, Pacific Northwest National Laboratory, Richland Washington.

Structural Design and Assessment	008

Rail Thermal Force Calculations for Continuous Welded Rails (CWR)

Constantin Ciobanu

MRes, CEng, FPWI, MCIHT
Permanent Way Design Team Leader
Engineering, Design and Project Management
Swindon, UK

Levente Nogy

EurIng, CEng, MICE, FPWI
Senior Design Engineer
Network Rail Design Delivery
Birmingham, UK

Abstract

This article describes the behaviour of the continuous welded rail (CWR), concentrating especially on the most sensitive part of the CWR – the stress transition zone, which is continuously being subjected to length variations in response to rail temperature changes.

Although the article refers to the United Kingdom's railway track standards and to the specific conditions of the British track infrastructure, it presents engineering principles that are of interest to a worldwide railway engineering community.

Keywords

Railway track; Continuous welded rail; Stress free temperature; Restrained thermal expansion track model

Winner of the Permanent Way Institution's 2017 Silver Journal Award

1. Introduction

1.1. CWR Track Definition

The restrained thermal expansion track model presented in the article “Rail thermal force calculations for jointed track” (Ciobanu, Nogy - 2017) describes the track response to rail temperature variations and highlights the intricate influence of different track components in this process. In the jointed track, a sufficient temperature variation eventually activates the longitudinal resistance forces along the entire rail length. In ideal conditions and for a homogenous track structure, each rail will have these resistances activated symmetrically relative to the mid-point of the rail and in theory this point is the only section that does not physically move. However, there is a rail length above which, the maximum possible rail temperature variation ΔT_{max} (the largest possible difference between the stress-free temperature and the actual range of rail temperatures experienced on the network), is not sufficient to activate the longitudinal resistance on the entire rail length. On such a length of rail, there will always be a central fixed zone – an area where no track longitudinal resistance is active and neither expansion nor contraction is taking place (Figure 1). Within the central fixed zone, the rail thermal forces are null at a specific rail temperature called the stress-free temperature (SFT). Activation of longitudinal resistance forces only occurs at the extremities of this long rail and these areas are called stress transition (breathing) zones (L_T). A stress transition zone is any section of CWR where the thermal force is variable, the longitudinal resistance (p) is activated and rail movement occurs due to rail temperature variations.

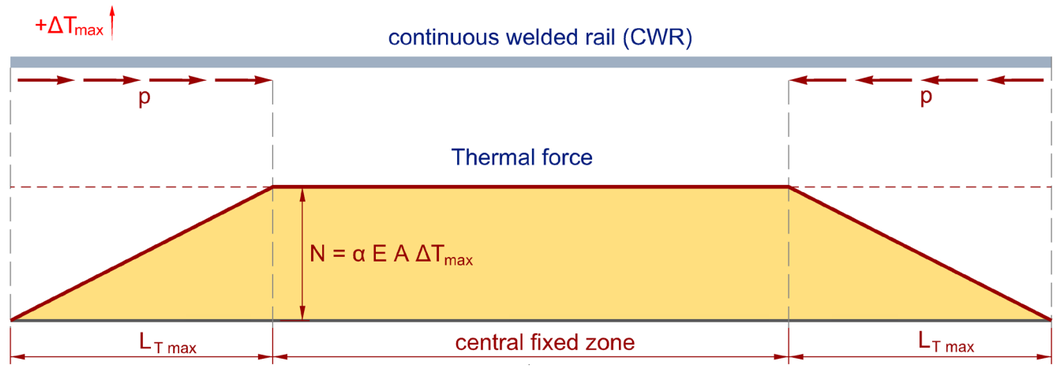

Figure 1: CWR definition

The long rails which contain a central fixed zone of constant thermal force, even for the maximum rail temperature variation, are called Continuous Welded Rails - CWR (AICF - 1959).

The maximum stress transition length L_{Tmax} mainly depends on the maximum rail temperature variation, ΔTmax, track longitudinal resistance (p), rail type, and also considers a set of safety factors. For consolidated ballast this maximum stress transition length is around 90 m, thus defining CWR as any section of non-jointed track over 180 m in length. However, from a maintenance perspective, it is prudent to classify track sections as CWR when these are composed of long rails.

1.2. Stress-Free Temperature (SFT)

On the British railway network the permitted range of SFT is 21°C to 27°C (NR/L2/TRK/3011). When the rail installation temperature is below 24°C the rail is extended by hydraulic tensors or heated along its entire length to reach an equivalent length at which the rail would be when it is at 27°C. If the rail temperature during the works is between 24°C and 30°C the CWR installation can be done via natural stressing (NR/L2/TRK/3011 – 9.2).

The SFT is therefore fixed at installation, with the intention of creating a balance between the potential maximum compression and tension thermal forces in the rail, during the yearly rail temperature variations.

1.3. Stress Transition Zone

At stress transitions the thermal forces are never zero except during installation, through natural stressing. On the central fixed zone, the thermal force (N) is constant and it can be calculated using the following equation:

$$N = \alpha E A \Delta T$$

where α is the coefficient of thermal expansion of steel, E is the Young’s Modulus of steel, A is the rail cross sectional area, ΔT is the temperature difference between the desired stress-free temperature (SFT) and the current rail temperature.

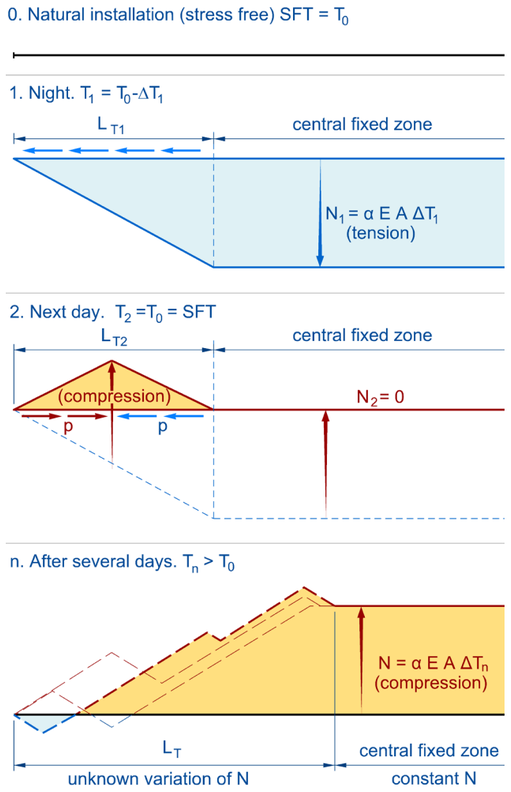

Figure 2: Stress transition zone

Figure 2 shows the development of the transition zone at the free end of a CWR section provided with an adjustment switch. The CWR is presumed installed naturally, at a suitable stress-free temperature T_0. During the night, the temperature falls to a minimum T_1 and in the central zone a constant tension force is developed, since no rail contraction can occur. The rail contracts at the ends of the CWR, gradually activating the track longitudinal resistance (p), and a stress transition zone L_{T1} is developed. In this zone the tension force varies linearly from the tensile force developed in the constant fixed value to zero, at the adjustment switch. This length can be theoretically calculated using the equation:

$$L_{T1} = \frac{N_1}{p} = \frac{\alpha E A \Delta T_1}{p}$$

The next day the rail temperature returns to the stress-free temperature ($T_2 = T_0$ = SFT). On the central zone the thermal force returns to zero. Over the stress transition zone the rail will tend to expand, the longitudinal resistance (p) is activated to oppose this tendency and will retain a variable compression force induced by the increase in temperature from T_1 to T_2. Even though the rail has now returned to the original installation temperature and on the central fixed zone there is no thermal force present, there is a thermal compression force on the stress transition length developed over night due to the temperature increase from T_1 to T_2.

After several days of rail temperature variations, the stress transition zone (L_T) will develop further and its length can no longer be accurately evaluated. The rail thermal force variation over this zone becomes irregular and will never again be null, at least not until a new natural re-stressing is undertaken. Within its length, it can contain higher thermal forces than the ones in the central zone and even have a combination of both compression and tension force sections at one and the same time (Figure 2). In time, the length of this zone can grow up to 90 m, for compacted ballast and rail fastenings able to provide the longitudinal resistance force required by BS EN 13481-2.

This complex behaviour is not prevented by the presence of an adjustment switch at the end of the CWR section and justifies the requirement of the CWR stressing procedures to unclip a rail length assumed to cover the stress transition zone and suspend it on rollers to release the rail of any stress prior to welding. This procedure is in place even for natural stressing – when the central fixed zone is free of any thermal forces (NR/TRK/L2/3011 – 9.14).

The location of the stress transition zone is not only limited to the extremities of a CWR track but it may also be present between two fixed zones inside the CWR (Figure 3).

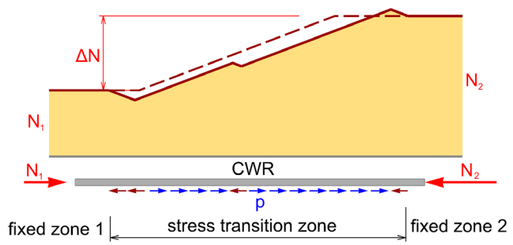

Figure 3: Stress transition zone within CWR

These internal stress transition zones are shorter than the ones formed at the end of CWR and can be generated by several factors which can be categorised into two main groups:

A. Stress Transition Zone Caused by Rail Temperature Changes.

These can be encountered in areas of CWR track where there is a consistent rail temperature difference between adjacent CWR sections:

> Between two CWR sections, each with different stress-free temperatures (SFT). Network Rail UK standards allow a 6°C SFT range, from 21°C to 27°C. For CEN60 rail this is the equivalent of up to 110 kN variation in thermal force which will generate an approximately 13-15 m stress transition zone between adjacent CWR sections installed at 21 and 27°C respectively.

> Tunnel portals. In tunnels the rail is not exposed to sunlight and, for sufficiently long tunnels, the rail temperature is significantly different than that outside the tunnel.

> Transition between sections of track with significant changes in track sunlight exposure – for example the transition from cutting to embankment.

> Transition from white-painted to un-painted rails. The painted rail has a temperature of around 6°C lower than the un-painted one. Hence, a short stress transition zone will develop where this change in rail temperature occurs.

> Transition from exposed to embedded rails (on longer level crossings or embedded rail slab track).

> Passage over a river (on a bridge) – the condensing water and air currents will reduce the rail temperature compared to the track on the abutting sections. The bridge itself also has an influence that is included in the second category of stress transition zones.

B. Stress Transition Zones Generated by Track Structure Changes.

The potential for variation/transition in rail thermal force may be created wherever the track structure changes. For example:

> Track across bridge – the movement bearing of a bridge allows thermal expansion of the structure due to temperature variation. If the track is continuous over a movement bearing, the bridge will tend to move longitudinally the track relative to the adjacent (often embankment) section (Figure 4). This action can significantly change the distribution of the rail axial forces, especially if the rail is directly fixed onto the bridge deck. For short ballasted bridge deck the impact is minimised, however, for long structures, the effect remains significant.

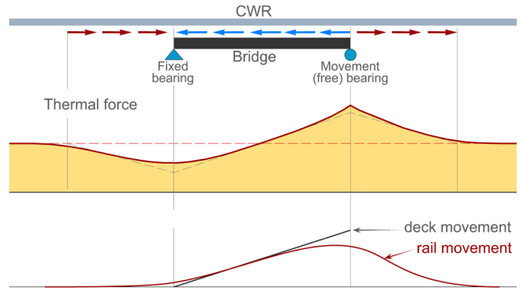

Figure 4: CWR over a bridge

A bridge also subjects the track to variable bending and other actions which influence the variation of the rail longitudinal (thermal) forces (UIC Code 774-3 – 2001).

To reduce the impact caused by the bridge induced forces, the CWR track can be interrupted by the placement of adjustment switches over the movement bearing. However, all the adjustment switches, even in layouts featuring longer switch-type rails (Figure 5) as opposed to the short overlapping rails normally used on the British railway network, create a track geometry irregularity which causes additional dynamic effects at vehicle and track levels, especially at high speed. Modern bridge structures and track can also be designed to optimise and minimise the track-bridge interaction and install continuous welded rails over the bridge (UIC Code 774-3 – 2001, Calçada - 2009). In both cases, with or without the presence of the adjustment switch, the track over a bridge will always develop a stress transition zone.

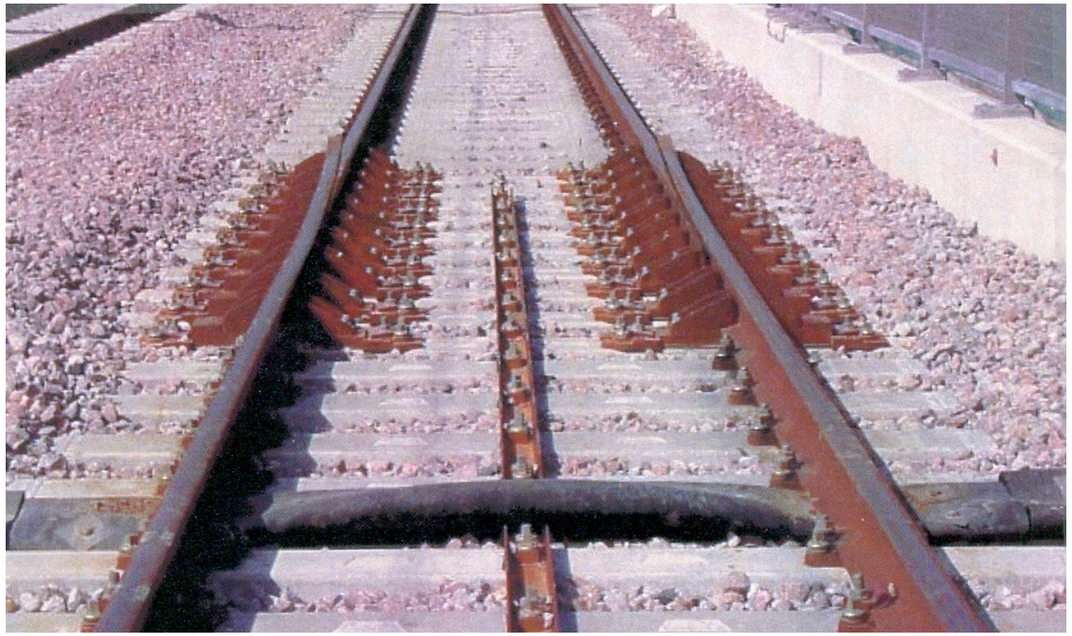

Figure 5: Adjustment switch on LGV line (photo by Nicolas Taveneaux, via Wikimedia Commons)

- Transition from ballasted to slab track or other higher fixity track systems (including glued ballast). In this section, changes in the track longitudinal resistance create the potential for generating a stress transition zone. When this track is in the central fixed zone of CWR the thermal force usually remains constant. If however, this section overlaps with other stress transition zones, it may add an additional level of variation in the rail thermal stress. Abutting sections with different types of sleepers may even have a similar effect.
- Change of rail section – the change in the rail section area changes the value of N even when all the other track parameters are the same. The rail thermal force in a CEN60 rail is 6.7% higher than that in a CEN56 rail. This generates a short stress transition zone (around 3 m for a 20°C variation from SFT) at the rail type change location.
- Presence of guard rails increases the thermal forces in the track. To reduce their influence, the guard rails are usually installed without being fastened to all sleepers and with fishplated joints to minimise the additional thermal forces caused by their presence (sometimes with bolts not tightened to the full torque required by a running rail joint).
- Stress transition over Switches and Crossings (S&C). For a single turnout abutted by plain line CWR there is a complex thermal force loading – two rails (two forces) at the switch toe and four rails (four forces) at the heel of the crossing (Figure 6). The entire S&C layout creates a complex stress transition zone with potentially significant thermal force variations compared to plain line. In plain line, with the modern fastenings, the clamping forces generate higher longitudinal resistance than those generated between the sleeper and the ballast. Thus, for plain line, the longitudinal movement of the rail will generally only occur at this level. In a layout with Switches and Crossings some rails are constrained from any movement (the stock rails, crossings, etc), others are free to expand or contract (the switch rails) or with restrained thermal movement (the closure rails). The length and weight of the bearers varies, the number of rails fastened to each bearer is variable, there are wing and check rails present in the crossing area. This sum of factors generates a complex longitudinal resistance response through the S&C both at ballast and rail fastening level.

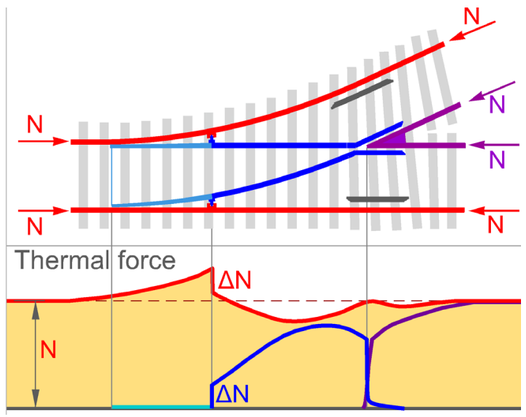

Figure 6: Thermal forces over a S&C (adapted from Wang, P. [2015])

The switch stock rails are continuous, but these rails accumulate thermal forces because they are prevented from expanding or contracting. The thermal forces will only tend to dissipate into "thermal breathing" movement (expansion or contraction) in the rails that have a free end – for example in the closure and the switch rails. This "breathing" must be limited to enable the switch to operate without adverse effect on the points operating and detection equipment. This limitation can be obtained by installing stress interaction devices at the heel of each of the switch rails. These devices can be:

- Stress transfer blocks - which rigidly connect the switch heel and stock rails for transferring the entire rail thermal stress from the closure rail to the stock rail.

2. Creep monitors or switch-stock rails interaction devices ("ball and claw") - allows a certain relative creep between the switch heel and stock rail (usually +/- 7 mm). The relative movement between the two rails is limited to a value that allows the expansion of the switch and closure rails without interfering with the normal operation of the points. If the expansion or contraction of the rail closes the creep monitor gap, the device prevents the further expansion of the closure rail and transfers the additional thermal force to the stock rail (ΔN in Figure 6). The creep monitors used on the UK network are designed to transfer up to 20% of the maximum thermal force (NR/L2/TRK/2102 – 5.10.5). For high-speed turnouts, where the switch and closure rails are longer than conventional speed turnouts, the thermal forces to be transferred are higher and alternative solutions are required. On the Spanish high-speed turnouts, multiple ball and claw units are installed (Figure 7). The German high-speed turnouts also use multiple or more robust creep-monitor designs (Wang – 2015).
3. Another option is to design the switch rail toe profile, the closure rail fastenings and the point operating mechanism to cope with the significant expansion of the internal rails of the high-speed S&C and not install any stress interaction devices between the stock rail and the heel of the switch rail.

In addition to these two main groups, a dynamic stress transition zone is created below a moving train – influenced by the vehicle loading and by the acceleration and deceleration of the vehicle. The longitudinal resistance is increased under the wheels and decreased in front/behind the vehicle and between bogies.

Slewing and lifting the track by on-track mechanical tamping machinery may also affect the track thermal forces. The SFT is altered and re-stressing will be required if the geometry changes are significant (NR/L2/TRK/001/Mod3 – 8.2).

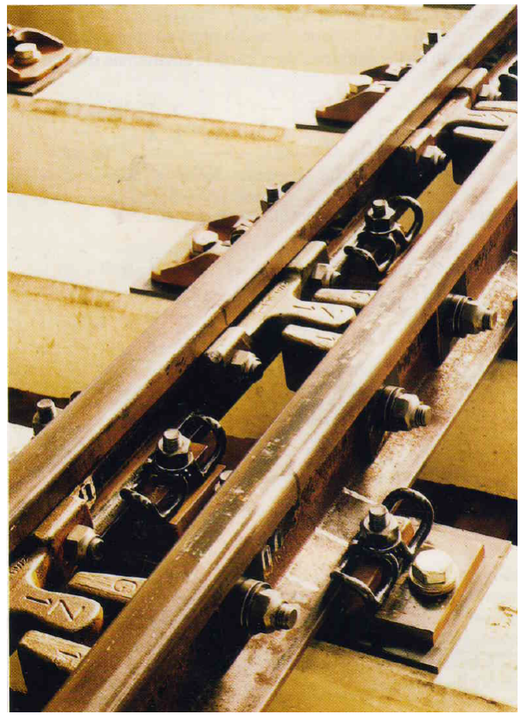

Figure 7: Multiple ball & claw units on a Spanish high-speed turnout (from García Díaz de Villegas & Bugarín [2005] – courtesy of JEZ Sistemas Ferroviarios – www.jez.es)

1.4. Adjustment Switch

The adjustment switch is a special joint with overlapping rail ends (scarf joint), which allows a range of longitudinal rail movements. It can be used to dissipate part of the thermal forces over the end CWR, where it abuts jointed track or other track features not designed to withstand thermal forces (NR/TRK/L2/3011).

Figure 8 presents an example of gap opening variation of an adjustment switch placed between CWR and a free-expansion jointed track. Even though the CWR track is on a restrained expansion superstructure – with an active longitudinal resistance, p – the movement on the CWR side of the adjustment switch varies significantly more compared to the jointed track side. In this example, the rail on the CWR varies between -9 mm and 20.9 mm and the rail on the free expansion jointed track varies from -2.7 mm to +4.3 mm. This is due to the long stress transition zone developed at the end of the CWR and to the dissipation of the expansion/contraction in the track joints. In this idealised model, the adjustment switch gap varies between 88 mm (at 53°C) and 125 mm (at -14°C). The history of the rail temperature variation has a direct influence on the present status. In this case, for a rail temperature of 20°C, and depending on how this moment is reached, the adjustment switch gap can be between 99 mm and 114 mm.

The installation of the adjustment switch at the end of CWR avoids the transfer of the thermal forces from the CWR to the adjacent section of track. An option used by other railway administrations is to allow this transfer on up to three jointed track panels (called buffer panels), which are installed with similar components to the CWR section (similar rail profiles, fastenings, ballast compaction). The joint gap variation of these buffer track panels is significantly affected by the adjacent CWR and it differs from the regular jointed tracks' behaviour (Ciobanu, Nogy – 2017-2).

1.5. Stressing Anchor

During the stressing works at the ends of the CWR or on the intermediate stress transition zones the thermal force is irregular, and it needs to be neutralised before applying the required pull force, by unclipping and supporting the rail on roller to allow unrestricted movement. On the fastened section of rail beyond the unclipped zone, a temporary stress transition zone (LT) will be formed – with a known variation of the thermal force (Figure 9).

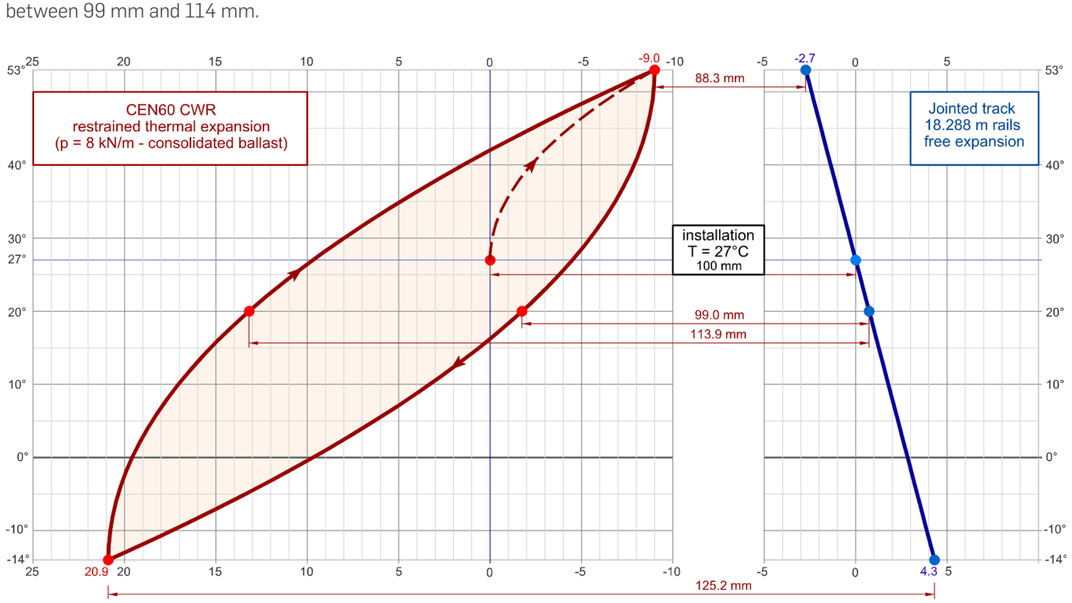

Figure 8. Gap variation for adjustment switch placed between CWR and jointed track

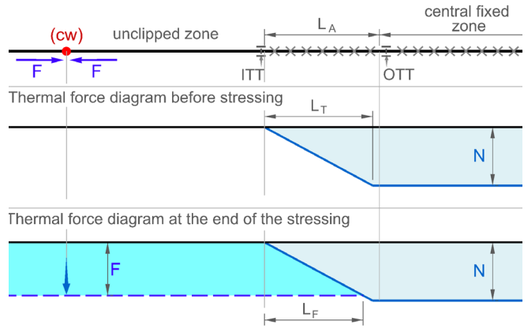

Figure 9: Anchor length

The rail stressing hydraulic tensing equipment applies an axial force (F) in the rails, by extending both free ends of rail at the point where the closure weld (cw) will be formed (Figure 9). If the temporary stress transition zone L_T overlaps with one of the stress transition zones described earlier, the pull force, F, might not be properly retained in the unclipped section of rail. In such a case the stressing process and/or the anchor length will need to be re-assessed to ensure that the adjacent stress transition does not affect the stressing process and the correct installation of the stress-free temperature on the stressed rail.

The stressing anchor L_A, needs to be of a sufficient length of clipped rail, from the first clipped fastening to a point where the rail thermal force is certainly constant and the rail is not moving. This is proved on site by two types of rail movement indicators:

- inner tell-tale (ITT), where rail movement will be recorded, first due to the development of the stress transition L_T and after, during the stressing, by the stressing pull. This is usually marked on the last unclipped sleeper, prior to cutting the rail.
- outer tell-tale (OTT), placed at the end of the anchor and in the central fixed zone. This confirms the adequacy of the anchor length by recording no rail movement during the stressing process. If movement is recorded at the OTT it indicates that the temporary stress transition L_T is longer than the estimated anchor length and the OTT must be repositioned, or the next OTT needs to be checked, if several have been placed on site.

The temporary stress transition length L_T (Figure 9) can be theoretically calculated using the formula:

$$L_T = \frac{N}{p} = \frac{\alpha E A \, \Delta T}{p}$$

where ΔT is the temperature difference between the current temperature and the SFT of the central fixed zone CWR. The anchor stress transition length required by the pull force F can be calculated using:

$$L_F = \frac{F}{p}$$

The anchor length L_A, needs to be, by a safe margin, greater than the two transition lengths:

$$L_A > \max(L_T, L_F)$$

Table 1 gives indicative values of the new stress transition length L_T formed after the ITT during the stressing process, following the rail unclipping and supporting on rollers.

p (kN/m rail)	5 [1]	8 [2]	12 [3]	F
ΔT (°C)	L_T (m)			(kN)
5	20.000	15.000	10.000	93
10	40.000	25.000	20.000	185
15	60.000	35.000	25.000	278
20	75.000	50.000	35.000	370
25	95.000	60.000	40.000	463
30	115.000	70.000	50.000	556
35	130.000	85.000	55.000	648

[1] Low longitudinal resistance for tamped ballast (Van – 1996)
[2] High longitudinal resistance for consolidated ballast (Van – 1996)
[3] Longitudinal resistance for creep only at fastening level (for fastenings compliant with EN 13481-2:2012)

Table 1: Length of the temporary stress transition formed after unclipping (CEN60 rail)

If the unclipped rails are exposed to significant temperature variations during the stressing process, peak thermal forces like the ones shown in Figure 2 (Stage 2 -T_2), can be created in the temporary transition length L_T. In such cases the stressing process should be re-assessed and, if required, a new stressing anchor length established before further unclipping undertaken. This will ensure the controlled release of the irregular thermal forces and obtain a known variation of the thermal force on the new anchor stress transition zone.

Table 2 of the British standard NR/L2/TRK/3011 provides the recommended anchor length for a variety of track conditions. However, bearing in mind the way the longitudinal resistance is activated at various levels in the track, it may not be safe to assume that the minimum 30 m anchor length for "high resistance" track is always sufficient for new modern fastenings in places with consolidated ballast, especially for high temperature difference, ΔT, between installation temperature and SFT. Although new modern fastenings (designed according to BS EN 13481-2:2012) will provide a reliable fastening longitudinal resistance, the rails, fastenings and sleepers will tend to move together in the ballast with only a minimum creep occurring at fastening level.

When comparing a stressing anchor to a regular stress transition, one important thing that should be considered is the significant difference between the regular stress transition at the end of CWR and the anchor, which is given by the temperature range and cycles that these two go through their respective operational “lives”.

A regular stress transition zone has a long lifespan (years) and it will potentially go through the entire rail temperature range [-14°C, 53°C] throughout many cycles during those years, whereas the temporary stress transition which appears within the anchor zone is a temporary arrangement during the stressing process, with a known thermal force variation, from zero to the constant value found on the central fixed zone.

The thermal forces which develop in the continuous welded rails are significantly higher than the ones found in the jointed rails. The response of the railway track to these forces is more complex, both in plain line and S&C.

The CWR, especially on the stress transitions, can have very complex, sometimes even unpredictable behaviour and it is useful for the rail stressing engineer to be familiar with the principles of rail thermal force calculations, so they can make the appropriate decisions during the stressing process.

Acknowledgements

The authors would like to thank Geoffrey Kennedy (Professional Head of Discipline – Permanent Way, Atkins) and Tom Wilson (Technical Discipline Leader - Track, WSP | Parsons Brinckerhoff) for their comments, suggestions and support in writing this article.

This article was originally published in the Journal of the Permanent Way Institution (UK), as part of a series of three articles presenting the general principles and theoretical considerations on railway track subjected to temperature variations. These articles are:

Ciobanu, C., Nogy, L. (2017) An introduction to rail thermal force calculations, PWI Journal April 2017 Vol 135 Part 1: 24-32.

Ciobanu, C., Nogy, L. (2017) Rail thermal force calculations for jointed track, PWI Journal April 2017 Vol 135 Part 2: 25-34.

Ciobanu, C., Nogy, L. (2017) Rail thermal force calculations for CWR, PWI Journal October 2017 Vol 135 Part 4: 14-18.

References

AICF (1959). Bulletin de l'Association internationale des chemin de fer. XXXVI,

BS EN 13481-2:2012. Railway applications - Track - Performance requirements for fastening systems Part 2: Fastening systems for concrete sleepers. British Standards Institution.

Calçada, R. (Ed.) (2009). Track-bridge interaction on high-speed railways. CRC Press/Taylor & Francis Group.

Code 774-3, UIC (2001). Track/bridge Interaction: Recommendations for calculations. International Union of Railways (UIC).

García Díaz de Villegas, J. M., & Rodríguez Bugarín, M. (2005). Desvíos Ferroviarios. Ingeniería Cántabra, SA.

Radu, C. (1979) Calea fără joante. Partea I. Institutul de Constructii Bucuresti.

NR/L2/TRK/001/mod03 (2012). Inspection and maintenance of Permanent Way. Plain line. Issue 6. Network Rail.

NR/L2/TRK/001/mod14 (2012). Inspection and maintenance of Permanent Way. Managing track in hot weather. Issue 6. Network Rail.

NR/L2/TRK/001/mod16 (2012). Inspection and maintenance of Permanent Way. Adjustment Switches. Issue 6. Network Rail.

NR/L2/TRK/2102 (2016). Design and Construction of Track, Issue 7. Network Rail.

NR/L2/TRK/3011 (2012). Continuous Welded Rail (CWR) Track, Issue 7. Network Rail.

Wang, P. (2015). Design of high-speed railway turnouts: theory and applications. Academic Press.

A Novel Approach for the Calculation and Presentation of Secondary Response Spectra

Chris Pearce

Chartered Engineer
Engineering, Design and Project Management, Infrastructure
Epsom, UK

Ian Ward

Technical Director
Engineering, Design and Project Management, Infrastructure
Epsom, UK

Abstract

"Secondary response" describes the behaviour of secondary systems inside a building subjected to dynamic loading. The design of secondary systems, such as process equipment, stairs, or other non-structural components, can be governed by these loads. Consequently, secondary response is an important consideration in the seismic design of structures. Since it is rarely feasible to employ detailed models of equipment arrangements throughout structural models to determine their dynamic behaviour, the design of equipment and other secondary systems are often based on Secondary Response Spectra (SRS). The SRS provide information about the maximum vibration levels experienced by the equipment over a range of frequencies.

SRS are typically calculated at a limited number of positions within a structure and then enveloped to produce bounding spectra. Inherent in this approach is the potential for the resulting SRS to be either overconservative, as the spatial resolution of the secondary response calculations is lost during enveloping, or to be nonconservative by missing peak values.

In this study, a novel "global SRS calculation and mapping" procedure is proposed, wherein SRS are calculated at all nodes within a finite element model of a structure. This approach has only recently become possible through the confluence of advances in computing power and efficient in-house solutions to the underlying mathematics. By preserving the resolution of the SRS calculations, this approach will avoid undue conservatism. It is amenable to automation and can significantly reduce the potential for user error. In addition, with SRS data available at all points, the variation in secondary response throughout a structure can be communicated in new and intuitive ways.

Keywords

Seismic design; Secondary response; Floor response spectra; SRS; FEA

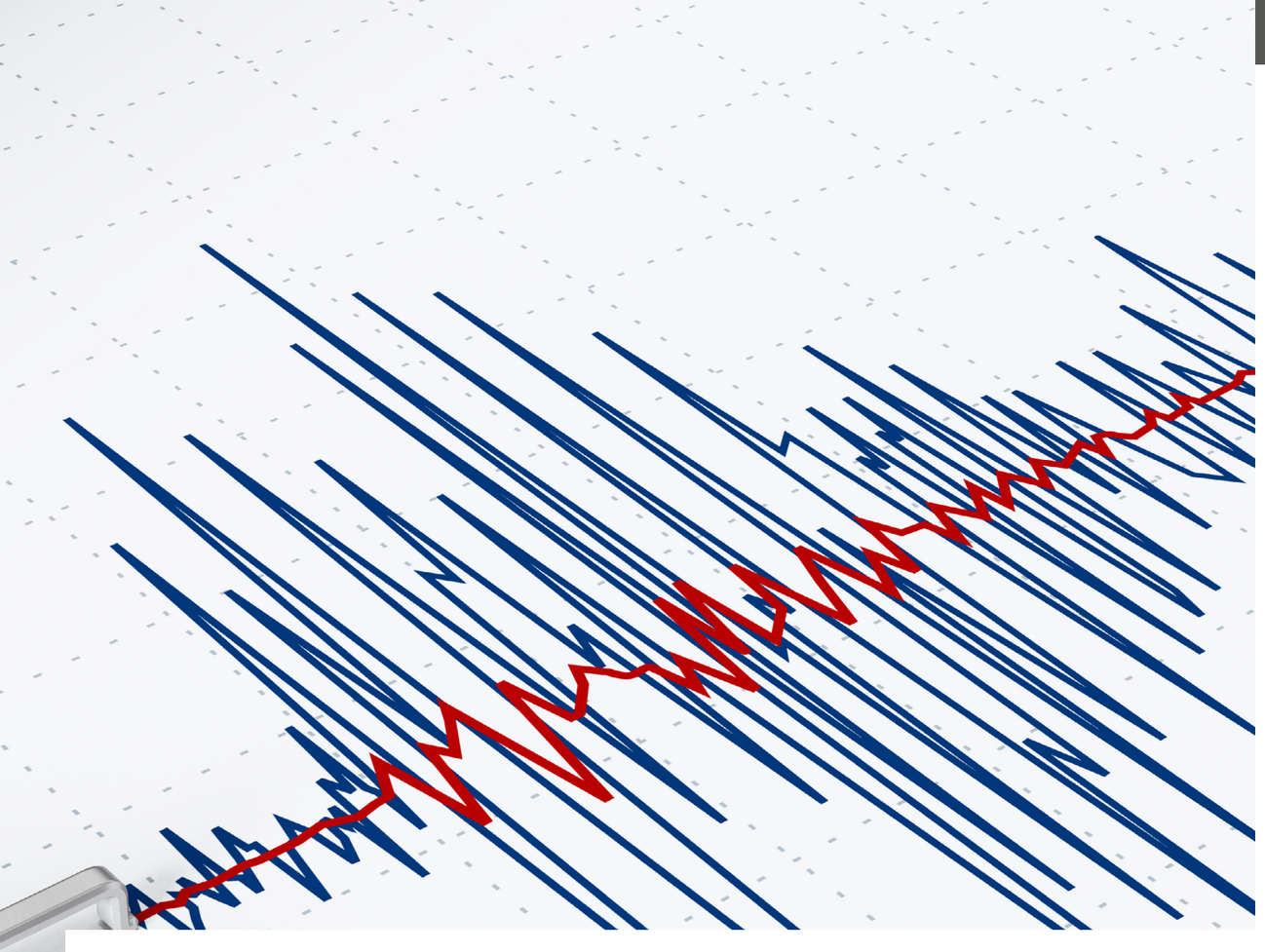

1. Introduction

Secondary response describes the behaviour of non-structural components within a building subjected to dynamic loading. Secondary response is most often considered in the design of seismically qualified structures, but may also be considered for structures experiencing blast, shock, or ground-borne vibration. When a structure is subjected to an earthquake, it will experience acceleration at its base, caused by motion of the ground. The structure, or "primary system," will respond dynamically, which will induce accelerations acting on the "secondary system" housed inside it. The secondary systems considered are most often process equipment or items such as stairs, walkways, etc. The objective of secondary response calculations is typically to obtain the peak accelerations experienced by the secondary systems during the dynamic event. The load generated by this peak acceleration will inform the specification or design of equipment, and any support structures or frames.

The most common method for determining secondary response is known as the "cascade approach" (Taghavi and Miranda, 2008). In this approach, the first step is to determine the acceleration time-history at a point in a structure, as a result of the application of a base acceleration time-history. The point selected is typically on a floor slab on which equipment will be located and the base acceleration time-history may represent seismic ground motion. With knowledge of the seismic design acceleration time-history, the response at any point in the structure can be determined through numerical or analytical models, such as the Finite Element (FE) method. The second step is then to determine the acceleration time-history of the equipment as a result of the structural acceleration. The fundamental assumptions of this approach are that the secondary system does not interact with the primary system and that the dynamic properties of the primary system are not affected by the presence of the secondary system. These assumptions are reasonable in the majority of circumstances, except when the primary system is expected to respond inelastically or the secondary system is of substantial mass (Taghavi and Miranda, 2008).

It is generally not feasible to model the equipment arrangements inside a structure in any great detail. The equipment is therefore typically modelled using a Single Degree of Freedom (SDOF) approximation. If the natural frequency and damping ratio of the piece of equipment is known or assumed, it can be represented by a SDOF system with equivalent properties. The response of an SDOF system to acceleration at its base can be readily obtained using numerical methods. Chopra (1995) describes several numerical methods available to calculate the behaviour of SDOF systems in response to discretised acceleration time-histories, such as the central difference method, and variants of Newmark's method. Of particular note is the recursive function developed by Nigam and Jennings (1969), which yields an exact solution for the behaviour of an SDOF system in response to an applied acceleration time-history assumed to vary linearly between discretised points. Guidance is available in codes such as ASCE 4-98 and ETC-C:2010 on the applicability of various numerical methods, based on the time-incrementation of the ground motion.

The dynamic properties of non-structural components, such as complex equipment arrangements, may not be known to the building designer, or may be subject to future alteration. As such, rather than determine the response of a single SDOF system, it is generally required to be knowledgeable of the peak acceleration response arising from a range of SDOF systems. This information is conveyed as Secondary Response Spectra (SRS). SRS describes the peak response of a series of SDOF systems with different dynamic properties. Example SRS, showing peak acceleration against the natural frequency for different levels of equipment damping, are shown in Figure 1. The production of SRS is

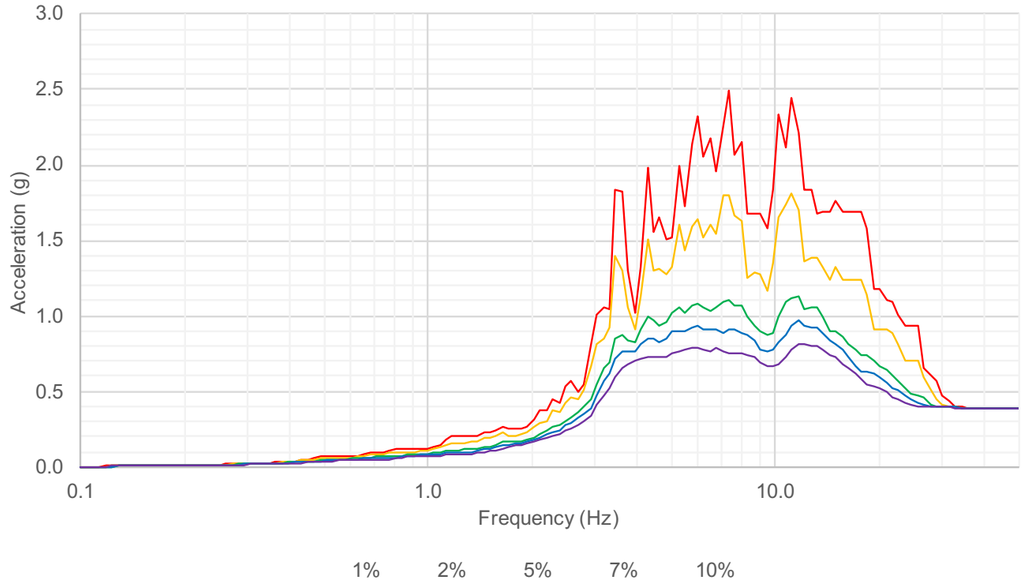

Figure 1: Example SRS plot detailing response of non-structural components vs. natural frequency. The various spectra correspond to different levels of equipment damping (from 1% to 10%).

often required during the design stage or to inform remediation measures post-construction.

3. Existing Method

In practice, it is necessary to characterise the secondary response for large areas of a structure, rather than at individual points. In order to do so, the standard procedure is to calculate SRS at a limited number of positions within the structure, which are then enveloped to produce bounding spectra. For example, in order to determine SRS characteristic of a floor in a structure the following procedure would be followed:

1. First determine suitable points on the floor that would capture the maximum secondary response. This typically requires additional analysis to predict the locations where maximum response would occur, or manual steps to select relevant points based on engineering judgement.
2. Calculate SRS at the selected points.
3. Envelope the resulting spectra to produce a bounding spectrum. The bounding spectrum represents the maximum secondary response of the area analysed.

The existing method is depicted in Figure 2 for an example floor. The enveloping of five SRS is depicted, although in practice many more may be used.

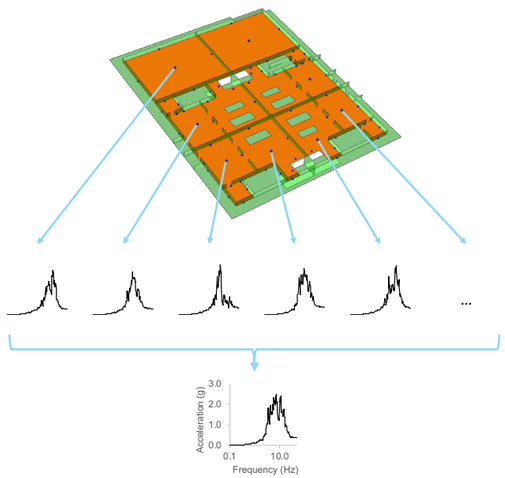

Figure 2: Diagram of existing SRS calculation procedure. To produce SRS characteristic of an example floor (highlighted orange), SRS are first determined at selected points (blue dots), and then enveloped.

3. Proposed Method

3.1. Analysis Philosophy

In this study, a novel approach to secondary response analysis is proposed: the "global SRS calculation and mapping" procedure, which is based on the calculation of SRS at all nodes within a FE model of a structure. This yields a number of benefits over the existing method:

Reduced conservatism/more control of conservatisms

In the existing method, the enveloped SRS determined for a particular region within a structure are assumed to be characteristic of the entire region. However, the response in some areas will be less onerous. In this study, it is proposed that SRS be calculated at all nodes within a model. Doing so removes the need to envelope SRS calculated at a limited number of points in order to characterise larger regions.

Fewer calculation steps

In the existing method, several additional calculation steps are required to determine the positions in the structure at which SRS are to be calculated. Defining SRS areas, or identifying and selecting positions that will give the greatest response, can be time-consuming manual steps. By comparison, in the global SRS calculation method, there is no longer a need for these additional steps.

High resolution

Despite the significant computational effort underlying the production of SRS, in the existing method the results are communicated in a relatively coarse fashion, by way of a few SRS plots per region. The resolution of the results, present in the calculations themselves, is therefore lost.

However, as a result of the proposed method, a higher density of SRS data is available, which allows the results to be communicated in novel ways. SRS results can be mapped onto computational models of structures and presented as contour plots. These contour plots could potentially be generated in any scriptable modelling software that would yield the most benefit for the analysis or design task at hand. For example, FE software such as Abaqus (Dassault Systèmes SE) or Robot Structural Analysis Professional (Autodesk Inc.) could be used, or Computer Aided Design (CAD) packages such as AutoCAD (Autodesk Inc.). This could benefit the positioning of equipment or other design processes that rely on SRS results, and would give designers and clients a more intuitive understanding of the behaviour of the structure and secondary systems. For instance, contour plots of SRS could be used to assess dropped-load hazards.

3.2. Complimentary Advancements

SRS calculations are computationally intensive and, as such, this approach has only recently become practical, due to advances in computing power. Enabling technologies include the proliferation of analysis computers with many high-speed processors, multi-processing software libraries, and the availability of systems with large amounts of Random Access Memory (RAM).

Efficient solutions to the underlying mathematics have also been employed to facilitate the global SRS calculation method. A variant of the modal dynamic time-history analysis technique has been developed that significantly decreases the number of times the equation of motion of an SDOF system needs to be solved. This is achieved by substitution of the function for the acceleration response of the primary system within that of the secondary system, resulting in a direct response function for the secondary system. This allows factoring by appropriate modal properties (i.e. modal displacements and mass participation factors) to be detached from the solution of the SDOF equations of motion, resulting in significant time savings when computing SRS at a large number of FE nodes.

4. Case Study

4.1. Software Implementation

In-house software has been developed to implement the proposed global SRS calculation and mapping procedure. The software (SpectroScope) has been written in the Python programming language and makes use of parallel processing, efficient array operations, and the other complimentary advancements described above in order to efficiently calculate secondary response. The exact solution to the equation of motion of SDOF systems is obtained using the recursive function presented in Nigam and Jennings (1969).

4.2. Analysis Example

The above-mentioned software has made it feasible to calculate equipment response at all points in computational models of floors, walls, or entire structures. This has enabled a detailed understanding of the secondary response both over wide areas or at individual equipment locations. It has been successfully employed on projects to determine secondary response for a wide range of structural models, of varying levels of complexity, and created in various software packages.

A case study is presented demonstrating the global SRS calculation and mapping procedure conducted using a detailed FE model of a large, seismically qualified structure. A FE model of the complex, partially-embedded, reinforced concrete building was created using the Abaqus/CAE software package (Dassault Systèmes SE). The model was composed of approximately 360,000 shell and beam elements, defined by approximately 350,000 nodes, with around 230,000 spring elements representing the soil.

A modal analysis was conducted to obtain the information required for the secondary response calculations, namely: the natural frequencies, damping ratios (determined using composite modal damping), and mass participation factors in the three Cartesian directions, for all modes of interest. A total of 812 modes were considered, which represents all natural modes up to 40 Hz. In addition, the modal displacements in the three Cartesian directions, corresponding to each of the modes of interest, were determined for all nodes in the model.

The SpectroScope software was used to calculate both the structural and equipment responses to a set of concurrent base acceleration time-histories, (i.e. time-histories in the x, y, and z directions, representing components of seismic ground motion). SRS were determined for a wide range of dynamic properties of the secondary system; specifically, seven equipment damping ratios between 1% and 15%, and 150 equipment natural frequencies between 0.1 Hz and 50 Hz. The time required to calculate SRS is dependent on many factors, including the analysis machine used, the size of the model, and the number of equipment damping ratios and natural frequencies considered. In this case study, the calculation time to determine the SRS for each equipment damping ratio was approximately equal to the time required to conduct a modal analysis of the structure.

A variety of contour plots were then produced utilising the SRS results determined at all nodes within the model. The large quantity of data can be visualised in different ways but are here presented as contour plots of either: SRS at a specific equipment frequency, the peak SRS enveloped across all 150 equipment frequencies or the equipment frequencies that give rise to the maximum SRS. In each case, the plotted results are specific to a single value of equipment damping. A few example contour plots are given in Figures 3 through 6 below.

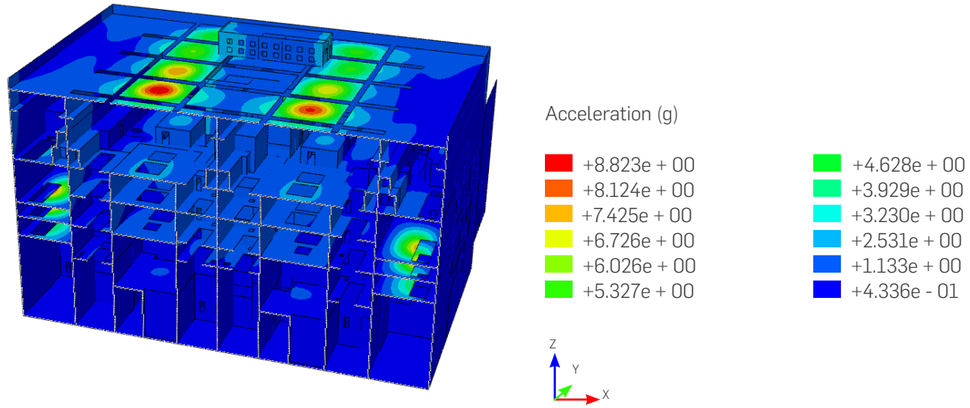

Figure 3: Contour plot of vertical (z-direction) SRS, computed for a specific equipment frequency of 10.2 Hz, with 5% equipment damping.

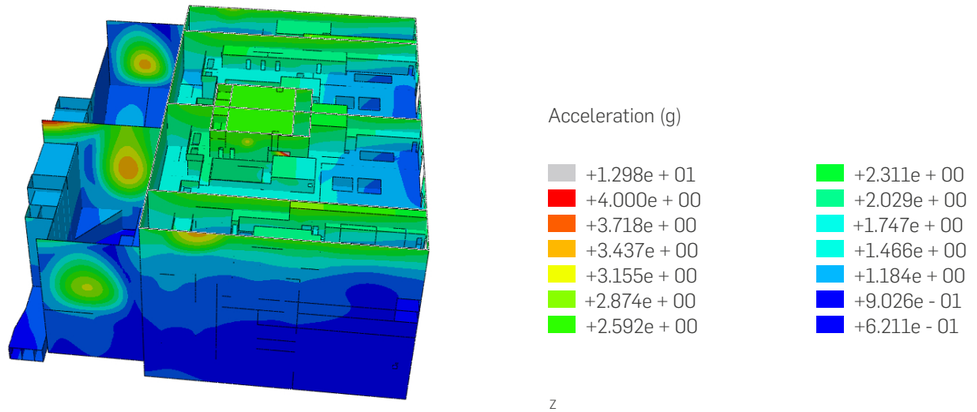

Figure 4: Contour plot of maximum horizontal (x-direction) SRS, enveloped across 150 frequencies between 0.1 Hz and 50 Hz, with 5% equipment damping.

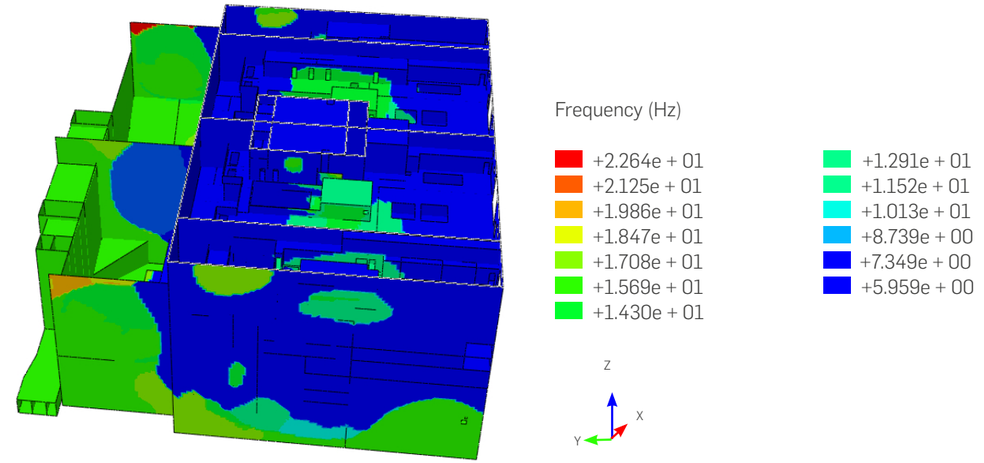

Figure 5: Contour plot showing equipment frequencies corresponding to the maximum horizontal (x-direction) SRS, enveloped across 150 frequencies between 0.1Hz and 50.0Hz, with 5% equipment damping.

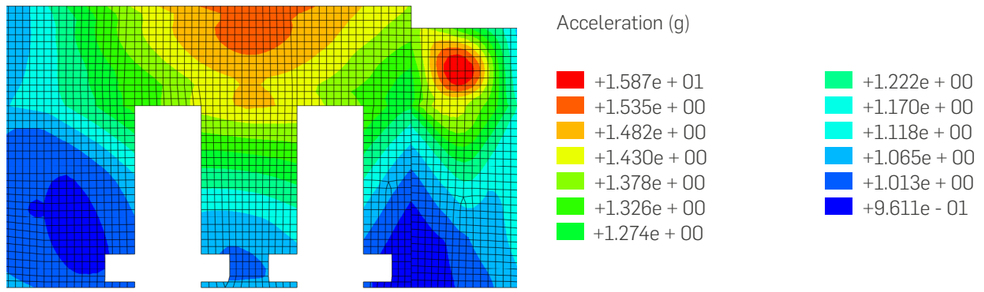

Figure 6: Contour plot of maximum vertical (z-direction) SRS, enveloped across 150 frequencies between 0.1 Hz and 50 Hz, with 5% equipment damping. Plan view of an individual floor, with FE mesh visible.

5. Discussion

There is a substantial amount of literature on methods to expediate the process of calculating SRS. Various "spectrum-to-spectrum" methods have been developed in which SRS are determined analytically from the ground spectrum of the design earthquake. Several different techniques have been employed in developing these methods. For example, Yasui et al. (1993) and Jiang et al. (2015) describe spectrum-to-spectrum methods based on Duhamel's integral. Calvi and Sullivan (2014) present a spectrum-to-spectrum method that makes use of an empirical relationship proposed by Sullivan et al. (2013), which derives from a large number of non-linear time-history analysis simulations. In Lucchini et al. (2016), a spectrum-to-spectrum method based on a probabilistic approach is presented, that allows SRS to be determined for a target mean annual frequency of exceedance. Reviews of the currently available spectrum-to-spectrum methods can be found in Lucchini et al. (2017), as well as the aforementioned publications. Although a number of spectrum-to-spectrum methods have been available for some time, they have not been widely adopted in the nuclear industry. This may be due to the fact that the approximations inherent in several of these methods result in varying levels of conservatism over different frequency ranges, which could produce overconservative or nonconservative results at certain frequencies (Jiang et al., 2015).

One of the principal advantages of spectrum-to-spectrum methods is the speed at which SRS can be determined. The other is the fact that generating SRS directly from the ground spectrum overcomes the variabilities in SRS derived from spectrum-compatible time-histories, which generally results in multiple base acceleration time-history sets being required during design calculations. The computationally efficient time-history method discussed here has made it feasible to calculate SRS at all nodes in a structure. Nevertheless, spectrum-to-spectrum methods could also be employed in the global SRS calculation and mapping procedure if such a method were preferable.

There appears to be little literature concerning the selection of nodes for SRS calculations or methods by which a greater understanding of the variation in secondary response throughout a structure can be obtained. A notable exception is Jussila et al. (2016), in which the authors conclude that the selection of nodes to be used for SRS calculations should not be based on engineering judgement alone, as this has the potential to be nonconservative. The authors then explore a systematic approach of selecting nodes in regular grid patterns of increasing density in order to provide recommendations on the grid size to use for SRS calculations in reactor buildings. The authors note that predicted SRS may vary significantly within a floor and in their study report a typical coefficient of variance of 0.2 for SRS in the horizontal directions and 0.45 for vertical SRS (Jussila et al., 2016).

The procedure presented in this study is in many ways similar to the philosophy of Jussila et al. (2016), which notes that previous numerical methods were limited to computationally efficient simplifications, whereas modern methods can take advantage of the increased computation capacity available. The global SRS calculation procedure, wherein SRS are determined at all nodes, could be regarded as a logical extension to grid-based methods of increasing resolution. However, unlike grid-based methods, no additional calculation steps are required to identify the nodes of interest. Furthermore, the results of the global SRS calculation procedure are amenable to contour plot production, which leads to an intuitive understanding of the variation in secondary response within the structure.

6. Conclusions

Design procedures should reflect the current state of technology, and take advantage of this to eliminate processes susceptible to error or oversight. To this end, a new global SRS calculation and mapping procedure has been developed and software has been written to implement this process. The approach has been demonstrated on a variety of buildings and found to give significant advantages by simplifying the overall process and producing higher resolution results.

Acknowledgements

Originally published as "A novel approach for the calculation and presentation of secondary response spectra" in the proceedings of the SECED 2019 Conference (Pearce and Ward, 2019).

The authors would like to thank EDPM colleagues Nick Hucker and Will Jarvis for their assistance in the development of the SRS calculation procedure and software.

References

ASCE 4-98, Seismic Analysis of Safety-Related Nuclear Structures, American Society of Civil Engineers (ASCE), 2000

Calvi PM, Sullivan TJ (2014), Estimating floor spectra in multiple degree of freedom systems, Earthquakes and Structures, 7: 17-38

Chopra AK (1995), Dynamics of Structures: Theory and Applications to Earthquake Engineering, Prentice-Hall

ETC-C:2010, EPR Technical Code for Civil Works, AFCEN, 2010

Jiang W, Li B, Xie W-C, Pandey MD (2015), Generate floor response spectra, Part 1: Direct spectra-to-spectra method, Nuclear Engineering and Design, 293: 525-546

Jussila V, Li Y, Fülöp L (2016), Statistical analysis of the variation of floor vibrations in nuclear power plants subject to seismic loads, Nuclear Engineering and Design, 309: 84-96

Lucchini A, Franchin P, Mollaioli F (2016), Uniform hazard floor response spectra for linear structures, Earthquake Engineering and Structural Dynamics, 46: 1121-1140

Lucchini A, Franchin P, Mollaioli F (2017), Spectrum-to-spectrum methods for the generation of elastic floor acceleration spectra, Procedia Engineering, 199: 3552–3557

Nigam NC, Jennings PC (1969), Calculation of response spectra from strong-motion earthquake records, Bulletin of the Seismological Society of America, 59: 909-922

Pearce CW, Ward IP (2019), A novel approach for the calculation and presentation of secondary response spectra, Proceedings of the SECED 2019 Conference, London, UK, 9-10 September

Sullivan TJ, Calvi PM, Nascimbene R (2013), Towards improved floor spectra estimates for seismic design, Earthquakes and Structures, 4: 109-132

Taghavi S, Miranda E (2008), Effect of interaction between primary and secondary systems on floor response spectra, Proceedings of the 14th World Conference on Earthquake Engineering, Beijing, China, 12-17 October

Yasui Y, Yoshihara J, Takeda T, Miyamoto A (1993), Direct generation method for floor response spectra, Proceedings of the 12th International Conference on Structural Mechanics in Reactor Technology (SMiRT 12), Stuttgart, Germany, 15–20 August, 367-372

Structural Design and Assessment | 010

Development of Reliability-Based Assessment Criteria Against Extreme Environmental Loading for Fixed Offshore Steel Structures with Significant Permanent Loading

Mark Manzocchi

Principal Engineer
Oil & Gas
Edinburgh, UK

Mohamed Atia

Principal Engineer
Oil & Gas
Abu Dhabi, UAE

Abstract

Many fixed offshore steel platforms in the Arabian Gulf are situated in shallow water and have a relatively high proportion of dead loading to environmental loading. As such, their capacity is governed by the combined effect of extreme environmental loading and vertical dead loading. Reliability-based assessment methods normally consider the probability of the lateral capacity being exceeded by the extreme environmental loading. This assessment is typically performed by considering the pushover capacity of the platform compared with the regional environmental hazard curve. Allowance is made for uncertainty in the capacity and load model when evaluating the reliability. In the presence of significant dead loading, and for some ultimate failure modes, the sensitivity of pushover capacity to dead load plays an important role in the reliability analysis.

This paper describes the methodology for reliability analysis against the extreme load hazard and which can be implemented into future assessment codes. Particular attention is focussed on the sensitivity of structures to high levels of dead load and how this may be incorporated into reliability analysis. The development of acceptance criteria for reserve strength ratios (RSRs) which depend on regional hazard curves and dead load is also described.

Keywords

Offshore Steel Jackets; Extreme Environmental Loading; Pushover Analysis; Structural Reliability; Safety Factors

1. Environmental Hazard Curves

Offshore structures are subjected to environmental loading arising from the action of waves, current, and wind on the structure. The magnitude of this environmental load hazard is described in terms of a hazard curve relating loading magnitude to its return period, defined as the mean time between occurrences of that loading being exceeded.

An established method for deriving hazard curves is through the use of a response-based metocean analysis (RBMA) (Tromans and Vanderschuren, 1995). The RBMA is a method of producing consistent environmental load hazard curves (of base shear or other response parameter) for different global regions and different types of fixed platforms.

For fixed steel jackets, the global jacket loading is defined in terms of the applied total base shear. In the RBMA, the base shear induced by the environment on a representation of the structure is derived for all storm events in the metocean dataset (e.g. from the hindcast dataset). Statistical analysis is performed on this derived response data, with due account being made of short-term variability within storms convoluted over the long-term variability. The outcome is a probability distribution of extreme annual base shear response, which in turns defines the hazard curve.

As described by Efthymiou et al. (1996), the hazard curve for a fixed platform subjected to storm loading is commonly normalised by the base shear having an annual probability of exceedance of 0.01 (i.e., a return period 100 years). The shape of the hazard curve is then generally found to have an exponential tail which plots as a linear relationship between the normalized response and the logarithm of return period.

The characersitics of environmental hazard curves for fixed-steel structures are specific to the environment at a given site, but they can be broadly categorized by geographical regions (Efthymiou, 2011). The ratio between the 10,000-year return period response, E_{10K} and the 100 year return period response, E_{100} defines the slope of the hazard curve, typically representative of a region.

The hazard curve relationship between environmental loading E at return period RP and return period for the log-linear hazard curve is:

$$\frac{E}{E_{100}} = 1 + \left(\frac{r_H - 1}{2}\right)\log_{10}\left(\frac{RP}{100}\right)$$

With parameter r_H being the hazard curve ratio

$$r_H = \frac{E_{10K}}{E_{100}}$$

A typical hazard curve is illustrated in Figure 1.

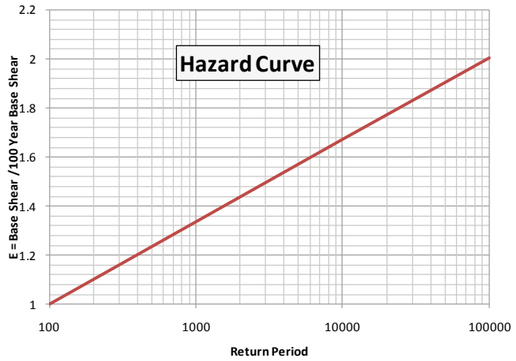

Figure 1: Typical environmental hazard curve

2. Structural Capacity Failure Surface

For steel structures, global structural resistance is generally determined by means of nonlinear pushover analysis (Figure 2). The Reserve Strength Ratio, RSR, is a measure of structural capacity and is defined as the the pushover capacity normalized by the 100-year environmental loading. This concept can be generalised to define a reserve strength ratio normalised by the environmental loading with return period RP.

$$RSR_{RP} = \frac{E_{Collapse}}{E_{RP}}$$

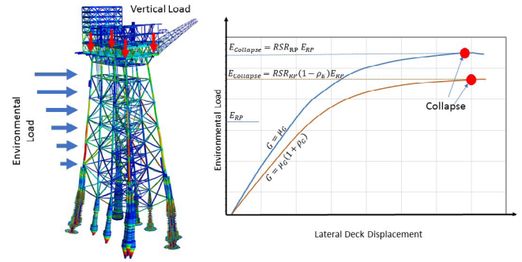

Figure 2: Pushover analysis

The influence of the permanent dead loading on the capacity of the structure plays an important role, depending on the failure mode of the structure. For failure modes which depend on the global applied shear force, such as failure of braced bays, the global capacity tends to be insensitive to variability in the dead loading. However, where the global failure mode is of an overturning type, such as local buckling in the braces, then the resistance to environmental loading is sensitive to the vertical dead loading. A failure surface defining the ultimate collapse load as a function of dead load derived from a series of pushover analyses (Figure 3).

E= Environmental Load

G= Dead Load

E_{nom}= Nominal Environmental Load (derived at return period RP)

μ_G= mean dead load

λ_E= environmental load factor applied to E_{nom}. i.e. $E = \lambda_E E_{nom}$

λ_G= load factor applied to μ_G. i.e. $G = \lambda_G \mu_G$

$\lambda_{E\mu}$= Environmental load factor at which collapse occurs when a pushover analysis is performed at the mean dead load. Note that $\lambda_{E\mu} = RSR_{RP}$

λ_R= factor on mean resistance

ρ_G= proportional increase in dead load

ρ_E= proportional decrease in environmental load at collapse

The sensitivity of the environmental load capacity to dead load may be expressed in terms of a sensitivity parameter, α_G, defined as the ratio in the proportionate reduction in environmental capacity to an increase in dead load. Consider two pushover analyses: one with mean dead load for $G=\mu_G$, and the second for at an incremented dead load $G=\mu_G(1+\rho_G)$. In the first case, the environmental load factor at collapse (or RSR) is $\lambda_{\mu E}$. In the second case, the environmental load factor at collapse is $\lambda_{\mu E}(1-\rho_E)$. The dead load sensitivity parameter is then here defined as

$$\alpha_G = \frac{\rho_E}{\rho_G}$$

For example, if an increase in dead load of $\rho_G = 10\%$ leads to a decrease in environmental collapse base shear of $\rho_E=5\%$ then $\alpha_G=0.5$.
When the resistance is multiplied by a factor λ_R, the whole failure surface expands radially by this factor in the space of the applied loading.

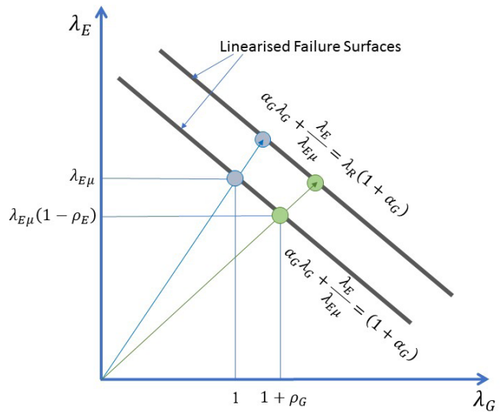

Figure 3: Linearised failure surface in dead load –Environmental load space

The failure surface in the space of the multiplicative factors $\lambda_G$on mean dead load, λ_E on nominal environmental load and λ_R on mean resistance and linearised around the point of mean resistance, dead load and collapse environmental load is then given by:

$$\lambda_R(1+\alpha_G) - \left(\alpha_G\lambda_G + \frac{\lambda_E}{\lambda_{E\mu}}\right) \le 0$$

Introducing random variables:

X_E= Random multiplier on environmental load

E_H= Random environmental load multiplier described by hazard curve

X_G= Random multiplier on mean dead load

X_R= Random multiplier on mean resistance

Thus:

$$\lambda_E = X_E E_H$$
$$E = \lambda_E E_{nom} = X_E E_H E_{nom}$$
$$\lambda_R = X_R$$

The limit state function then takes the form:

$$(1+\alpha_G)X_R - \left(\alpha_G X_G + \frac{X_E E_H}{\lambda_{E\mu}}\right) \le 0$$

One important observation is that the sensitivity of environmental pushover capacity to dead load needs be accounted for even if the dead load variability is small or deterministic. Let $X_G=1$ (i.e., a deterministic dead load). Then the failure surface becomes:

$$(1+\alpha_G)X_R - \alpha_G - \frac{X_E E_H}{\lambda_{E\mu}} \le 0$$

With $\alpha_G \neq 0$ the effect can be captured with an effective resistance variable X'_R with an increased CoV:

$$X'_R - \frac{X_E E_H}{\lambda_{E\mu}} \le 0$$

With $X'_R=(1+\alpha_G)X_R-\alpha_G$. If $E[X_R]=1$ then:

$$CoV[X'_R] = (1+\alpha_G)CoV[X_R]$$

The implication is that, even where there is no uncertainty in the dead loading, the effect of sensitivity of the collapse load to dead load sensitivity is to increase the effective uncertainty in the resistance.

3. Reliability-Based Assessment Criteria

The environmental loading is the primary Type I aleatoric (or physical) random variable to which a platform is subjected. Other uncertainties included in a structural assessment (Efthymiou et al., 1996; Moses and Stahl, 2000; Moses, 1991; Turner, 2003) include Type II uncertainties in resistance, modelling uncertainty in environmental loading. A comprehensive framework for reliability analysis and enumeration of potential uncertainties to which is given in Fraser et al. (2015).

Reliability analysis has been used to calibrate safety factors that can be used in the context of an assessment using pushover analysis. These factors are applied to the dead load and to the reserve strength ratio and are required to ensure that a given target probability of collapse is achieved. The probabilistic model is detailed in Table 1.

Limit State Function $(1+\alpha_G)X_R - \left(\alpha_G X_G + \frac{X_E E_H}{\lambda_{E\mu}}\right) \le 0$

Symbol	Description	Probability Distribution
E_H	Type I Environmental Load Uncertainty	Defined by Hazard Curve $E_H = 1 + \frac{(r_H-1)}{2}\log_{10}\left(\frac{RP}{100}\right)$
X_R	Resistance Uncertainty	Lognormal Distribution Median = 1.0 Coefficient of Variation (CoV) Failure mode involving braced bay CoV = 5% Failure mode involving tubular leg with no local buckling (D/t < 60) CoV = 10% Failure mode involving tubular leg with local buckling (D/t > 60) CoV = 15%
X_G	Uncertainty in Dead + Live Vertical Load	Normal Distribution Mean = 1.0 CoV = 10%
X_E	Type II Environmental Modelling Uncertainty	Normal Distribution Mean = 1.0 CoV = 12%

Table 1: Definition of probabilistic model for pushover analysis

The RSR is denoted RSR_{RP} and is defined as the load factor applied to the environmental load set with a return period of RP years and which results in system collapse of the platform.

$$RSR_{RP} = \frac{E_{Collapse}}{E_{RP}}$$

Where:

$E_{Collapse}$ is the collapse load factor

E_{RP} is the extreme environmental loading with a return period or RP years

If an assessment is being performed to a target return period of collapse, RP_{targ}, then it is recommended that E_{RPtarg} is applied as the reference load to the structure.

For jacket structures, and in the absence of wave-in-deck loading, the relationship between environmental load magnitude and return period is region specific. It may be approximated by the following hazard curve relationship:

$$E_{RP} = E_{100}\left(1 + \frac{r_H - 1}{2}\log\left(\frac{RP}{100}\right)\right)$$

Where r_H denotes the hazard curve ratio defined by:

$$r_H = \frac{E_{10,000}}{E_{100}}$$

For a pushover analysis performed with the objective of achieving a specified target return period to failure the RSR must satisfy:

$$RSR_{RP_{Targ}} > C_C$$

C_C is a probability factor which accounts for variability in resistance and load modelling. Values of C_C for target return periods to failure of 2,500 and 10,000 years, for different resistance coefficient of variation, and for a range of hazard curve ratio r_H, have been calibrated using reliability analysis and are given in Table 2 for failure modes involving structural members

The resistance coefficient of variation (CoV) depends on the structural failure mode. The following are recommended:

- Failure mode involving braced bay CoV = 5%
- Failure mode involving tubular leg with no local buckling (D/t < 60) CoV = 10%
- Failure mode involving tubular leg with local buckling (D/t > 60) CoV = 15%

Return Period of Collapse		2,500 Years				10,000 Years			
Hazard Curve Ratio, r_H		1.5	1.7	1.9	2.1	1.5	1.7	1.9	2.1
CoV Resistance	5%	1.08	1.06	1.05	1.04	1.09	1.07	1.06	1.06
	10%	1.12	1.09	1.08	1.07	1.14	1.11	1.09	1.08
	15%	1.20	1.15	1.12	1.11	1.22	1.18	1.15	1.13

Table 2: Values of probabilistic factor C_C for pushover analysis

The sensitivity to overall permanent + variable load in a pushover analysis is investigated by performing pushover analyses for two levels of permanent and variable load. The permanent load sensitivity factor is defined as:

$$\alpha_G = \frac{\%\ Decrease\ in\ Environmental\ Load\ Factor\ at\ Collapse}{\%\ Increase\ in\ Permanent + Variable\ Load}$$

The pushover analysis should then be performed by factoring the best estimate (median) permanent + variable load by a factor C_G such that:

$$G+Q=C_G\,(G_{BE}+Q_{BE})$$

Values of C_G are given in Table 3.

Return Period of Collapse			2,500 Years				10,000 Years			
Hazard Curve Ratio, r_H			1.5	1.7	1.9	2.1	1.5	1.7	1.9	2.1
Dead Load Sensitivity Factor α_G	0.1	5%	1.04	1.02	1.02	1.02	1.04	1.03	1.03	1.02
	0.1	10%	1.12	1.09	1.08	1.07	1.14	1.11	1.09	1.08
	0.1	15%	1.28	1.23	1.19	1.17	1.32	1.26	1.23	1.20
	0.3	5%	1.05	1.04	1.03	1.03	1.05	1.04	1.04	1.03
	0.3	10%	1.15	1.12	1.10	1.09	1.17	1.13	1.11	1.10
	0.3	15%	1.33	1.27	1.22	1.20	1.38	1.31	1.27	1.24
	0.5	5%	1.07	1.05	1.04	1.04	1.07	1.06	1.05	1.04
	0.5	10%	1.19	1.14	1.12	1.10	1.21	1.16	1.14	1.12
	0.5	15%	1.40	1.32	1.27	1.23	1.47	1.37	1.32	1.28

Table 3: Values of permanent + variable load factor C_G

4. Concluding Remarks

In this paper, the influence of vertical gravity loading on assessment criteria for fixed offshore structures subject to significant vertical loading has been considered. A structure whose RSR under horizontal environmental loading is sensitive to the level of vertical permanent loading has a greater failure probability than one which is insensitive to dead load. This sensitivity can be assessed by performing two pushover analyses and quantified by a parameter α_G.

A series of calibrated safety factors have been derived and presented in Table 3. These account for the uncertainty present in the structural assessment and are presented for different target return periods of collapse, regional hazard curve characteristics, resistance uncertainty, and sensitivity of pushover capacity to vertical dead load. These factors provide criteria for use in the context of pushover analysis and can be used for assessment against a given target return period to failure.

Acknowledgements

This paper was originally prepared for presentation at the Abu Dhabi International Petroleum Exhibition and Conference held in Abu Dhabi, UAE, 9–12 November 2015 (Society of Petroleum Engineers). The authors have benefited from technical discussion on the subject matter of this paper with Dr. Ramsay Fraser, Dr. Peter Tromans, Dr. Mike Efthymiou, Dr. Graham Stewart, Dr. Richard Gibson, Pat O'Connor, Alastair Smith and Salvador Vargas.

References

Banon, H., Cornell, C. A., Crouse, C. B., Marshall, P. W., Nadim, F., Younan, A. H., (2001) "ISO Seismic Design Guidelines for Offshore Platforms," Proceedings of OMAE:20th Offshore Mechanics and Arctic Engineering Conference – OMAE 2001, Rio de Janeiro, Brazil, 3rd – 8th June 2001.

Cornell, C. A., (1996) "Calculating Building Seismic Performance Reliability: A Basis for Multi-Level Design Norms," Proceedings of Eleventh World Conference on Earthquake Engineering, Acapulco, Mexico, 1996.

Efthymiou, M., van de Graaf, J. W., Tromans, P. S., and Hines, I. M., (1996), "Reliability Based Criteria for Fixed Steel Offshore Platforms," Proceedings of the 15th International Conference on Offshore Mechanics and Arctic Engineering, Florence, Italy, pp. 129–141.

Fraser, R, Manzocchi, M, Gibson, R, (2015) "Pushover Load factors for Fixed Steel Platforms Sensitive to Topside Load and Wave-in-Deck Load", Proceedings of the 34th International Conference on Ocean, Offshore and Arctic Engineering, St. John's, Newfoundland, Canada, OMAE2015 – 41605

Moses, F. (1991), "A Global Approach for Reliability-based Offshore Platform Codes", Proc. 4th Integrity of Offshore Struct. Symp. D. Faulkner et al (eds), Glasgow, Elsevier 1991.

Moses, F., and Larrabee, R. D., (1988). "Calibration of the Draft LRFD-RP2A for Fixed Platforms," Proceedings of the Offshore Technology Conference, Houston, TX, 1988

Moses, F., Stahl, B., (2000) "Calibration Issues in Development of ISO Standards for Fixed Steel Offshore Structures", Trans. AMSE, 52, vol. 122, Feb 2000.

Tromans, P. S., and Vanderschuren, L., (1995), "Response Based Design Conditions in the North Sea – Application of a New Method", OTC 7683, Huston, May 1995.

Turner, R. C., (2003), "Component-based calibration of North West European annex environmental load factors for the ISO fixed steel offshore structures code 19902", Research Report 088, UK HSE, 2003.

SNC·LAVALIN

snclavalin.com

Contact information
Akshaye Sikand
Manager, Knowledge Management
Akshaye.Sikand@snclavalin.com

5356_SL19